Award Number: W81XWH-12-2-0038

TITLE: Prevention of Blast-Related Injuries

PRINCIPAL INVESTIGATOR: Albert I. King

CONTRACTING ORGANIZATION: Wayne State University
Detroit, MI 48201

REPORT DATE: July 2015

TYPE OF REPORT: Annual

PREPARED FOR: U.S. Army Medical Research and Materiel Command
                           Fort Detrick, Maryland 21702-5012

DISTRIBUTION STATEMENT: Approved for Public Release;
                                         Distribution Unlimited

REPORT DOCUMENTATION PAGE

Form Approved
OMB No. 0704-0188

1. REPORT DATE	2. REPORT TYPE	3. DATES COVERED
07/14/15	Annual	15 June, 2014 to 14 June, 2015

4. TITLE AND SUBTITLE

Prevention of Blast-Related Injuries

5a. CONTRACT NUMBER
W81XWH-12-2-0038

5b. GRANT NUMBER

5c. PROGRAM ELEMENT NUMBER

6. AUTHOR(S)

Albert King, John Cavanaugh, King Yang, Liying Zhang, Xin Jin, Feng Zhu

E-Mail: king@rrb.eng.wayne.edu

5d. PROJECT NUMBER

5e. TASK NUMBER

5f. WORK UNIT NUMBER

7. PERFORMING ORGANIZATION NAME(S) AND ADDRESS(ES)
Wayne State University
5700 Cass Ave., Suite 4900
Detroit, MI 48202-3692

8. PERFORMING ORGANIZATION REPORT

9. SPONSORING / MONITORING DAGENCY NAME(S) AND ADDRESS(ES)
U.S. Army Medical Research and Materiel Command
Fort Detrick, Maryland 21702-5012

10. SPONSOR/MONITOR'S ACRONYM(S)

11. SPONSOR/MONITOR'S REPORT NUMBER(S)

12. DISTRIBUTION / AVAILABILITY STATEMENT
Approved for Public Release; Distribution Unlimited

13. SUPPLEMENTARY NOTES

14. ABSTRACT

This report covers work done on blast testing of live anesthetized swine and on unembalmed cadavers. A detailed histological study of blast-exposed swine brain showed that there was damage to both the axons and the neuron cell bodies in the form β-APP immunoreactivity and other tests, suggesting that the mechanism of injury may be different from that of blunt impact. We have also developed computer models of the swine and human brain and are in the process of validating them against the acquired experimental data. It is proposed that future research concentrate on seeking injury mechanisms to brain cells caused by a pressure wave.

15. SUBJECT TERMS
Keywords: Blast-related brain injury, Open field testing of swine and PMHS, Computer modeling of swine and human brain, brain injury mechanisms

16. SECURITY CLASSIFICATION OF:			17. LIMITATION OF ABSTRACT	18. NUMBER OF PAGES	19a. NAME OF USAMRMC RESPONSIBLE PERSON
a. REPORT	b. ABSTRACT	c. THIS PAGE			USAMRMC
U	U	U	UU	80	19b. TELEPHONE NUMBER *(include area code)*

TABLE OF CONTENTS

**

INTRODUCTION

This research project is designed to determine the cause of mild traumatic brain injury due to blast overpressure and, if possible, the human tolerance to blast overpressure. It consists of an experimental portion in which 12 swine and 6 post-mortem human subjects (PMHS) are to be exposed to blast. The experimental effort is supplemented by a computer modeling section which can extend the results of the tests to blast scenarios not easily achievable experimentally. In the second report, we reported on the results of our experimental research and of our modeling effort, In this report, we report the completion of our swine testing and results of our histological findings in the swine brains. We were only able to do one more cadaver test due to specimen unavailability and thus need an extension of the award to complete this task as well as the cadaver head modeling task that depends on the data to be collected. We will submit a final report upon completion of the tasks associated with cadaver testing.

STATEMENT OF WORK

The Statement of Work (SOW) for this project is as follows:

I.   Perform open field blast testing on 6 anesthetized minipigs to obtain biomechanical data and on 12 anesthetized minipigs to obtain pathohistological data
II.   Perform open field blast testing on 6 unembalmed post-mortem human subjects (PMHS) also known as cadavers to obtain biomechanical data
III.   Develop and validate a computer model of the pig brain simulating the effects of a blast over-pressure
IV.   Develop and validate a computer model of the human brain simulating the effects of a blast over-pressure

TASK I REPORT

Task I - Perform open field blast testing on 6 anesthetized minipigs to obtain biomechanical data and on 12 anesthetized minipigs to obtain pathohistological data (Original Proposal)

In this task, there were three separate work items:
1.   Blast testing of instrumented swine
2.   Blast testing of noninstrumented swine
3.   Brain histology to assess brain injury in blast exposed swine

1.   Blast Testing of Instrumented Swine

a)   Test Methodology

In our plan of work, we were scheduled to perform open field blast testing of 6 anesthetized swine to obtain biomechanical data of brain response due to blast overpressure. The target incident overpressures (IOP) were nominally 150 kPa (low), 300 kPa (medium) and 450 kPa (high). Swine-related instrumentation consisted of 6 intracranial pressure (ICP) sensors inserted into various regions of the brain, 2 surface pressure sensors (SP), a triaxial linear accelerometer (LA), a triaxial angular rate sensor (AS) and 4 strain gage (SG) rosettes mounted on the swine skull. Additional instrumentation consisted of a pencil transducer mounted near the head of the swine to measure the free-field IOP and two high-speed video cameras to record the blast event. One of the cameras was focused on the head of the swine and ran at 20,000 frames/second (fps). The other provided an overall view of the blast site and ran at 10,000 fps. A Dewetron 64-channel data acquisition system was used to collect data. A 1-MHz sampling rate was used for collecting SP data, 500-kHz sampling rate for ICP data, and 200-kHz sampling rate for LA, AS and SG data collection.

In 2014, we completed open field blast testing of anesthetized swine to obtain biomechanical data of brain response due to blast overpressure. The target incident overpressures (IOP) were nominally 150 kPa (low), 300 kPa (medium) and 450 kPa (high).

In order to achieve a better survival rate and to reduce the time of instrumentation, we proposed a revised sensor array for the remaining swine tests. The revised protocol was approved by IACUC of Wayne State University and by ACURO of MRMC. The new protocol involved the use of 4 intracranial pressure sensors as compared to the 5 or 6 sensors listed in the original protocol. The new sensor array is shown in Figure 1, each animal was exposed to one or two directions of blast instead of three. These changes reduced preparation time as well as time to complete the scheduled 9 blast tests without loss of data. These changes were put into effect for all the open field blast tests done in 2014. The survival rate of swine was significantly improved as all animals tested survived all the scheduled tests that lasted the whole day. Also all the tests were completed within the time limit set by ARES, Inc. Table 1 summarizes all the instrumentation used in the swine blast tests.
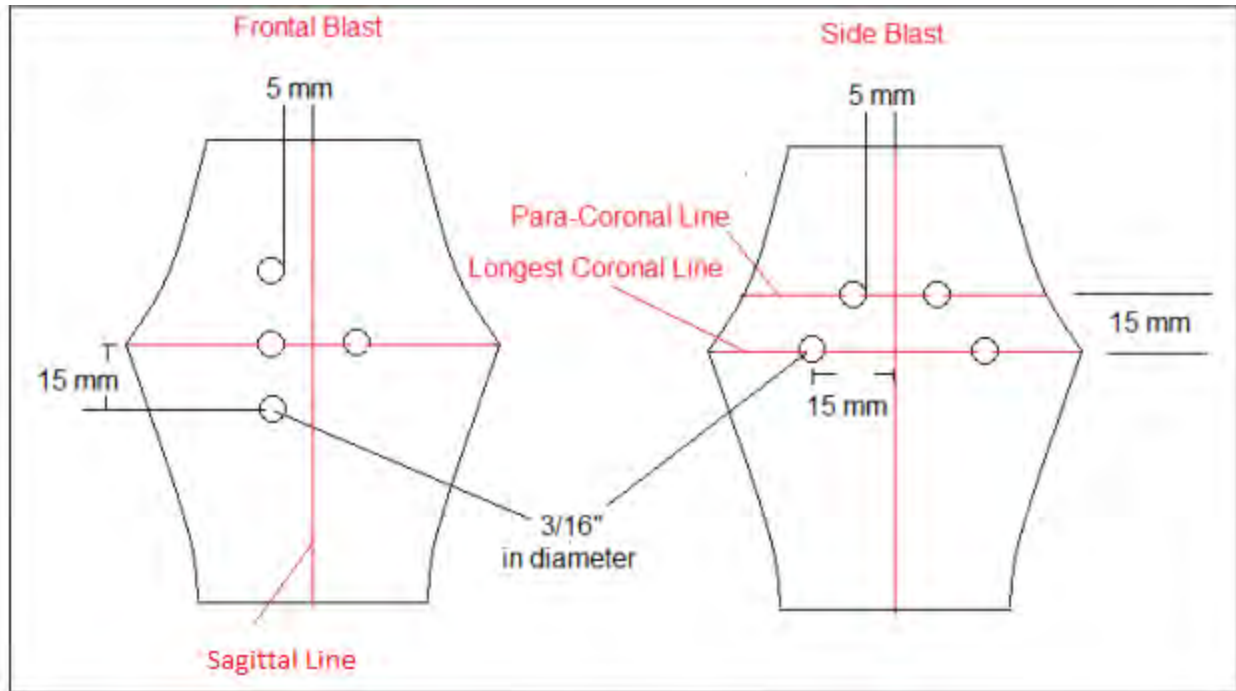
Figure 1. New layout of ICP sensor array in 2014

Based on the templates in Figure 1 pressure sensors were inserted in the brain of anesthetized swine in the climate-controlled ambulance at the ARES test site, while other preparations were being made for the blast tests. Upon completion of the insertion procedure, the animal was moved onto a sling for the blast experiment. While in the sling and before the test, strain gages were attached to the skull and a triaxial accelerometer package with a 3-D angular rate sensor was mounted on the skull on the occipital bone. The level of anesthesia was maintained and monitored by a veterinarian to ensure adequate depth of anesthesia. The preparation on site took 2 to 3 hours, including the hooking up of all transducers to the recording equipment, the set-up of two high speed cameras and verification of each channel. The IOP was monitored by a pencil transducer placed near the head of the test subject. Figure 2 shows the overview of the blast setting.

b)   Data Processing and Analysis

ICP data were filtered with a 10 KHz Butterworth low-pass filter. LA, AS and SG data were filtered with a 5 KHz Butterworth low-pass filter. All statistical analyses were performed using DIAdem 2012 software (National Instruments Corporation, Austin, TX). All the data were grouped into three incident overpressure levels according to recorded IOP by the pencil transducer located next to the swine head. The range for the nominal low level blasts (150 kPa) was between 148 kPa to 161 kPa; while that for the nominal

Figure 2. Blast experiment setting. The left photograph shows the anesthetized swine placed in a steel-covered sling hanging from a metal beam which is anchored to the ground. The arrow at "A" points to the C4 charge. The distance of the C4 explosive to the test animal was adjusted to vary the IOP. Arrow B shows the pencil pressure sensor used to record the incident pressure. Arrow C shows the head of the test animal directly facing the oncoming blast wave front. Arrow D shows the location of high-speed cameras and blast shielding. The right photograph shows the swine in a metal harness anchored to the ground and covered with a foam-lined lead shield over the torso.

medium level blasts (300 kPa) was between 218 kPa to 341 kPa; and that for the nominal high level blasts (450 kPa) was between 341 kPa to 552 kPa (Tables 1 and 2). Within each group, the pig head was oriented to the blast wave in one or two different directions: front and rear, or side. A detailed analysis was conducted on the mechanical data from frontal blasts. All the data were grouped into three incident overpressure levels according to recorded incident pressure by the pencil transducer located next to the swine head.

Frontal blast data analysis: Duration of the blast wave, which was the time the incident pressure was above ambient pressure, was determined with Diadem. Incident pressure impulse was defined as the area of the positive phase of the incident pressure wave and was obtained through integration with respect to time. Peak ICP values, positive duration time, and impulse of recorded data were determined for each blast level for statistical analysis. Mean, standard deviation and standard error were calculated for each group when the sample size was more than two. Linear regression models were constructed to predict the relative relationship between ICP readings within groups. Peak pressure rise time and rate were also captured to characterize the feature of the ICP within the brain. Resultant linear acceleration and angular rates were also calculated in each group and relationships between incident pressures and these responses were determined. ICP box plots were drawn to show the distribution of

pressure within each group, Statistical analysis was carried out on both pressure data and motion data. More specifically, one-way ANOVA test was performed on ICP data between different pressure level groups and followed by t-tests which were performed to compare readings at different levels within the same brain region.

Data from side and rear blasts were also collected and analyzed. Due to sensor malfunction and data acquisition system failures, the sample size in side and rear blast was smaller than that for frontal blast. All data were grouped into three incident overpressure levels according to the recorded incident pressure by the pencil transducer located next to the swine head for both the rear and side blasts. Linear regression models were also constructed to predict the relative relationship between ICP readings within groups. Resultant linear acceleration and angular rates were also calculated in each group and relationships between incident pressures and these responses were determined.

c)   Results

In this reporting period, we performed 30 blasts on three instrumented pigs. Combined with the 19 tests performed in 2013, a total of 49 tests were performed at different levels in different orientations.

A summary of the instrumented pig tests is listed in Table 1, with the grouping based on the previously defined nominal IOPs.

Table 1: Summary of Tests on Instrumented Pigs

	Low IOP	Medium IOP	High IOP
Front	6	7	6
Rear	6	5	5
Side	5	6	3

For each test a summary of peak values is listed below (Tables 2 and 3). Some data points were lost due to sensor malfunction and are left blank in the tables.

Table 2: Summary of Test Schedule with IOP Peak Values

Blast No.	Test No.	Level	Subject	Pencil Pressure(kPa)	Pencil Pressure(psi)	Head orientation
				7/15/2014		
1	20	Medium	swine	n/a	n/a	Front
2	21	Low	swine	142.72	20.7	Front
3	22	Low	swine	150.31	21.8	Front
4	23	Low	swine	157.89	22.9	Rear
5	24	Low	swine	148.93	21.6	Rear
6	25	Medium	swine	300.61	43.6	Rear
7	26	Medium	swine	309.57	44.9	Rear
8	27	High	swine	468.15	67.9	Rear
9	28	High	swine	551.58	80	Rear
				8/19/2014		
1	29	Low	swine	145.5	21.1	Side
2	30	Low	swine	146.9	21.3	Side
3	31	Low	swine	159.3	23.1	Side
4	32	Medium	swine	284	41.2	Side
5	33	Medium	swine	271	39.3	Side
6	34	Medium	swine	317.8	46.1	Side
7	35	Medium	swine	308.2	44.7	Side
8	36	High	swine	355.1	51.5	Side
9	37	High	swine	481.9	69.9	Side
				9/9/2014		
1	38	Low	swine	148.2	21.5	Front
2	39	Low	swine	152.37	22.1	Front
3	40	Medium	swine	285.44	41.4	Front
4	41	Medium	swine	325.43	47.2	Front
5	42	High	swine	341.29	49.5	Front
6	43	High	swine	432.3	62.7	Front
7	44	Low	swine	160.65	23.3	Rear
8	45	Low	swine	150.31	21.8	Rear
9	46	Medium	swine	317.85	46.1	Rear
10	47	High	swine	395.8	57.4	Rear
				9/23/2014		
1	48	Low	swine	148.9	21.6	Side
* 2	49	Medium	swine	297.16	43.1	Side

Table 3: Summary of Head Linear Acceleration and Angular Rate Response

Test date	Blast No.	Test ID	Incident (kPa) Pencil Pressure	Orentation	Linear Head Accelerations (g) Resultant	Angular Head Velocities (rad/s) Resultant
7/15/2014	2	21	142.7	Front	412.1	20.8
7/15/2014	3	22	150.3	Front	425.6	14.2
9/9/2014	1	38	148.2	Front	298	46.4
9/9/2014	2	39	152.37	Front	297.5	32.8
7/15/2014	1	20	284.1	Front	806	101.1
9/9/2014	3	40	285.44	Front	370.8	314.8
9/9/2014	4	41	325.43	Front	679.4	26.6
9/9/2014	5	42	341.29	Front	336.8	
9/9/2014	6	43	432.3	Front	364.1	
7/15/2014	4	23	157.9	Rear	236	15.2
7/15/2014	5	24	148.9	Rear	459	20
9/9/2014	7	44	160.65	Rear	251.8	13.8
9/9/2014	8	45	150.31	Rear	182.3	16.5
7/15/2014	6.0	25.0	300.6	Rear	328.5	38.2
7/15/2014	7	26	309.6	Rear	290.1	388.3
9/9/2014	9	46	317.85	Rear	342	32.8
7/15/2014	8	27	468.2	Rear	489.4	191.8
7/15/2014	9	28	551.6	Rear	319.7	
9/9/2014	10	47	395.8	Rear	446.7	66.7
8/19/2014	1	29	145.5	Side	179.1	19.3
8/19/2014	2	30	146.9	Side	193.9	14.1
8/19/2014	3	31	159.3	Side	241.4	12.8
9/23/2014	1	48	148.9	Side	612.1	23.4
8/19/2014	4	32	284	Side	411.2	41.6
8/19/2014	5	33	271	Side	384.4	33.3
8/19/2014	6	34	317.8	Side	516.1	33.9
8/19/2014	7	35	308.2	Side	546.7	53.9
9/23/2014	2	49	297.16	Side		
8/19/2014	8	36	355.1	Side	439.7	58.4
8/19/2014	9	37	481.9	Side		75.3

Frontal Blast Data Analysis:

Data from a total of 19 frontal blasts were available for analysis. Peak IOP, positive phase duration, and IOP impulse of each test are listed in Table 4. Peak IOP vs. impulse, shown in Figure 3 clearly indicates the 3 blast levels used in the tests. Examples of IOP and ICP curves in a frontal blast are shown in Figure 4.

Table 4: Summary of incident pressures in frontal blast tests - peak value, duration of the first positive wave and the impulse of the first positive waveform. * indicates test in which swine had already expired during testing

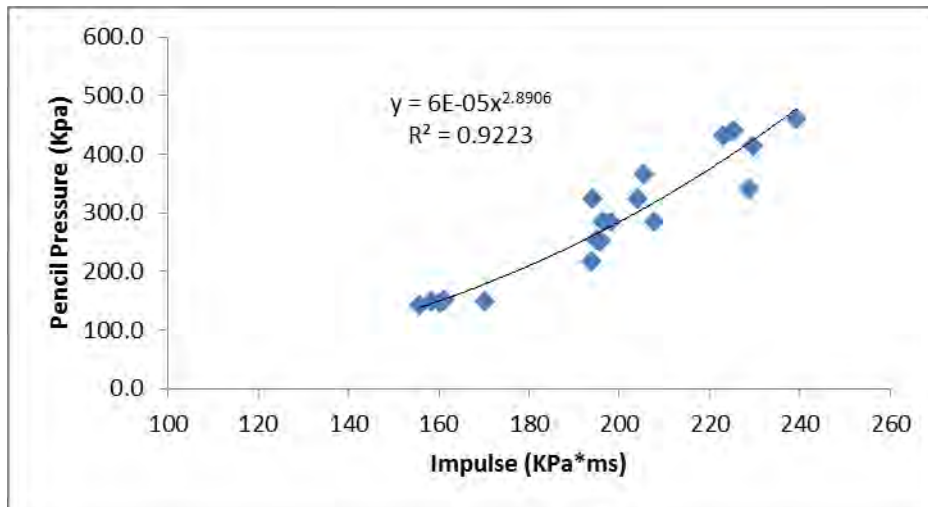| Test ID	Incident (kPa)	Duration (ms)	Incident Impulse (kPa*ms)
*1	150.3	2.80	170.3
*2	142.7	2.90	155.7
3	150.3	2.90	158.3
4	148.2	2.90	160.3
5	152.4	3.10	161.0
6	218.0	2.10	193.9
7	253.4	2.20	195.7
8	255.2	2.00	194.9
9	324.2	2.30	194.1
*10	285.5	2.30	207.7
*11	284.1	2.10	198.1
12	285.4	2.00	196.4
13	325.4	2.00	204.0
14	366.0	1.60	205.4
*15	441.3	1.70	225.2
*16	413.7	1.60	229.6
*17	460.6	1.70	239.2
*18	341.3	2.40	228.8
19	432.3	2.40	222.9

Figure 3: Correlation between the incident peak pressure and its impulse for the three different and distinct blast levels.
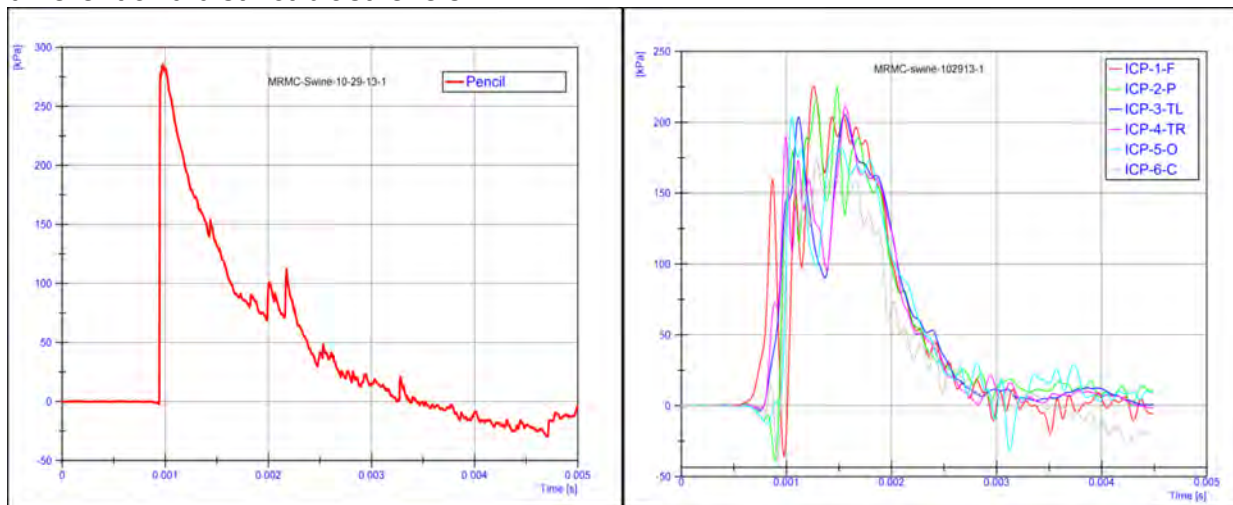

Figure 4: Pencil reading from a medium level blast (left) and the ICP results of the swine brain from the same blast. The positive phase duration of IOP is 2.30 ms, and the IOP impulse is 207.7 kPa*ms.

The relationships between IOP and ICP, LA and AS data are illustrated in Figures 5-11. With higher IOPs, ICP increased in different regions of the brain. For frontal blasts, among all the regions of the brain, ICP readings in the parietal region had the highest values at the medium and high IOP levels, as shown in Figure 5.
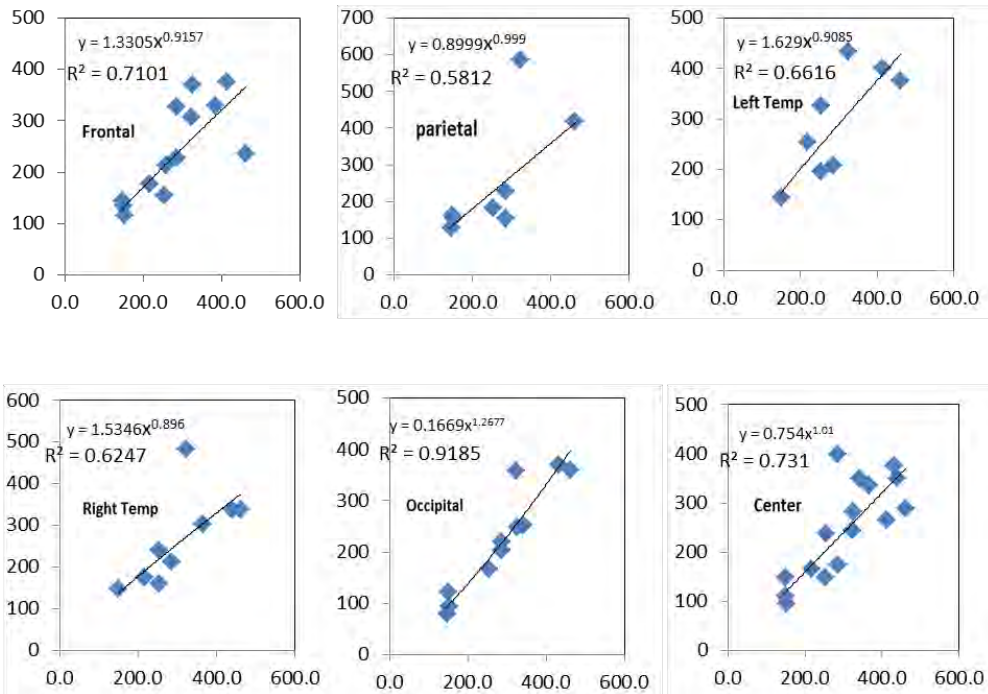
12

Figure 5: Scatter plots of ICP vs. IOP at different locations of the brain. IOP (x axis) and the ICP (y axis) are in units of kPa. Linear regression model and R^2 values are shown in each plot.

ICP readings in the central region of the brain were much lower than those in the parietal region. However, ICP readings were not significantly different from the incident readings in all blast levels. In terms of impulse, ICP impulses appeared to correlate with those of the IOP but they were not a good predictor of peak ICP. Figure 6 shows the relationship between ICP and IOP impulse.
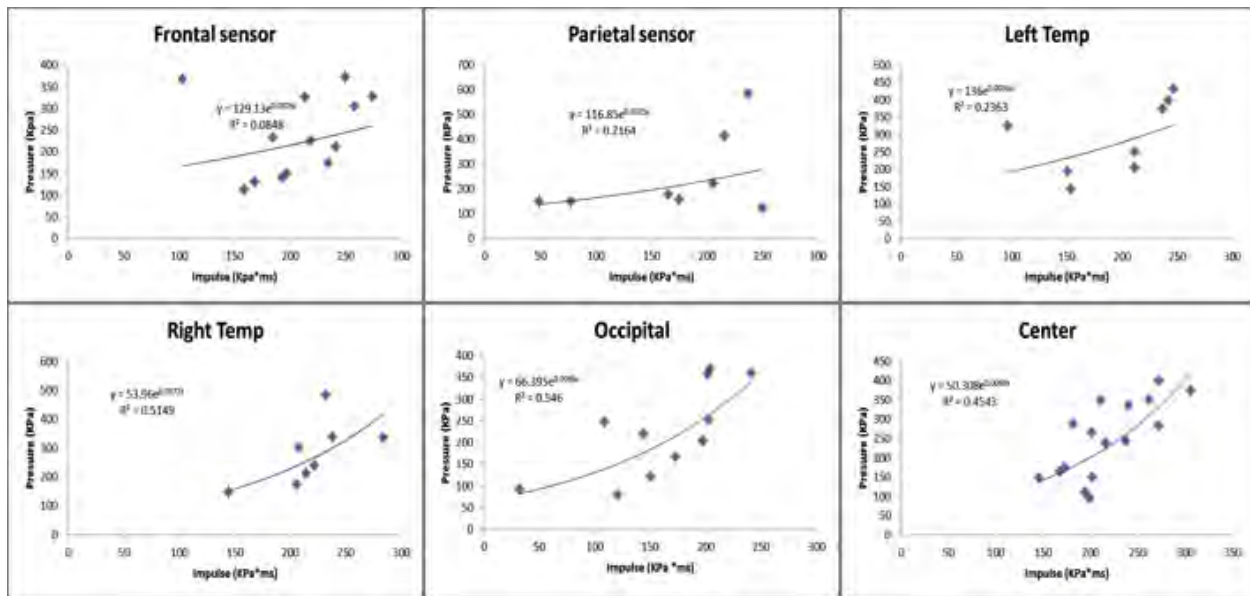
13

Figure 6: ICP impulses at different locations were correlated with corresponding IOP readings. Exponential regression gave the best R^2 value. However, impulse was not a significant predictor of peak pressure.

There was not much of a difference between peak readings at various locations in the brain (Figure 7). In the frontal, occipital and center areas of the brain, sensor readings were significantly increased at medium and high level blast groups (Figure 8 and 9).
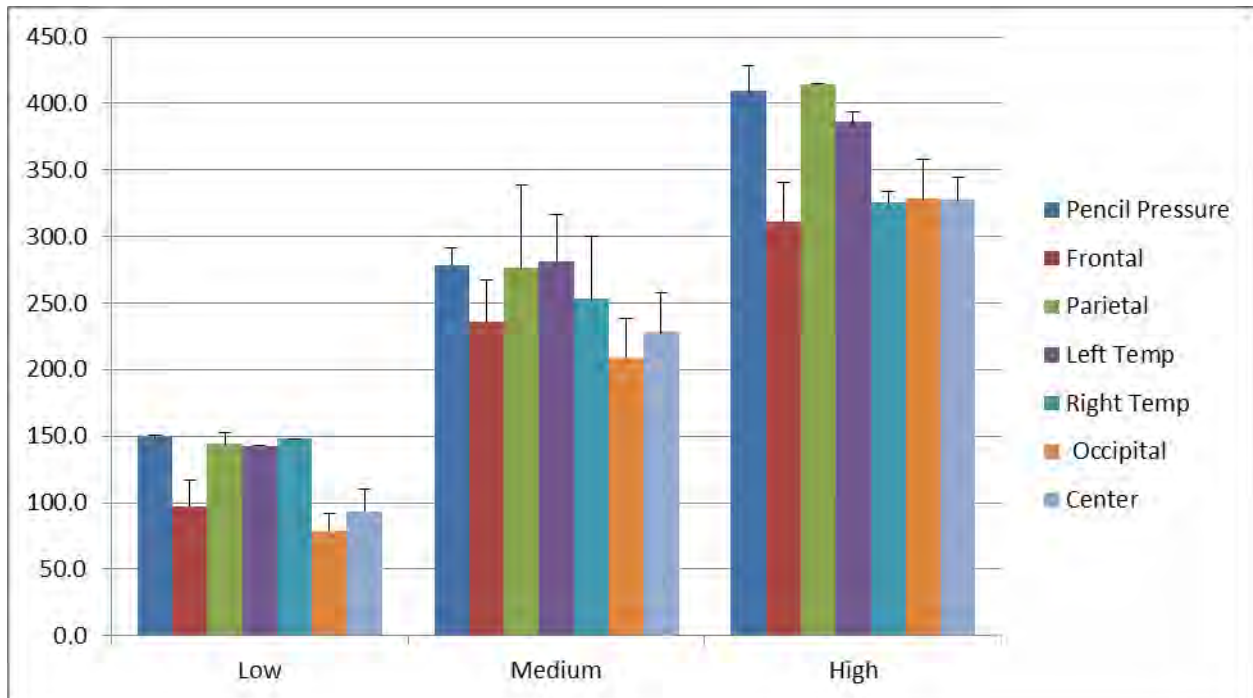
Figure 7: ICP peak readings at various brain regions at different levels of blasts. The mean values and the ±1 SD are shown. Pencil pressure (IOP) is also shown.
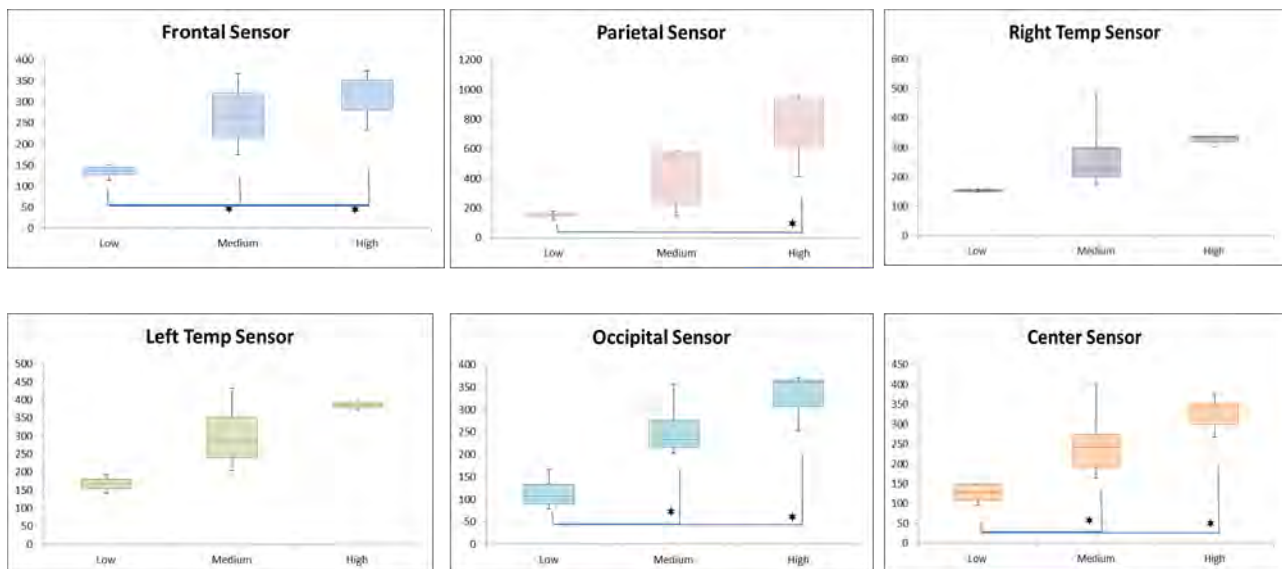

Figure 8: Box plots of ICP peak readings at different locations of the brain. One-way ANOVA was carried out on each set of readings followed by a Tukey test to indicate significant differences within each group. A black dot indicates that the difference is significant at $p<0.05$. Pressure values are in kPa.
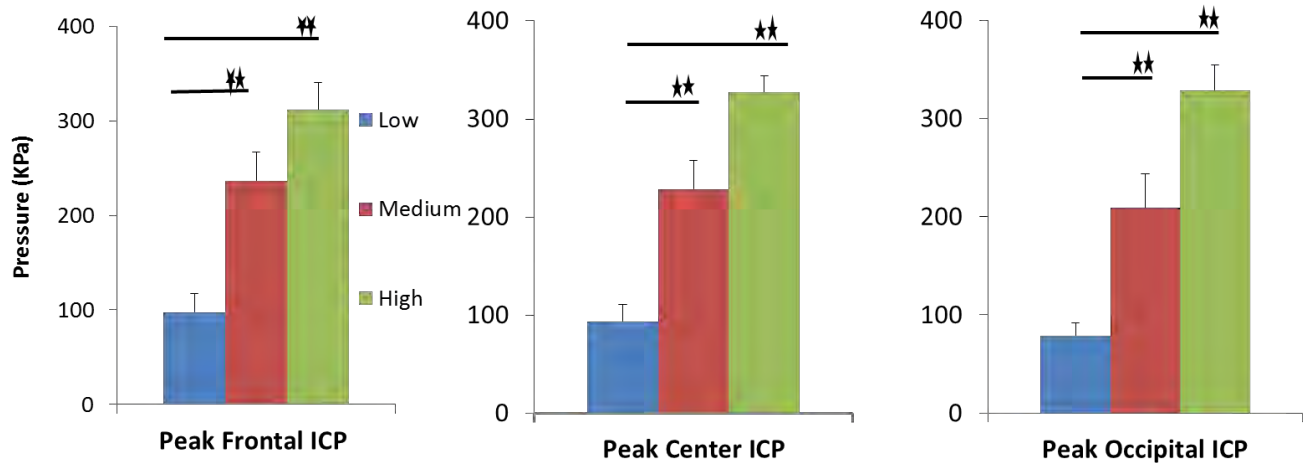
15

Figure 9: Peak ICP readings at frontal, center and occipital regions of the brain show significant increase with higher blast levels. T-tests indicate significant differences between blast levels. (** $p < 0.02$)

Maximum pressure rise rate (MPRP) increased significantly with increased IOP levels. A series of t-tests was performed between every two locations at same blast levels. However, differences between various locations of the brain within same level were not clear except frontal vs. occipital readings at the medium blast level ($p < 0.05$, Figure 10). Results at different blast levels also show that frontal, occipital, and center ICP were significantly increased between low and high blast groups. Frontal ICP also showed increase from low to medium blast group (Figure 10).
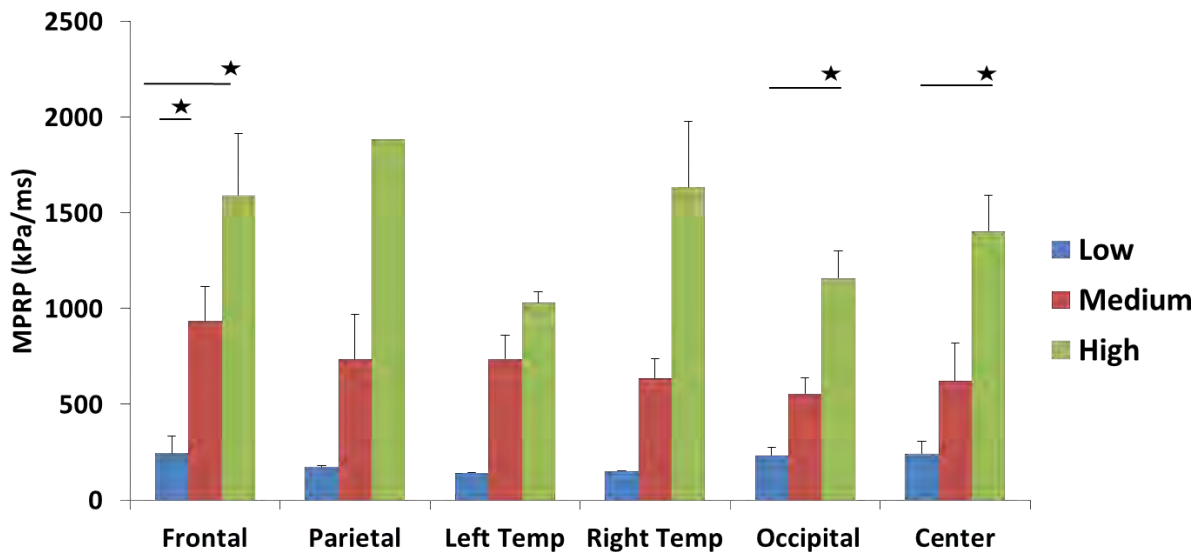

Figure 10: Maximum pressure rise rate at each ICP location. T-test was performed between blast level groups at each sensor location, *$p < 0.05$.

16

Peak resultant acceleration correlated well with peak incident overpressure as shown in Figure 11. Most of the angular velocity data were not credible at the high blast levels due to oscillation of the sensors. The durations of the linear acceleration were typically less than 3 ms, indicating there was little translational movement of the head during primary blast.
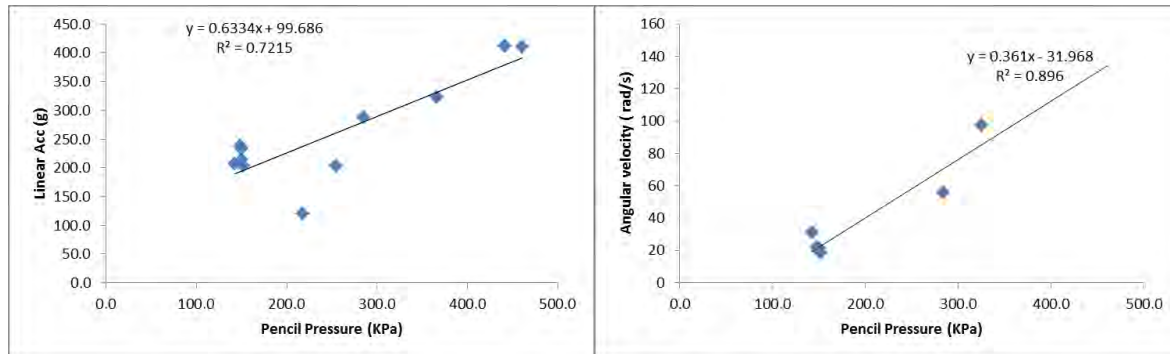

Figure 11. Head linear acceleration and angular velocity at various levels of IOP

Rear Blast Data Analysis:

In rear blasts, ICPs at different brain regions increased with increases in IOP with some exceptions at center brain region, as shown in Figure 12. ICP readings in the parietal region had the highest values among all the measured ICPs. The sensor located in this region was the closet one to the blast while frontal sensor was at the contrecoup location relative to the rear blast, but there was no evidence of a contrecoup pressure occurring there.
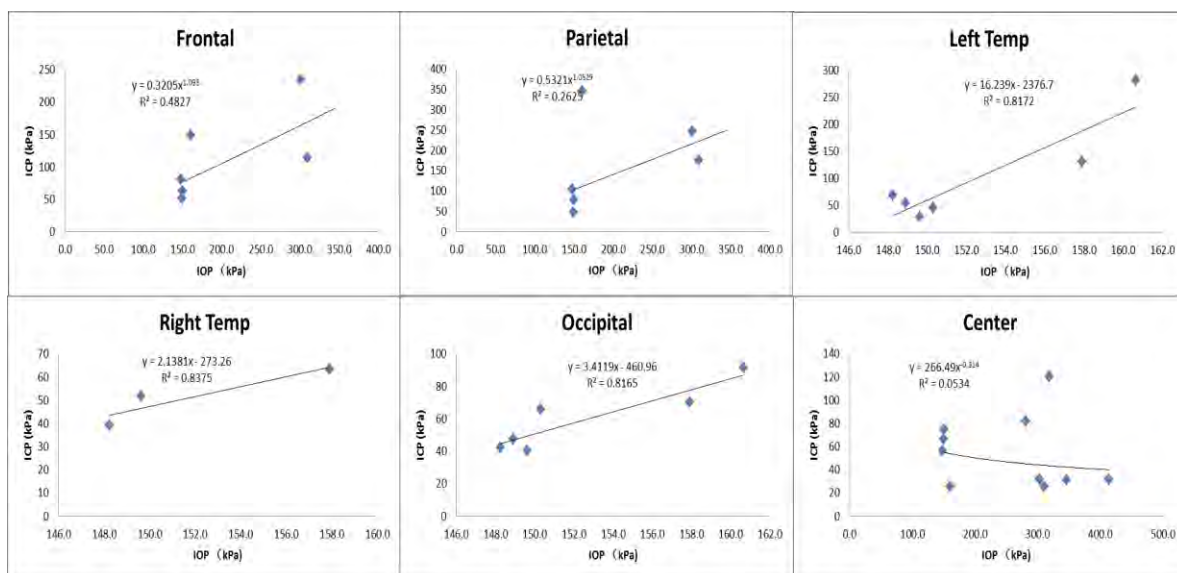

Figure 12. Scatter plots of ICP vs. IOP at different locations of the brain for rear blast tests. Linear regression model and R^2 values are shown in each plot.

17

Resultant linear head accelerations increased with increases in IOP in rear blast exposure of the head. Similar trends were also observed in resultant angular velocities of the head (Figure 13).
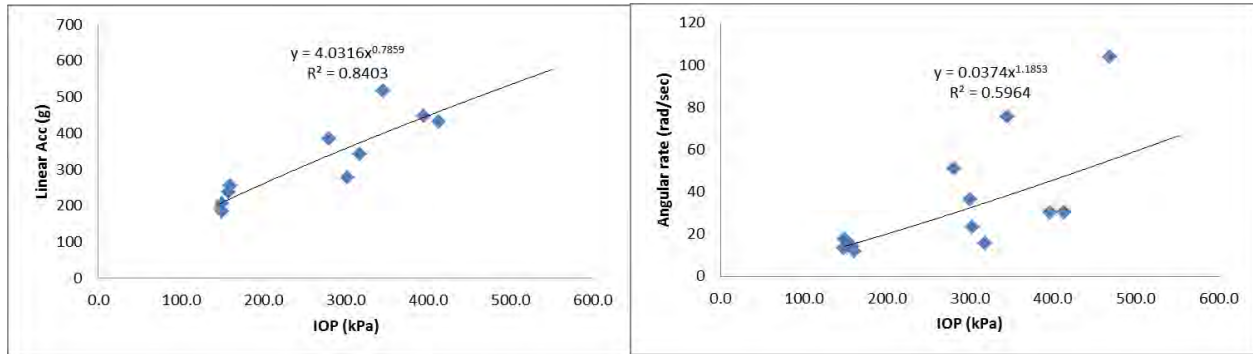

Figure 13. Scatter plots of the motion on the head in rear blasts. Resultant linear acceleration correlated well with peak IOP in a linear regression model; resultant angular velocity was minimally correlated with peak IOP in a linear regression model.

Side Blast Data Analysis:

In side blast, IOP at left temporal region is in the coup location while the sensor in the right temporal region is at the contrecoup location of the blast. There was less correlation shown between peak IOP and peak ICP data (Figure 14). In some locations of the brain, the sensor readings were significantly different from each other at the same blast level. This may be due to the changes made in the sensor arrays in 2014 and the exact cause is being investigated. Resultant linear and angular motions of the head were highly consistent with the IOP levels in side blasts (Figure 15).
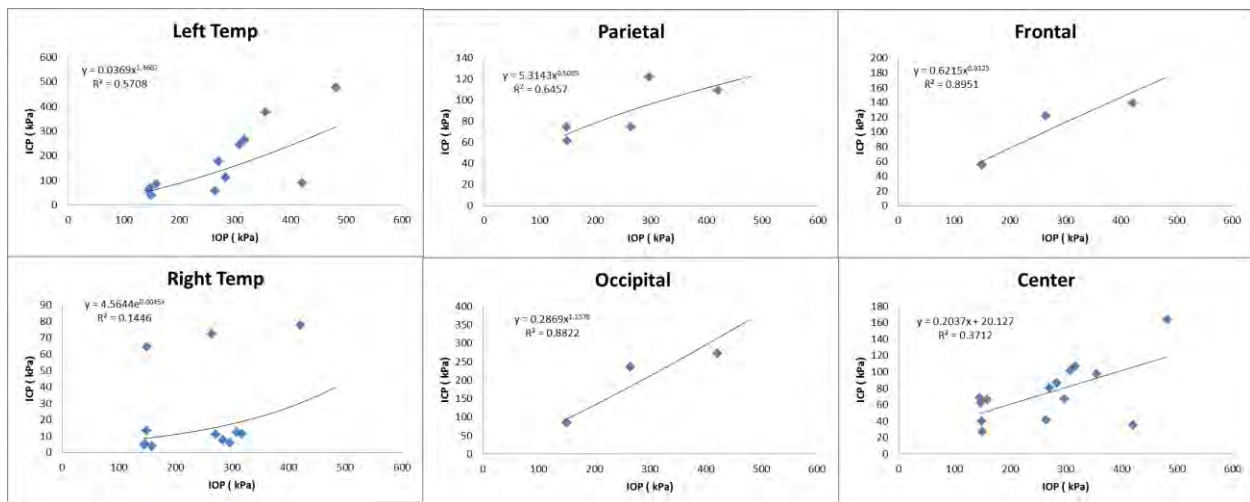

Figure 14. IOP vs. ICP at various regions of the brain in side blasts

In the left plot:
$$y = 1.0511x^{1.0604}$$
$$R^2 = 0.8672$$

In the right plot:
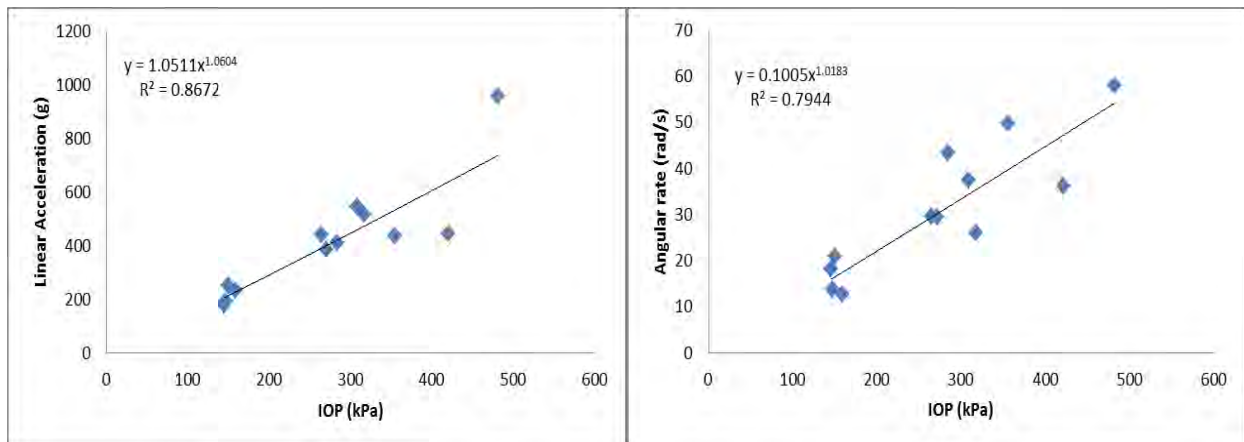$$y = 0.1005x^{1.0183}$$
$$R^2 = 0.7944$$

Figure 15. Relationship between ICP and head motion in side blasts (head linear acceleration and angular velocity) demonstrates that primary blast imparts a high acceleration to the head although the duration is short.

d.   Discussion

In this report, we provided data on ICP distribution in a live swine brain subjected to free-field blasts. The data are more detailed than what is available in the literature because we have data for blasts from three directions and have inserted multiple sensors into the brains of the animals tested.

Data in the literature on the mechanical responses of the brain due to blast are often contradictory, partly due to the lack of understanding of the physics of blast, and partly due to a wide range of experimental animals and models being used (Cernak et al, 2010, 2014). Our ICP results showed that the measured ICP was close to or lower than the IOP. This finding is consistent with some of the published experimental data. In a shock tube study by Chavko et al (2007), an optic fiber pressure sensor was used to measure ICP in a rat brain. They found that the ICP was lower than the IOP. Similarly, Shridharani et al (2012) conducted porcine blast experiments in a compressed gas shock tube, and found that the ICP was lower than the reflected pressure and also the IOP. However, there was also literature that indicated the contrary. Leonardi et al (2011) reported that the peak ICP in rats was larger than the peak IOP and suggested that the global skull flexure in the immature rats used was the source of the pressure increase.

We also noticed that the profile of ICP curves differ due to changes in blast orientation. It can be seen from Figure 15a that, in side blasts, the duration of the positive ICP is longer compared with that in frontal blasts. This finding is in agreement with the experimental results conducted on rats by Chavko et al (2007). Our rear blast ICP recordings are less consistent compared with those for frontal and side blasts. One of the reasons is that it was difficult to fully expose the occipital area of the swine to a rear

19

blast. Another reason could be sensor failures occurring during rear blast tests which were usually conducted at the end of the day.
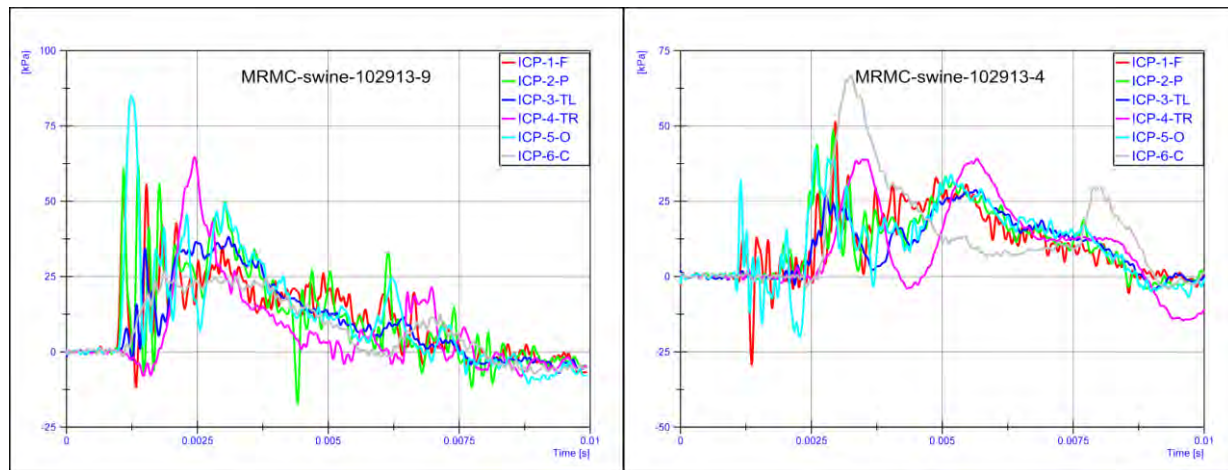

Figure 15a: Sample ICP curves in side blast (left) and rear blast (right).The units for ICP are kPa. There is a distinct difference in the ICP profile depending on the orientation of the blast.

The data reported here were acquired from live or recently deceased animals exposed to primary free-field blasts. The setup itself provided fundamental mechanical responses of blasts. The ICP and kinematic data can be used to validate computer models designed to simulate blast exposures.

Upon completion of the histological study, brain injury data will be correlated with the mechanical response data provided here, in the hope that tolerance of the porcine brain to primary blast can be established. Of course, it is still not possible to deduce human tolerance directly from these data. Scaling methods being worked on will be utilized to achieve this aim.

e.   References

Cernak, I, Noble-Haeusslein LJ (2010) Traumatic brain injury: an overview of pathobiology with emphasis on military populations. J Cereb Blood Flow Metab, **30**(2):255-66.

Cernak, I. (2014) Blast-induced neurotrauma models and their requirements. *Front Neurol. (5):128.*

Chavko, M., et al. (2007) Measurement of blast wave by a miniature fiber optic pressure transducer in the rat brain. J Neurosci Methods, 159 (2):277-281.
Shridharani, J.K., et al. (2012) *Porcine head response to blast.* Front Neurol, **3**:70.

Leonardi, A.D., et al. (2011) Intracranial pressure increases during exposure to a shock wave. J Neurotrauma, **28**(1):85-94.

2.   Blast Testing of Non-Instrumented Swine

Test Methodology

The noninstrumented swine were exposed to a single blast to assess the injuries sustained. Thus, the test methodology is as follows:

The animal was anesthetized at Wayne State University and transported in an ambulance to the test site on the day of the experiment, arriving at about 8 am, after a 90-120 minute drive from Detroit, MI to Port Clinton, OH. Anesthesia levels were maintained until it was ready for testing. The wait was due to the time needed to prepare the instrumented swine or cadaver which was to be tested alongside the non-instrumented swine. So for the first test of the day, there were generally two test subjects exposed to the same blast. In one case, the noninstrumented swine was tested alone. After the non-instrumented swine was exposed to blast, it was taken back into the ambulance and driven back to Wayne State University for observation and blood draw. It was sacrificed on the third day and the brain was removed and preserved for histological study.

The experimental protocol calls for the testing of 12 swine at two pressure levels –six at 300 kPa and 6 at 450 kPa, nominally. The protocol also included 6 sham animals which underwent the entire test protocol but were not exposed to blast. That is, the sham animals were anesthetized, transported by ambulance to Ohio where they waited for about 2 hours, put in the sling used to test blast animals for about 45 minutes, returned to the ambulance and driven back to Wayne State University for observation and blood draw. They were sacrificed on the third day and the brain was removed and preserved for histological study.

3   Brain histology to assess brain injury in blast exposed swine

During the period of June 2014 to June 2015, an additional 5 brains from high pressure blasts, 2 from medium pressure blasts and 1 from a sham animal were obtained and fixed for histology. With these new samples, the total number of brain samples is as follows: Sham = 5; Medium Pressure = 7, High Pressure= 5. Table 5 shows the test dates and pencil pressures of all the animals studied. Furthermore, blood was collected at various time points for subsequent temporal assessment of the serum for injury biomarkers. Biomarker analyses allow for additional correlations with histological outcome performed at the terminal survival point of 72 hours.

Many histological techniques were developed to assess blast induced neurotrauma on these brains. Axonal injury changes were assessed by beta amyloid precursor protein (β-APP), neurofilament light chain (NF-L) and medium chain (NF-M)

immunocytochemistry as well as by silver staining. Inflammatory response was assessed by glial fibrillary acidic protein (GFAP) and microglial (Iba1) immunocytochemistry to assess changes in the expression of astrocytes and microglia respectively. We will continue to investigate cellular injury using caspase 3 immunocytochemistry, FluoroJade C (FJ-C) and TUNEL staining and by haematoxylin eosin (H&E) staining. Additionally, the presence of hemorrhages will be assessed by Prussian blue staining.

Table 5: Details of blast and sham swine showing their test dates and the peak blast overpressures.

animal #	test date	test type	pressure level	peak filtered pencil pressure (psi)	peak filtered pencil pressure (kPa)
1	September 24, 2013	non-instrumented blast	medium	32.4	223.5
2	October 22, 2013	non-instrumented sham	sham	NA	NA
3	November 5, 2013	non-instrumented blast	medium	48.2	332.3
4	November 5, 2013	non-instrumented blast	medium	44.3	305.4
5	November 19, 2013	non-instrumented sham	sham	NA	NA
6	November 19, 2013	non-instrumented sham	sham	NA	NA
7	December 9, 2013	non-instrumented blast	medium	32.2	222.0
8	December 9, 2013	non-instrumented blast	medium	38.1	262.7
9	December 10, 2013	non-instrumented sham	sham	NA	NA
10	July 15, 2014	non-instrumented blast	medium	not recorded	not triggered
11	October 28, 2014	non-instrumented sham	sham	NA	NA
12	November 3, 2014	non-instrumented blast	high	52.2	359.9
13	November 3, 2014	non-instrumented blast	high	52.2	359.9
14	November 10, 2014	non-instrumented blast	high	58.5	403.3
15	November 10, 2014	non-instrumented blast	high	58.5	403.3
16	November 18, 2014	non-instrumented blast	medium	42.1	290.3
17	December 9, 2014	non-instrumented blast	high	50.8	350.3

Serum harvested at the stated time points (pre blast or sham test, 6 hrs, 24 hrs, 48 hrs and 72 hrs after blast or sham test) is being assessed for temporal changes in various biomarkers (S100B, NSE, MBP, NF-H, SBDP, IL-6, HSP-70).

Techniques used to section and stain the brain:

During this period, the focus of the histology was on processing brain tissue from all sham, mild and high pressure blast groups. Our focus was directed at processing at least 6 blocks from the frontal lobe of each brain. This resulted in a total of 102 blocks with 30 blocks from 5 sham swine, 42 blocks from 7 medium pressure (222-232 kPa) exposed swine and 30 blocks from 5 high pressure (290-403 kPa) exposed swine. Overall, we completed sectioning all the blocks (6 blocks/animal) from all the animals. As part of obtaining blocks of brain tissue, each brain was cut into 5 mm blocks (anterior to optic chiasm) using the custom made brain matrix from Zivic Instruments as shown in Figure 16. These blocks (Figure 17) were further cut into 35-40 µm thick frozen sections and collected in multi-well plates. 48 sections from each block were collected (Figure 18) which resulted in 4896 sections thus far from 6 blocks/animal from all the 17 animals (Table 6). Then, two representative sections from each block were used to perform different stains to assess injury changes. Astrocytic and microglial expression changes were assessed by incubating sections in antibody solutions against glial fibrillary acidic protein (GFAP) and ionized calcium-binding adapter molecule 1,

respectively. Axonal injury was assessed by incubating sections in antibody solutions against neuroflilament light chain (NF-L), neurofilament medium chain (NF-M) and also against beta amyloid precursor protein (β-APP). Axonal injury was also assessed by a silver impregnation technique.
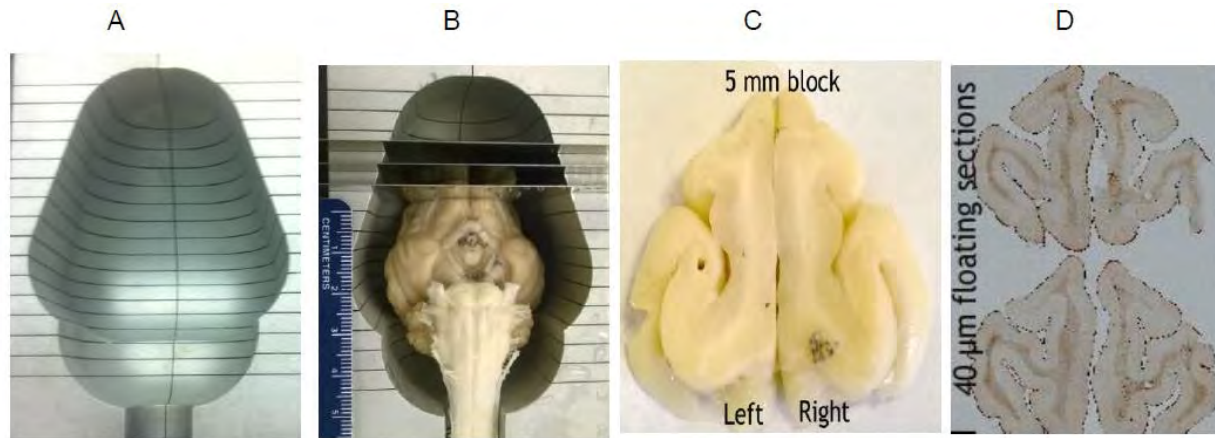

Figure 16. A. Top view of the brain matrix mold. B. The mold with a swine brain in it and with blades positioned to obtain a block. C. A representative 5–mm block obtained from the brain. D. A representative 40-µm thick section

Figure 17. A representative view of the 6 blocks obtained from a swine brain to show the anterior posterior aspect of the tissue processing performed thus far. The blocks encompass frontal cortical region and the underlying white matter
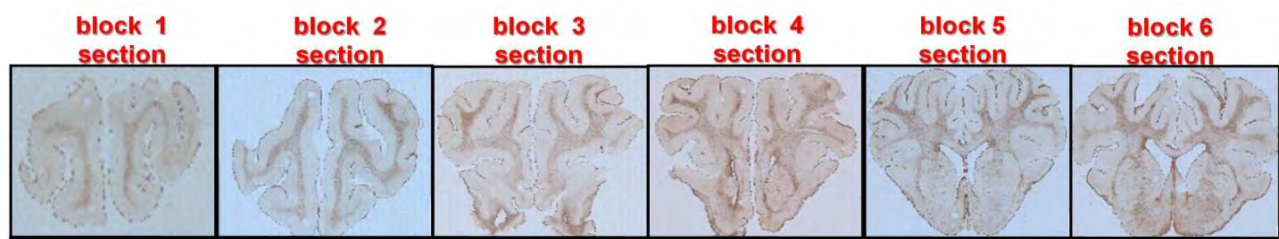

Figure 18. A series of panoramic images of sections obtained from the corresponding blocks shown in the above Figure 17. Sections from each block were stained to assess various injury markers.

Table 6. The number of blocks and sections obtained for each group as part of this study thus far.

Group	Blocks/animal	# of blocks/group	#of sections per animal/group
Sham (n=5)	6/animal	30	288/1440
Medium pressure (n=7)	6/animal	42	288/2016
High pressure (n=5)	6/animal	30	288/1440

Assessment of axonal injury by β-APP immunohistochemistry:

Using the standardized β-APP immunostaining technique described in previous quarterly reports, we continued with staining sections from all 6 blocks of all the animals to assess axonal injury. Thus far, we completed β-APP staining in 12 sections encompassing the six blocks from each animal resulting in a total of 204 sections from all the animals. Sections were incubated in antibodies raised against β-APP (Cat # 51-2700, Life Technologies, Grand Island, NY) and processed by routine avidin biotin peroxidase method. The presence of neuronal injury as evidenced by β-APP reactive zones was quantified from one section of each block from sham (n= 5 animals x 6 blocks per animals = 30 total sections), medium pressure (n=7 animals x6 blocks per animal = 42 total sections) and high pressure (n= 4 animals x 6 blocks = 24 total sections) groups. In the grey matter, an immunoreactive zone was defined as the region encompassing intense β-APP-reactive cell bodies (Figure19) that was observed in various cortical layers as well as in the subpial region. In the white matter, immunoreactive zones were defined as aggregates of intense β-APP-reactive axon-like processes, individual retraction balls, axonal swellings, axons with multiple beaded profiles or intensely stained stellate-like cells. For quantification, each section (encompassing left and right hemispheres) was viewed under a light microscope (Leica DMLB, Leica Microsystems Ltd, Heerburg, Switzerland) at 5x magnification for the presence or absence of an immunoreactive zone by a blinded investigator and the total number of immunoreactive zones for each section were recorded. The number of β-APP zones was significantly higher in the high-pressure brain samples compared to samples from medium pressure and sham sections (Figure19). One striking observation is the presence of patches of β-APP reactive zones both in the white and grey matter. Immunoreactive zones in the grey matter were observed in various cortical layers characterized by 1-3 intensely stained cell bodies with plaque-like deposits with the extended processes of the cell bodies. These immunoreactive zones were also observed in the sub-pial regions of the cortex (Figure 20 high pressure).   The

immunoreactive zones in the white matter were associated with stellate-like cells with their dark stained processes surrounded by retraction balls and axons showing signs of swellings. Other components of β-APP immunoreactive zones in the white matter regions were the presence of axons undergoing injury changes. These injury changes were in the form of single or multiple axonal swellings, swollen axons with terminal retraction balls and retraction balls with or without tail-like profiles. These axonal injury profiles were particularly predominant in the sub-cortical coronal radiations ending in various sulci, more so in the dorsal aspect of the cerebral hemispheres. Other areas that also showed injured axons were the internal capsule, white matter bundles of the striatum, and white matter fibers near the vomeronasal organ in the most frontal sections. Occasionally, axonal injury was also observed in the periventricular white matter tracts and corpus callosum.

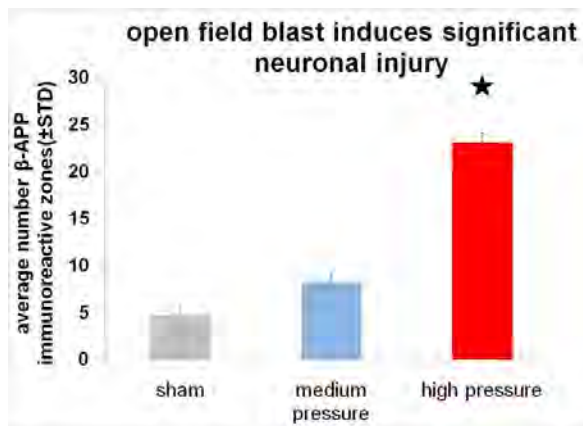Figure 19. Histogram showing the extent of β-APP immunoreactive zones in sections from sham, medium pressure and high pressure groups. The number of immunoreactive zones was significantly higher in the high pressure group ($p<0.05$) compared to those in the medium pressure group.
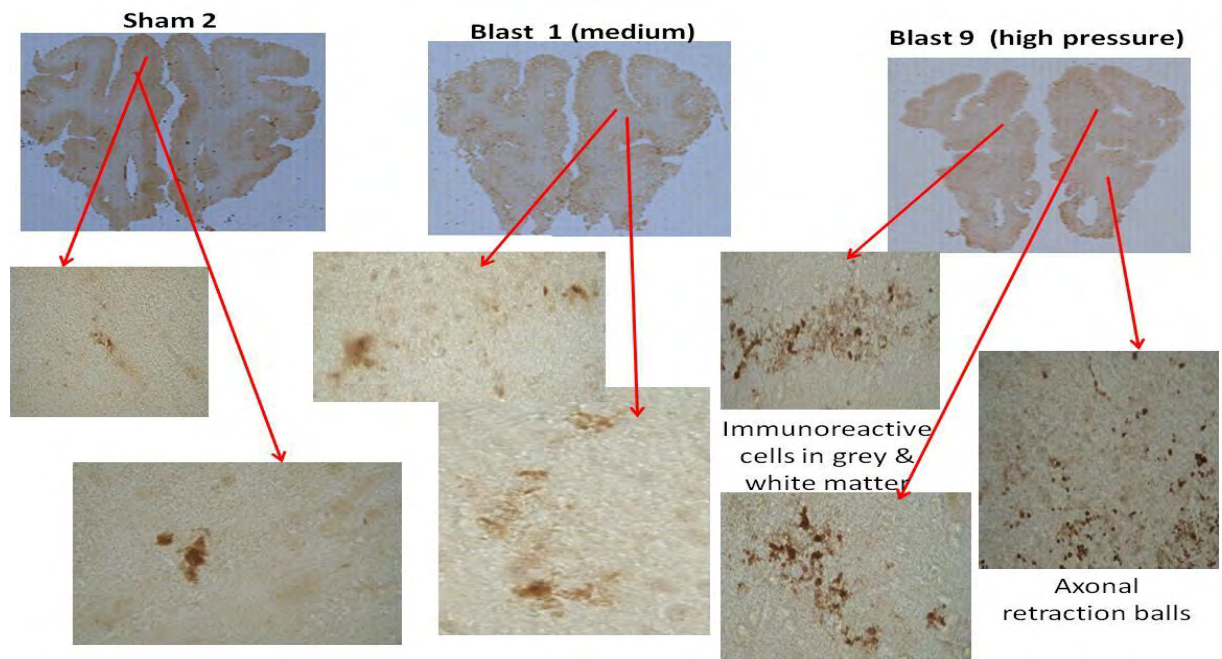

Figure 20. Images showing the extent of β-APP immunoreactive zones in representative sections from the three groups.

<u>Assessment of axonal injury by NF-L and NF-M (RMO-14) immunohistochemistry and immunostaining</u>:

Axonal injury changes in all brain samples were also investigated by neurofilament light (NF-L) chain and medium chain (NF-M) immunohistochemistry. For NF-L, we completed staining in 12 sections encompassing the six blocks from each animal resulting in a total of 204 sections from all the animals. Sections were incubated in antibodies raised against NF-L (Cat#AB9568; Millipore, Temecula CA). NF-M staining was performed in 3 sections each from blocks 2, 4 and 6, thus resulting in a total of 15 sections (3 sections from each block/animal x 5 animals) for sham, 21 sections for medium pressure (3 sections from each block/animal x 7 animals) and a total of 15 sections (3 sections from each block/animal x 5 animals) for high pressure. All the sections were incubated in neurofilament-medium RMO-14 antibodies (cat # 34-1000, Invitrogen, Camarillo, CA, 1:750) that were previously shown to reveal neurofilament compaction**.** Immunostaining was completed by routine avidin biotin peroxidase method. It is well established that the pathology of traumatic axonal injury involves distinct injury processes, neurofilament compaction (NFC) and impaired axoplasmic transport (IAT)[1]. In rat blunt trauma studies NFC was evidenced by immunoreactive axons that were thin, elongated and sometimes with vacuolations as revealed by RMO14 antibodies that target areas of compaction[1]. On the other hand, IAT is routinely visualized by using beta amyloid precursor protein immunostaining[1,2]. In addition to immunohistochemical staining, we also stained representative sections with a silver impregnation technique. For silver staining, we completed staining in 3 representative sections from three blocks each animal resulting in a total of 51 sections from all the animals.

In sections from medium and high pressure although NF-L reactive axons with uniform caliber and well-stained axonal core were observed, a population of large caliber axons with altered morphology were also observed (Figure 21A-C). These axons tended to have membrane boundaries that appeared to be disrupted in the form of semilunar empty space or sometimes with filamentous projections originating from their membranes. Besides, some of the large caliber axons appeared to be swollen and at times with the presence of vacuoles in their axonal core. In addition, some axons with terminal retraction bulbs appearing as clubs were also observed. The location of the observed changes was predominantly the sub-cortical white matter tracts. In the corpus callosum, no such prominent observations could be made considering the predominant nature of small fiber axons in its population. Qualitatively, in sections from sham animals, NF-L reactive axons running for extended lengths in the white matter tracts were observed. These axons appeared to have uniform caliber with well stained NF-L reactive core (Figure 21D).

A preliminary analysis of axonal injury changes assessed by NF-M immuno-histochemistry revealed putative RMO-14 immunoreactive axons that appeared to be linear with occasional swollen regions (arrow) and also axons with putative vacuolations (Figure 22). Preliminary analysis of silver stained sections revealed putative signs of

axonal injury in blast exposed sections. Sham section appeared to have normal looking sections with occasional axons showing signs of injury. A detailed analysis of silver stained sections is still ongoing.
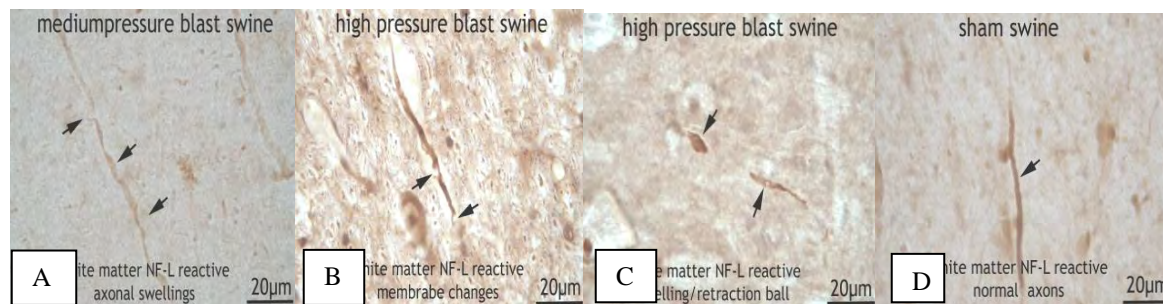

Figure 21. NF-L immunostaining showing injured-like and normal looking axons in blast and sham brain sections.
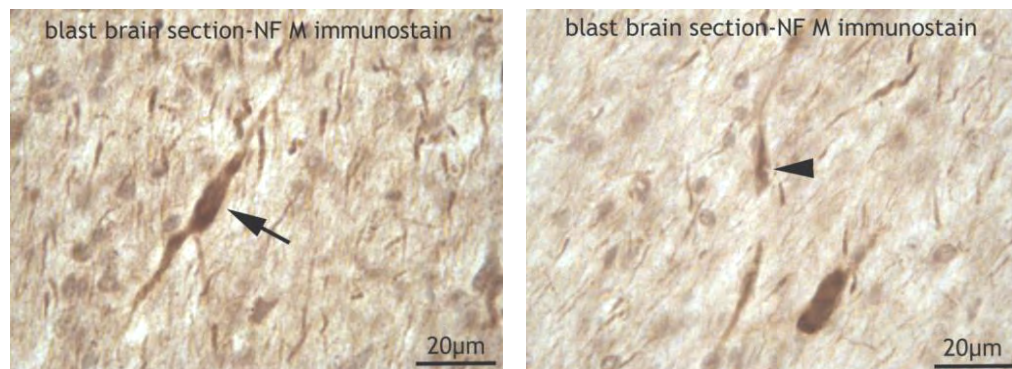

Figure 22. Blast brain sections showing putative neurofilament compaction (NFC) as evidenced by RMO14 immunoreactive axonal swellings (arrow) and areas with vacuolations (arrow head).

Assessment of astroglial changes following open field blast exposure

Using the standardized GFAP immunostaining technique described in previous quarterly reports, we continued with staining sections from all of the 6 blocks of all the animals to assess astrocyte proliferation changes in all brain samples. Thus far, we have completed astrocyte staining in 12 sections encompassing the six blocks from each animal resulting in a total of 204 sections from all the animals. For assessing astrocyte reactivity changes, representative sections were incubated in solution containing antibodies against glial fibrillary acidic protein (GFAP for identifying astrocytes, cat # NE1015, Calbiochem, La Jolla, CA; 1:5000). Sections were incubated in antibodies raised against glial fibrillary acidic protein (GFAP) (Cat # 51-2700, Life Technologies, Grand Island, NY) and processed by routine avidin biotin peroxidase method.

For quantifying the number of astrocytes and microglia in blast and sham groups in a blinded fashion, a x50 composite panoramic image from two sections each per block per stain (sham n= 32 sections: blocks 1-4; medium pressure n= 40 sections: blocks 1-4; high pressure n= 18 sections: blocks 1-3) was taken using OASIS software (Objective Imaging Inc, Kansasville, WI 53139). These panoramic images were further used in guiding the location to obtain x10 images, which in turn were used for the quantification. For this purpose, using a measurement tool in the Surveyor Software, the average length of the white matter track was determined for each corresponding panoramic image. Then representative x100 images were taken at equidistant points (each point approximately 5 mm apart) throughout the white matter, thereby fixing 5 specific points along the track in each hemisphere for each section. This allows for each section to be imaged in the same location given a fixed starting point to measure from. For counting purposes, each image was inverted (Figure 24) using the invert option in ImageJ software and the number of astrocytes was counted using the cell counter function in ImageJ. The GFAP staining was predominantly found in the white matter tracts. Thus representative images (x100 magnification) spaced approximately 5 mm apart encompassing the white matter regions were obtained to count the number of astrocytes in each image (10 images per section; 120 images for six blocks per animal; 2040 images for all animals).

A significantly higher number of GFAP reactive astrocytes (Figure 23 histogram) in sections from the high pressure (Figure 24A) group were observed compared to sections exposed to mild pressure (Figure 24B) and sham (Figure 24C) conditions. Sections from the medium pressure group also showed an increased number of
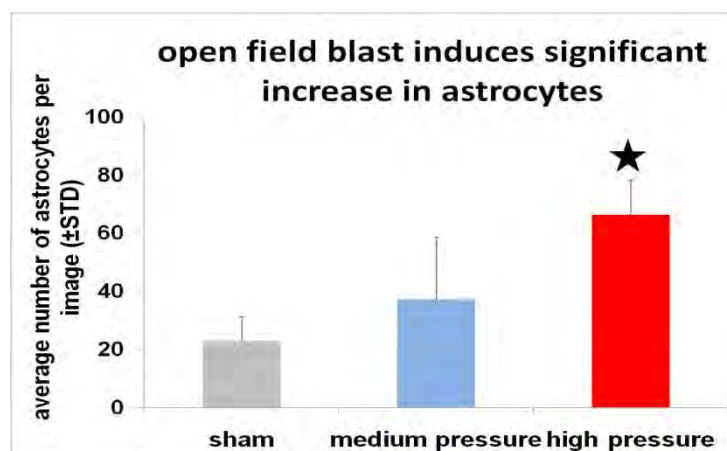

Figure 23: Histogram showing the number of astrocytes per image from sham, medium pressure and high pressure blast groups. The number of astrocytes was significantly high in sections from high pressure group.

astrocytes albeit at insignificant levels. Astrocytes in blast group tended to be intensely stained by GFAP with numerous processes. Besides, astrocytes in the blast group appeared to be more prominent with enlarged cell bodies (Figure 24). In the cortex, the astrocytes were almost exclusively localized to the white matter tracts highlighting them as distinct tracts   and thus images were exclusively obtained from the white matter tracts for the quantification purposes. Astrocytes were also observed in sub-pial cortical layer and sporadically in other cortical areas.
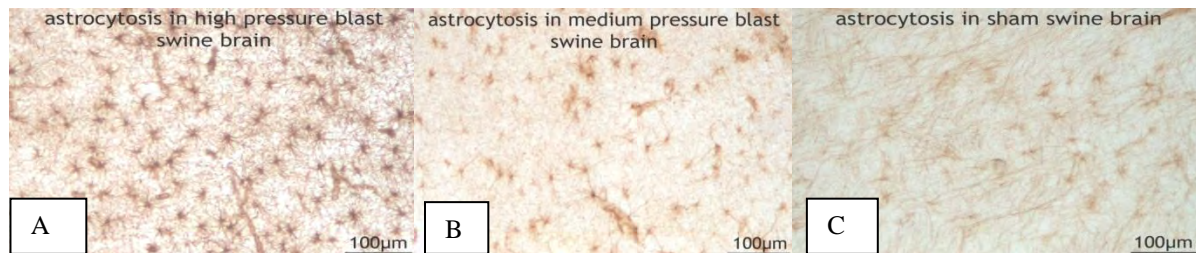

Figure 24 shows the representative GFAP images from (A) the high pressure, (B) medium pressure and (C) sham group.

Assessment of microglial changes following open field blast exposure

We have previously reported the development of a reliable staining technique to assess activation of microglia using rabbit anti Iba1 (ionized calcium-binding adapter molecule 1) antibody (cat # 019-19741, Wako Chemicals, Richmond, VA; 1:20000). Thus far, we completed microglial staining in 12 sections encompassing the six blocks from each animal resulting in a total of 204 sections from all the animals. Observation of these sections under light microscope revealed well stained microglia in both blast and sham exposed swine sections. For preliminary quantification purposes, five representative images (Figure 25) per hemisphere from both grey and white matter regions were obtained (sham n= 32 sections; medium pressure n= 44 sections; from blocks 1 thru 4). Then the total number of microglia in each were counted by the cell counter function in ImageJ. Our initial results indicate significant microglial counts in blast exposed brain sections compared to sham brain sections (Figure 25). These results support microglial activation following exposure to blast overpressure. Furthermore, considering the known role of microglia in the release of inflammatory mediators, microglial activation following blast exposure may be one of the initial cellular changes that contribute to the ensuing inflammatory and associated degenerative changes following open field blast exposure.
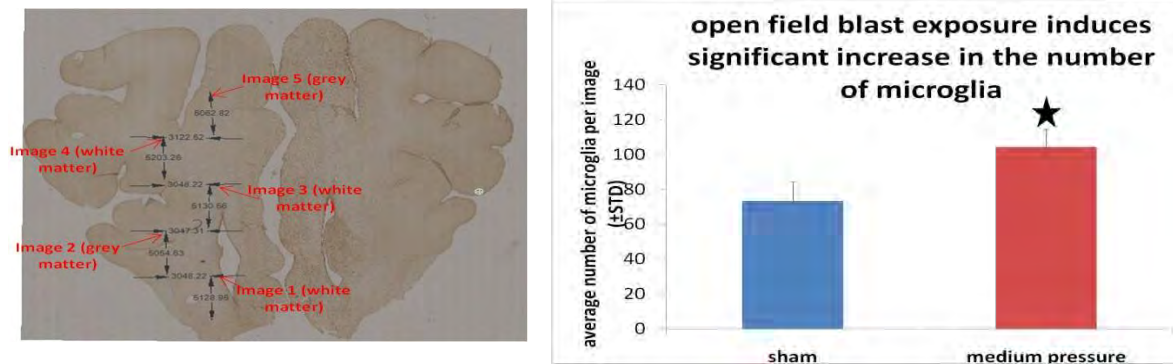
Figure 25. Image showing a methodology to take representative images of grey and white matter regions to quantify microglia. Histogram shows that a significantly higher number of microglia were observed in sections from medium pressure compared to sham

Development of a staining technique to assess apoptosis

Our initial efforts to assess apoptosis following open field blast were directed at staining 40 μm brain sections from blast and sham brains by incubating them in anti-Cleaved - Caspase-3 (Asp175) antibody and further incubation in an appropriate secondary antibody followed by routine avidin biotin peroxidase technique. These trials are ongoing. We also undertook dual labeling of apoptotic cells by immunofluorescence. As part of this double label immunofluorescence staining technique, representative sections were incubated in anti-Cleaved-Caspase-3 antibody and visualized by secondary antibodies tagged with Dylight 488 (green color). The sections were then counterstained with DAPI (blue color) to visualize nuclei. In the attached image taken from a white matter region, Cleaved Caspase-3 antibodies were tagged with Dylight 488 (green color, Figure 26A) and counterstained with DAPI (blue color, Figure 26B). In figure A, only a limited number of cells stained by Cleaved Caspase3 could be seen with a large number of DAPI stained nuclei (Figure 26B). Figure 26A+B shows the specific co-localization of Cleaved-Caspase 3 in DAPI nuclei as evident in this merged image from a representative medium blast section. Our current efforts are directed at continuing with routine immunohistochemistry and double label immunofluorescence staining to assess apoptosis following open field blast exposure.
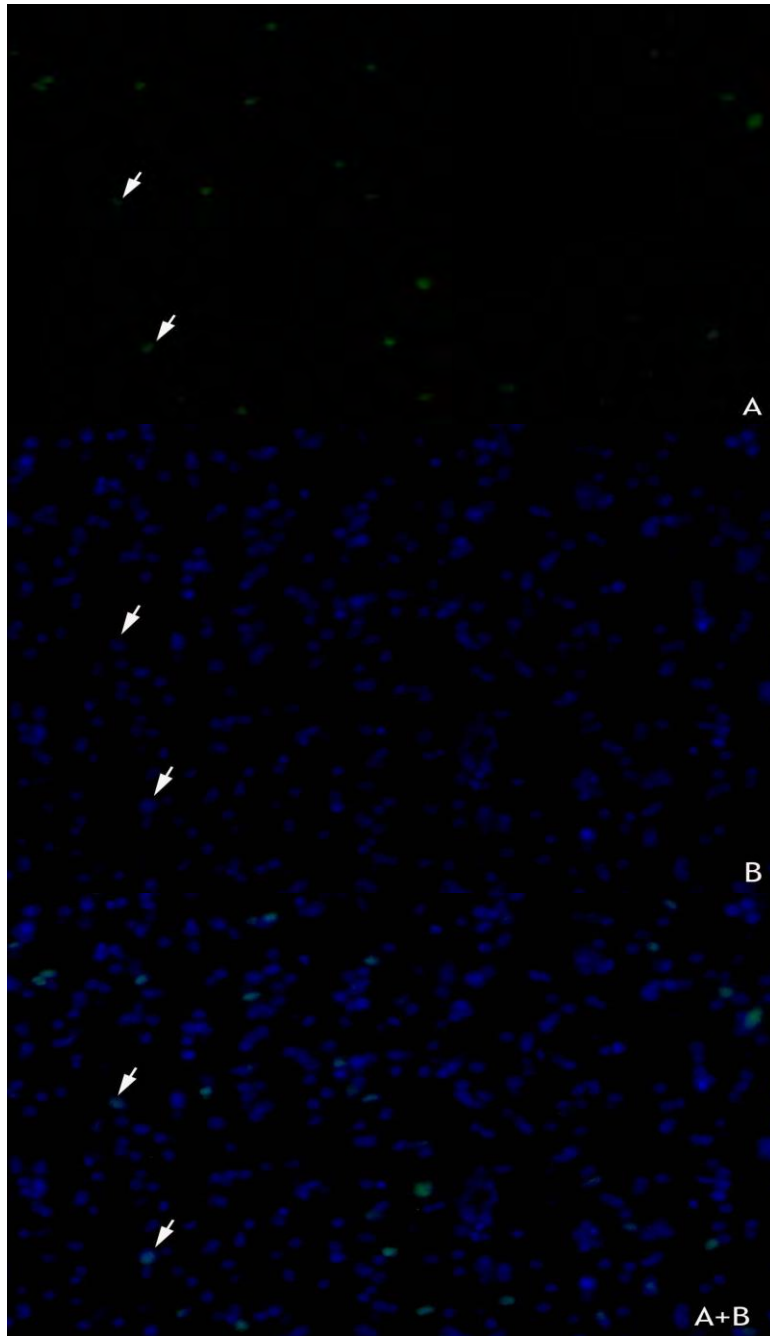
Figure 26 shows representative images of Cleaved Caspase-3 staining (green stained neurons in A) counter stained by DAPI (blue stain in B) with co-localization (arrows in A+B).

Development of a staining technique to assess cell injury using Fluoro-Jade C and cresyl violet

A preliminary staining of representative brain sections from 1 blast and 1 sham animal by Fluoro-Jade C was performed. Fluoro-Jade C is a sensitive fluorescent staining technique to visualize injured neurons. Free floating sections were immersed in 100% ethyl alcohol for 3 minutes followed by a 1 minute change in 70% alcohol and a 1 minute change in distilled water. The sections were then transferred to a solution of 0.06% potassium permanganate for 15 minutes and were gently shaken on a rotating platform. The sections were rinsed for 1 minute in distilled water and were then incubated in Fluoro-Jade C solution (0.0001%) for 30 minutes. The sections were then rinsed with three 1 minute changes of distilled water, mounted on a slide and coverslipped with D.P.X. Figure 27 shows Fluoro-Jade C labeled neurons, indicated by arrows. Current efforts are directed at optimizing this staining technique and implementing this method by using sections from all the blast (n=12) and sham animals (n=5). Furthermore, a preliminary cresyl violet staining was performed on representative sections (Figure 28). This staining technique will be used in conjunction with FJC and Cleaved Caspase to compare cellular injury between blast and sham sections.
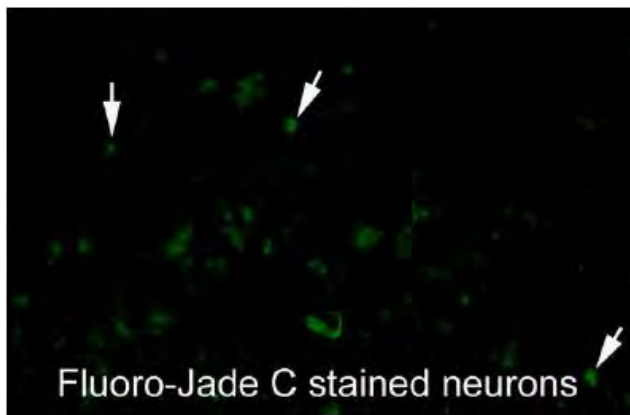
Figure 27. This is a representative area showing cortical neurons stained by FJC staining
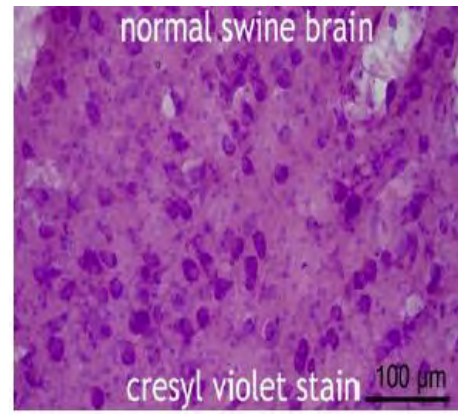
Figure 28. This is a cresyl violet stained representative area showing cortical neurons in a normal swine brain

Serum analysis for injury markers

During this period, we also performed an ELISA analysis of serum samples from 5 sham, 7 medium blast and 5 high pressure blast tests. The serum samples were collected before sham or blast testing and at 6 hrs, 24 hrs, 48 hrs and 72 hrs after blast or sham procedures. They were tested for changes in the expression of phosphorylated neurofilament heavy chain (pNF-H Elisa Kit, Encor Biotechnology, Gainesville, FL), glial fibrillary acidic protein (GFAP: cat#NS830, EMD Millipore, Billerica, MA) and interleukin-6 (IL-6: ESIL6, Life Technologies, Carlsbad, CA) as potential candidates of serum markers of blast injury. ELISA data from the three markers were compared for

statistical significance using generalized estimating equations. Baseline biomarker data were entered as a covariate to address possible baseline imbalance. Of the three biomarkers analyzed, there was some evidence of higher GFAP in the severe blast group than the sham group (p = 0.08). No apparent difference in GFAP was found between sham and medium pressure group. No significant changes were observed with regard to pNF-H and IL-6 serum levels.

Discussion:

To the best of our knowledge, our study is the first of its kind to attempt to address the fundamental question whether an open field blast exposure causes injury in the gyrencephalic brain. Although there were other studies that attempted to address the same question in a gyrencephalic model, animals in those studies were exposed to a simulated open field blast in a shock tube [3-5] unlike the true free field nature of our set-up. Blast durations in a shock tube tend to be longer than those in an open field blast. A previous study that performed open field exposure by positioning the animal on a steel shelf mounted to the concrete wall of the bunker nevertheless studied only physiological parameters namely; respiration, circulation and cortical activity but not histological analyses of the brain for injury[6].

Based on the observations made thus far, we propose that open field blast exposure causes neuronal injury as well as an increase in the number of astrocytes and microglia as early as three days after blast. These injury changes can continue to manifest and can extend to more chronic time periods as supported by the findings from Lanerolle et al who studied changes 2 weeks after blast in swine[3]. Neuronal injury was strikingly observed in the form of beta amyloid immunoreactive cell bodies, stellate cells and axons undergoing degenerative changes in both the white and grey matter regions, more prominently in the high pressure group. The presence of β-APP reactive neuronal injury especially in the frontal cortical region may have wide clinical implications. The microscopic nature of these changes may not allow them to be detected either by routine or advanced radiological assessments and may render diagnosis of blast related pathology even more difficult. These neuronal injury changes in the grey matter that appeared as intensely stained regions in and around cell bodies are reminiscent of Amyloid β reactive staining in Alzheimer's disease (AD). Immunoreactive zones in grey matter may suggest accumulation of β-APP in the cell bodies that may be related to impaired axoplasmic transport and its ultimate release into the surrounding extracellular matrix. This, in turn, can trigger neurotoxicity, presuming that it breaks down into the smaller amyloid beta fragments, Further validation of this process is needed. For that matter, an increased cytoplasmic β-APP staining in the perikarya following traumatic brain injury was also previously reported[7,8]. Additionally, up-regulation of β-APP in cells including Purkinje cells and hippocampal neurons was also observed in a rodent model of cranial blast[9]. Furthermore, some of the beta amyloid stained regions in the white matter resembled glial cells with projections, which may suggest a breakdown of amyloid precursor protein and its uptake by the microglial cells as a way of clearance.

This is further supported by the increase in the number of microglia in both the grey and white matter regions of sections from blast exposure group compared to sham. The β-APP reactive axonal profiles, more prominently in the high pressure group, were observed in all sections encompassing the prefrontal and frontal sub cortical regions. They were observed predominantly in the dorsal sub cortical white matter structures, which may entail wider clinical implications. Our study further supports axonal injury changes in the cortical white matter tracts using NF-L and NF-M immunohistochemistry. Axonal injury changes evidenced by NF-L immunoreactive swollen profiles, with vacuolations and club like terminations were observed in various sub cortical white matter tracts. In fact NF-L immunohistochemistry was previously used to show the pathogenesis of diffuse axonal injury following traumatic brain injury [10] with others showing cell body changes evidenced by accumulation of phosphorylated neurofilament heavy chain[11]. Although further validation is needed, we also show putative signs of neurofilament compaction using RMO-14 antibodies. Neurofilament compaction is one of the components of traumatic axonal injury revealed by RMO-14 antibodies[1] with the other being impaired axoplasmic transport revealed by β-APP immunohistochemistry[1,2]. In fact the predominance of presence of β-APP reactive profiles in the blast groups supports the dominance of impaired axoplasmic transport which was reported to be localized to the thin caliber axons[12] as revealed by very thin β-APP reactive profiles especially in the sub cortical white matter. In addition, the utility of β-APP immunohistochemistry was also reported by other investigators studying blast related changes in rodents[13,14]. Presence of intense GFAP reactive astrocytes is another hallmark of open field blast induced changes in the brain. The presence of GFAP reactive astrocytes delineating the white matter tracts implicates and supports their strong association with ongoing injury changes in the axons and other support cells. In fact, blast activity was shown to induce functional changes with profound astrocytic proliferation in the corpus callosum in a rodent blast model[15]. Furthermore, the response of astrocytes appears to be graded with their number increasing with increase in blast pressure as indicated by our preliminary analysis.

In our study, a high number of microglia were observed in all areas of the brain with no specific distribution pattern in both sham and blast exposed brains. Preliminary quantification supports elevated microglial counts in medium blast brain sections compared to sham brain sections.   This observation is different from that of Lanerolle et al who reported microglia in the central white matter of the corpus callosum with no differences being observed in the areas of superior frontal cortex and hippocampus between blast and sham animals[3]. With only very limited studies reporting on the microglial response in a gyrencephalic model, much of the previous reports on microglial response were from blast studies using rodents[16,17] and impulse noise[18].   A putative pathological implication for microglia comes from studies by Kane et al (2012) who reported an increased expression of microglial genes related to immune function and inflammatory responses in cultured microglia subjected to overpressure[19]. In a recent investigation, Sajja et al (2014) have shown a differential activation of microglia and astrocytes with selective activation of microglia at low magnitude blast overpressure and increased astrocytic activation with moderate blast overpressure[20]

What are the potential implications of the observed astrocytic and microglial activation? One possible implication is their potential role in neurodegeneration. It was recently shown that TGF beta from immature astrocytes could initiate synaptic elimination in postnatal thalamus by regulating the expression of C1q, a subcomponent of C1 complex of complement activation in the retinal ganglion cells[21]. C1q can trigger classic complement pathway that can lead to tagging of the supernumerary synapses with C3b fragment derived from complement activation and their ultimate elimination by microglia [22,23]. Furthermore, the indiscriminate microglial invasion of cortical and sub cortical regions as observed in the current study may also have other neurodegenerative implications considering the enhanced β-APP immunoreactive zones. It was shown that microglial functions such as directed process motility and phagocytic activity were impaired in mice with Alzheimer's disease-like pathology (AD-like) with their impairment being temporally and spatially correlated with Aβ plaque deposition[24] There may also be a bidirectional relationship that may exist between the activation of astrocytes and that of microglia. For example, the attenuation of reactive gliosis in a model of AD led to a high number of microglia in the vicinity of plaques and cortex[25] while the attenuation of astrocytic activation in a mouse model of Batten disease was shown to be accompanied by increased number of microglia in the brain [26]. In fact the role of microglia and astrocytes contributing to the release of various inflammatory mediators has been well reported. For that matter, studies by Bauman et al and others have shown increased levels of tumor necrosis factor (TNF), interleukin 1 beta (IL-1β), and interferon-γ in cerebrospinal fluid and serum following of blast [5,27] lending support to the inflammatory nature of blast pathology.

In conclusion, our investigation of a gyrencephalic brain three days after open field blast exposure supports the presence of a robust neuronal injury accompanied by extensive astrocytic and microglial activation in the frontal cortical region. The functional implication of these changes may be related to neuronal, axonal and dendritic degeneration combined with a cascade of inflammatory mediator release. Investigation of whether these injury changes extend to other parts (posterior aspects including brainstem) of the brain is ongoing.

Key findings:
     1. Open field blast induces marked axonal injury changes as evidenced prominently by β-APP immunohistochemistry in the cortex and subcortical white matter tracts of the frontal lobe.
     2. Open field blast induces profound changes in the number of astrocytes and microglia in the medium pressure blast group.
     3. Presence of GFAP almost exclusively in the white matter tracts may support an ongoing axonal injury.
     4. Evidence suggestive of higher serum GFAP levels in the high pressure blast group lends credence to astroglial changes as shown by histology.
     5. GFAP may be considered as one of the key serum markers of blast induced injury changes considering a) high astrocyte counts in blast sections; b) close

association of GFAP staining in the white matter tracts suggesting putative injury changes in the white matter tracts; c) evidence of higher GFAP levels in the serum in the high pressure group.

Our immediate objectives:
- Complete the quantification of the remaining APP, GFAP and Iba1 stained sections. This data will be incorporated into the manuscript in preparation to be submitted to a high quality journal.
- Continue with Cleaved Caspase, Fluoro-Jade C, H&E and Prussian blue staining.
- Continue with processing the remainder of the brain tissue, to assess changes in the parietal, temporal, and occipital lobes and in the brainstem.

References
1. Stone JR, Singleton RH, Povlishock JT. Intra-axonal neurofilament compaction does not evoke local axonal swelling in all traumatically injured axons. *Exp Neurol.* Dec 2001;172(2):320-331.

2. Kallakuri S, Li Y, Zhou R, et al. Impaired axoplasmic transport is the dominant injury induced by an impact acceleration injury device: An analysis of traumatic axonal injury in pyramidal tract and corpus callosum of rats. *Brain research.* May 3 2012;1452:29-38.

1. Stone JR, Singleton RH, Povlishock JT. Intra-axonal neurofilament compaction does not evoke local axonal swelling in all traumatically injured axons. *Exp Neurol.* Dec 2001;172(2):320-331.
2. Kallakuri S, Li Y, Zhou R, et al. Impaired axoplasmic transport is the dominant injury induced by an impact acceleration injury device: An analysis of traumatic axonal injury in pyramidal tract and corpus callosum of rats. *Brain research.* May 3 2012;1452:29-38.
3. de Lanerolle NC, Bandak F, Kang D, et al. Characteristics of an explosive blast-induced brain injury in an experimental model. *J Neuropathol Exp Neurol.* Nov 2011;70(11):1046-1057.
4. Gyorgy A, Ling G, Wingo D, et al. Time-dependent changes in serum biomarker levels after blast traumatic brain injury. *J Neurotrauma.* Jun 2011;28(6):1121-1126.
5. Bauman RA, Ling G, Tong L, et al. An introductory characterization of a combat-casualty-care relevant swine model of closed head injury resulting from exposure to explosive blast. *J Neurotrauma.* Jun 2009;26(6):841-860.
6. Axelsson H, Hjelmqvist H, Medin A, Persson JK, Suneson A. Physiological changes in pigs exposed to a blast wave from a detonating high-explosive charge. *Military medicine.* Feb 2000;165(2):119-126.

7. Itoh T, Satou T, Nishida S, Tsubaki M, Hashimoto S, Ito H. Expression of amyloid precursor protein after rat traumatic brain injury. *Neurol Res.* Feb 2009;31(1):103-109.

8. Kilbourne M, Kuehn R, Tosun C, et al. Novel model of frontal impact closed head injury in the rat. *J Neurotrauma.* Dec 2009;26(12):2233-2243.

9. Kuehn R, Simard PF, Driscoll I, et al. Rodent model of direct cranial blast injury. *J Neurotrauma.* Oct 2011;28(10):2155-2169.

10. Povlishock JT. Pathobiology of traumatically induced axonal injury in animals and man. *Ann Emerg Med.* Jun 1993;22(6):980-986.

11. Saljo A, Bao F, Haglid KG, Hansson HA. Blast exposure causes redistribution of phosphorylated neurofilament subunits in neurons of the adult rat brain. *J Neurotrauma.* Aug 2000;17(8):719-726.

12. Marmarou CR, Walker SA, Davis CL, Povlishock JT. Quantitative analysis of the relationship between intra- axonal neurofilament compaction and impaired axonal transport following diffuse traumatic brain injury. *J Neurotrauma.* Oct 2005;22(10):1066-1080.

13. Koliatsos VE, Cernak I, Xu L, et al. A mouse model of blast injury to brain: initial pathological, neuropathological, and behavioral characterization. *Journal of neuropathology and experimental neurology.* May 2011;70(5):399-416.

14. Garman RH, Jenkins LW, Switzer Iii RC, et al. Blast exposure in rats with body shielding is characterized by diffuse axonal injury. *Journal of neurotrauma.* Mar 30 2011.

15. Turner RC, Naser ZJ, Logsdon AF, et al. Modeling clinically relevant blast parameters based on scaling principles produces functional & histological deficits in rats. *Experimental neurology.* Oct 2013;248:520-529.

16. Kaur C, Singh J, Lim MK, Ng BL, Yap EP, Ling EA. The response of neurons and microglia to blast injury in the rat brain. *Neuropathol Appl Neurobiol.* Oct 1995;21(5):369-377.

17. Readnower RD, Chavko M, Adeeb S, et al. Increase in blood-brain barrier permeability, oxidative stress, and activated microglia in a rat model of blast-induced traumatic brain injury. *J Neurosci Res.* Dec 2010;88(16):3530-3539.

18. Saljo A, Bao F, Hamberger A, Haglid KG, Hansson HA. Exposure to short-lasting impulse noise causes microglial and astroglial cell activation in the adult rat brain. *Pathophysiology.* Dec 2001;8(2):105-111.

19. Kane MJ, Angoa-Perez M, Francescutti DM, et al. Altered gene expression in cultured microglia in response to simulated blast overpressure: possible role of pulse duration. *Neuroscience letters.* Jul 26 2012;522(1):47-51.

20. Sajja VS, Ereifej ES, Vandevord PJ. Hippocampal vulnerability and subacute response following varied blast magnitudes. *Neuroscience letters.* Apr 12 2014;570C:33-37.

21. Bialas AR, Stevens B. TGF-beta signaling regulates neuronal C1q expression and developmental synaptic refinement. *Nat Neurosci.* Dec 2013;16(12):1773-1782.

22. Schafer DP, Lehrman EK, Kautzman AG, et al. Microglia sculpt postnatal neural circuits in an activity and complement-dependent manner. *Neuron.* May 24 2012;74(4):691-705.

23. Stevens B, Allen NJ, Vazquez LE, et al. The classical complement cascade mediates CNS synapse elimination. *Cell.* Dec 14 2007;131(6):1164-1178.

24. Krabbe G, Halle A, Matyash V, et al. Functional impairment of microglia coincides with Beta-amyloid deposition in mice with Alzheimer-like pathology. *PLoS One.* 2013;8(4):e60921.

25. Kraft AW, Hu X, Yoon H, et al. Attenuating astrocyte activation accelerates plaque pathogenesis in APP/PS1 mice. *FASEB J.* Jan 2013;27(1):187-198.

26. Macauley SL, Pekny M, Sands MS. The role of attenuated astrocyte activation in infantile neuronal ceroid lipofuscinosis. *J Neurosci.* Oct 26 2011;31(43):15575-15585.

27. Svetlov SI, Prima V, Glushakova O, et al. Neuro-glial and systemic mechanisms of pathological responses in rat models of primary blast overpressure compared to "composite" blast. *Front Neurol.* 2012;3:15.

TASK II REPORT

Task II – Perform open field blast testing on 6 unembalmed post-mortem human subjects (PMHS) also known as cadavers to obtain biomechanical data

Blast testing was performed on one PMHS during this reporting period. This was the second specimen tested out of the 6 scheduled for this task. We obtained one female specimen from the University of Michigan. It arrived in the lab about four days after death and it was tested on the sixth day. Also, during the post-mortem period prior to instrumentation, the specimen was kept at 4 °C. Relevant biological data on the specimen are provided in Table 7.

Table 7. PMHS information

PMHS ID	Sex	Age	Height	Weight	Cause of Death
UM34869	Female	32	60"	105 lb	Colon cancer

1. PMHS Preparation

The PMHS preparation was the same as in the first test. In brief, six intracranial pressure (ICP) sensors were inserted into the frontal, parietal, left/right temporal, and occipital region of the skull. An acceleration block containing three linear accelerometers and three angular rate sensors, and two strain gages (frontal and right temporal) were fixed onto the skull surface (see Figure 29).
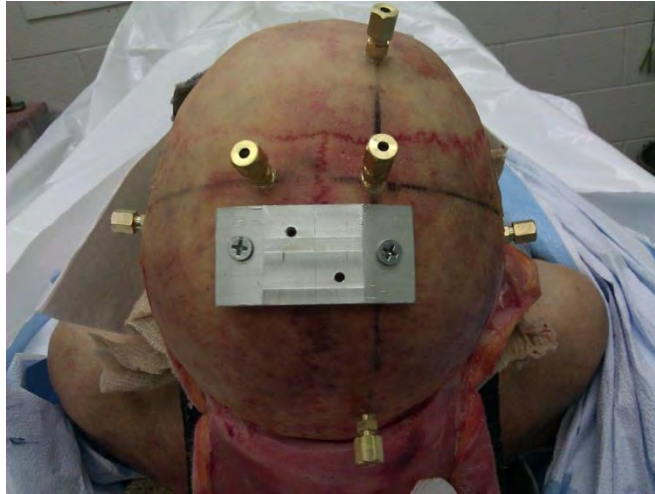
Figure 29. Location of ICP sensors and accelerometer block

2.   Blast Testing of PMHS

PMHS blast tests were conducted on 5/21/15 at ARES, Inc. in Port Clinton, OH. The explosive used was 8 lb of C4 placed at varying distances from the cadaver's head. The three pre-determined peak pressure levels were nominally 150, 300 and 450 kPa. A total of 8 tests were conducted on the cadaver. The test subject was hung upside down at the knee on the A-frame (see Figure 2.2) so that it can be easily turned to accomplish frontal lateral and rear blasts. A T-frame was fixed to the cadaver's back using a five-point harness system. Sand bags and straps were attached to the T-frame to limit the motion of the upper body of the cadaver. In addition to the measurement of intracranial pressure, strain, head linear acceleration, head angular velocity and frontal and occipital head surface pressure were measured.

Figure 30. Test site and set up for the cadaver test

During this testing, a custom-made perfusion device (Figure 31) was used to perfuse and pressurize brain with artificial cerebrospinal fluid (aCSF) before each blast. The purpose of the perfusion was to prevent air bubbles from affecting the ICP measurement during the blast.
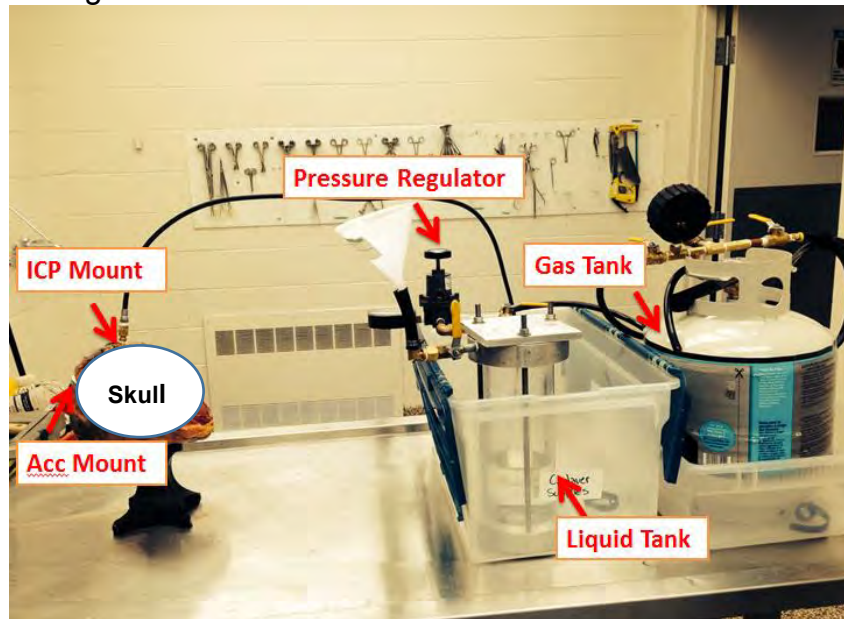

Figure 31. Custom-made brain perfusion device

3. Summary of Results

Eight blast tests were performed. They are low, medium, and high level blasts for frontal and side direction as well as low and medium level blast for rear direction. ICP sensor readings at parietal location were found to be abnormal during frontal blasts. A backup sensor was damaged after the high level frontal blast test. Data were not collected for that location for the rest tests.

ICP and accelerometer data were filtered at CFC 6000 and angular rate data were filtered at CFC 3000. All data from this cadaver have been processed.

Figure 32 is a plot of ICP as a function of time for a low level frontal exposure. The symbols F, P, T, O and C stand for frontal, parietal, temporal, occipital and central sensors respectively.
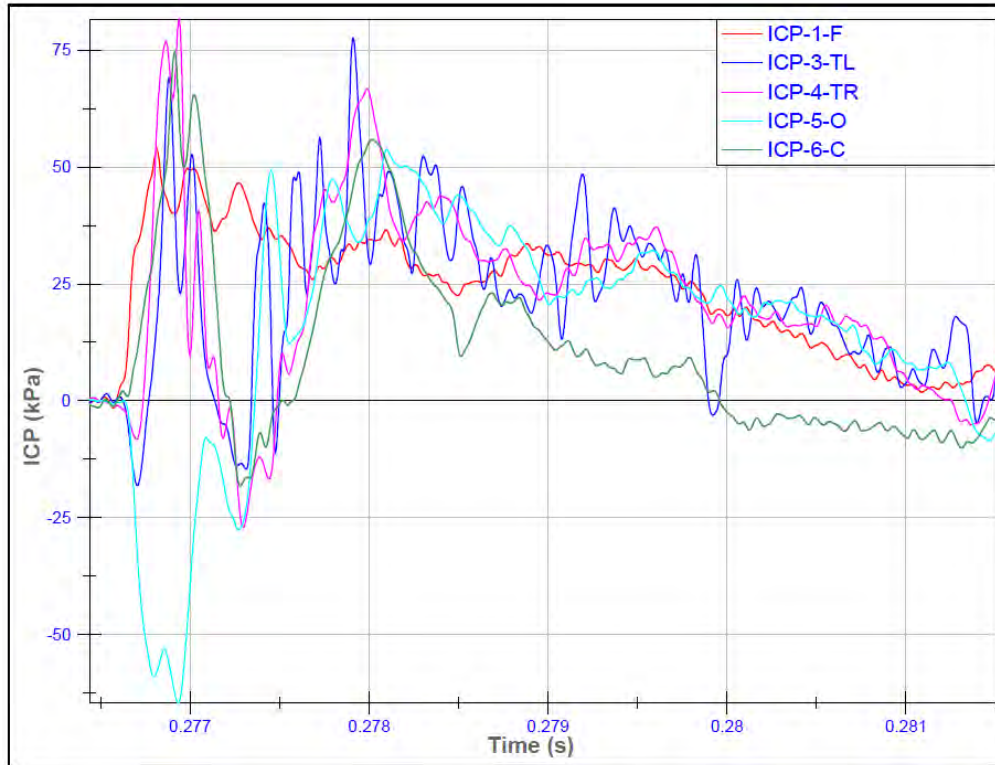
Figure 32. Intracranial pressures at various locations for a low level frontal blast.

For medium and high level frontal blasts, the intracranial pressures are shown in Figure 33 and 34.

Figure 33. Intracranial pressures at various locations for a medium level frontal blast
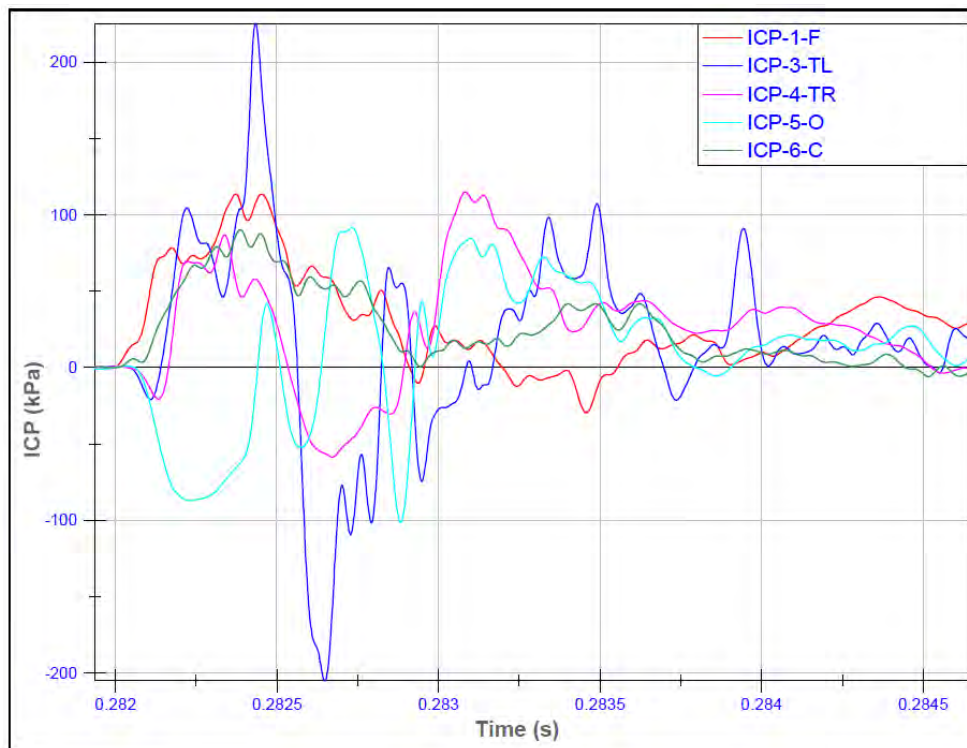
Figure 34. Intracranial pressures at various locations for a high level frontal blast

Intracranial pressures for side and rear blast tests are shown in Figure 35 to 39.

Figure 35. Intracranial pressures at various locations for a low level side blast

Figure 36. Intracranial pressures at various locations for a medium level side blast

Figure 37. Intracranial pressures at various locations for a high level side blast
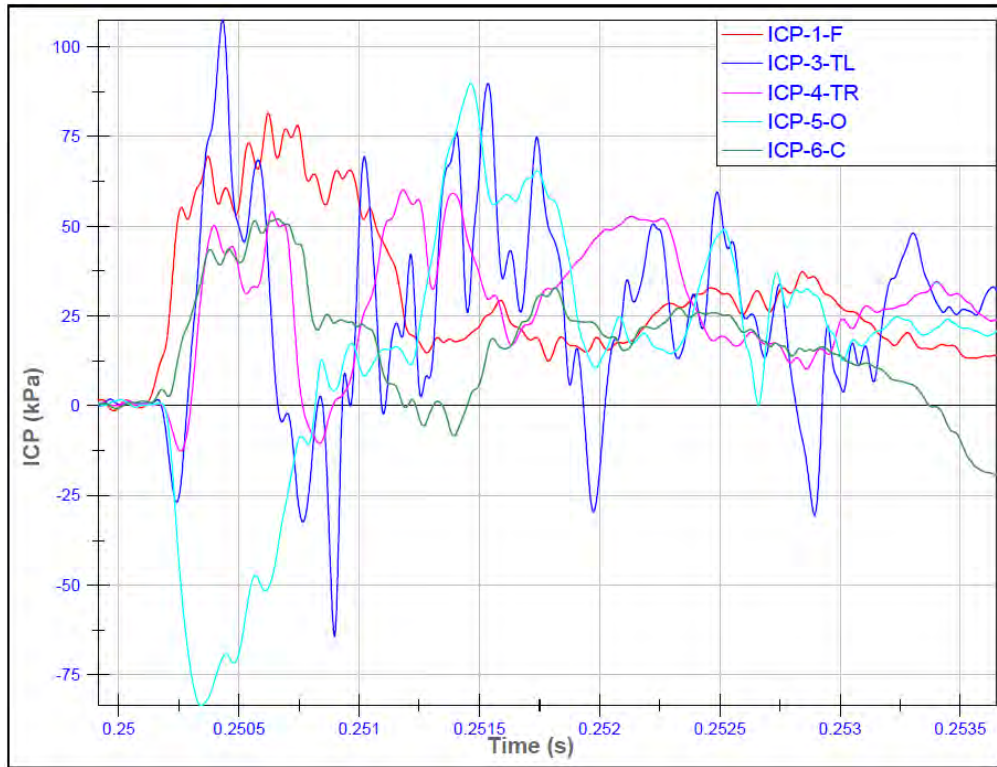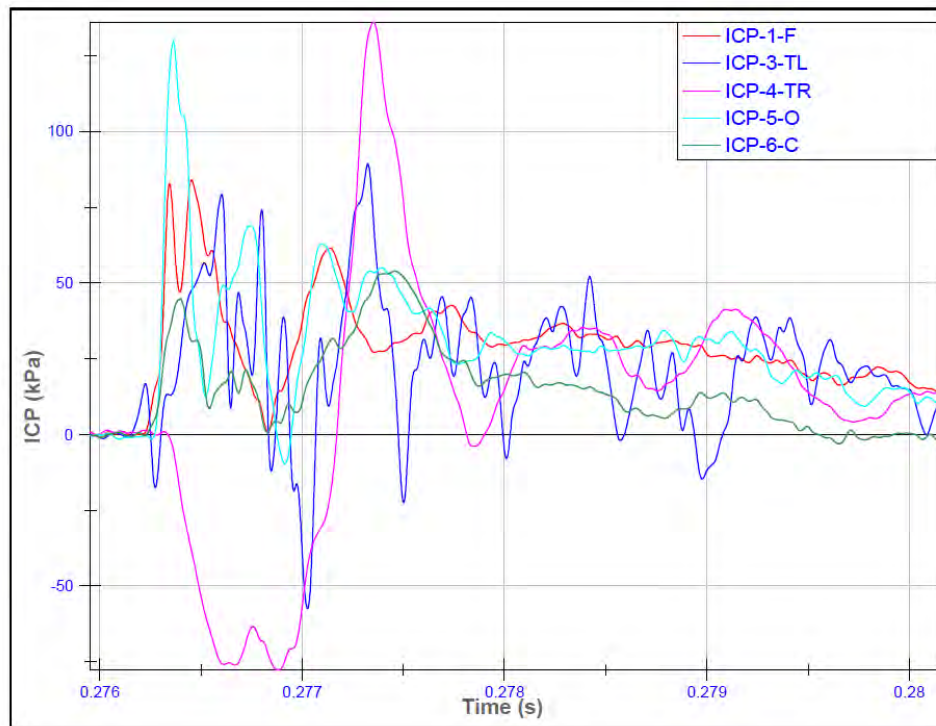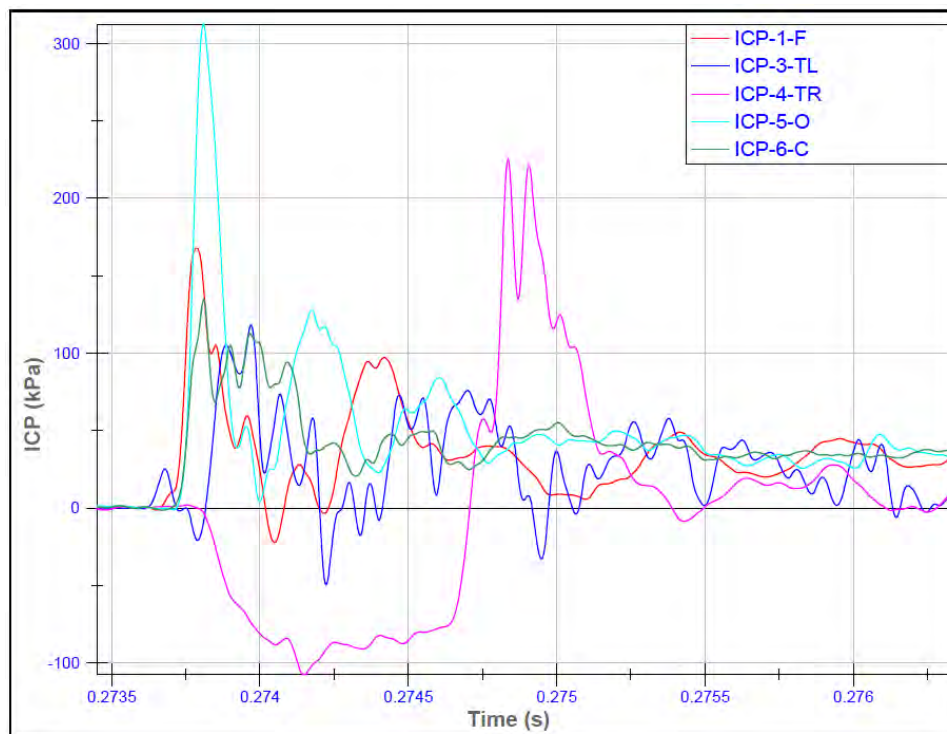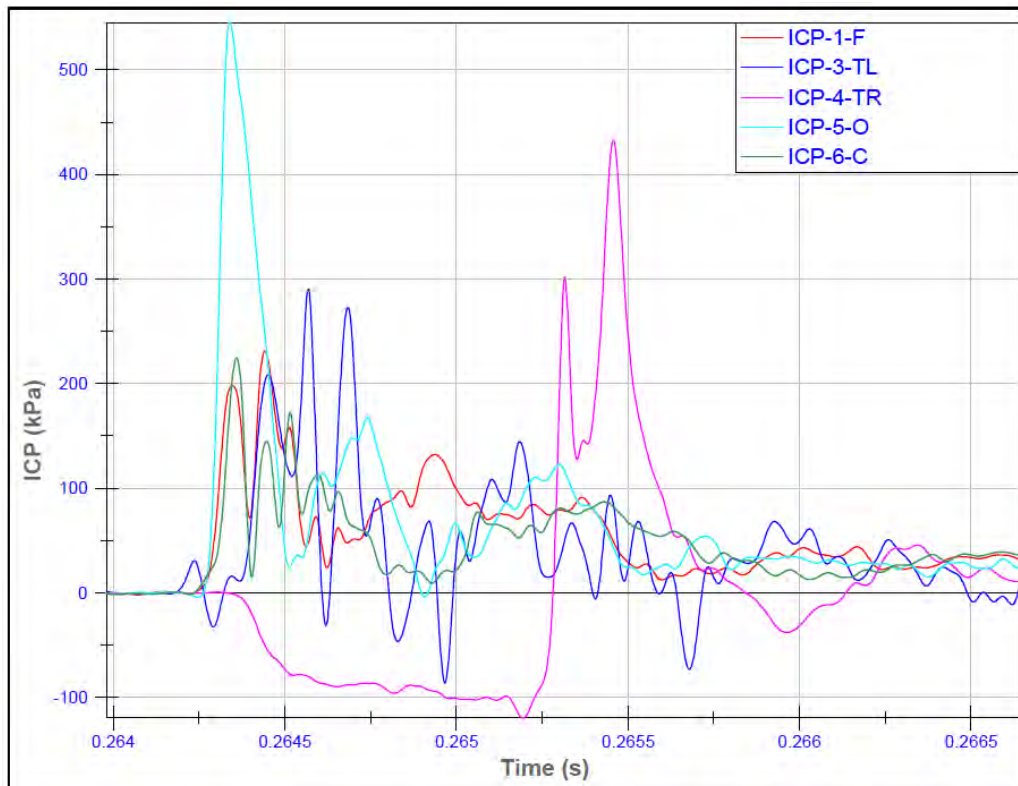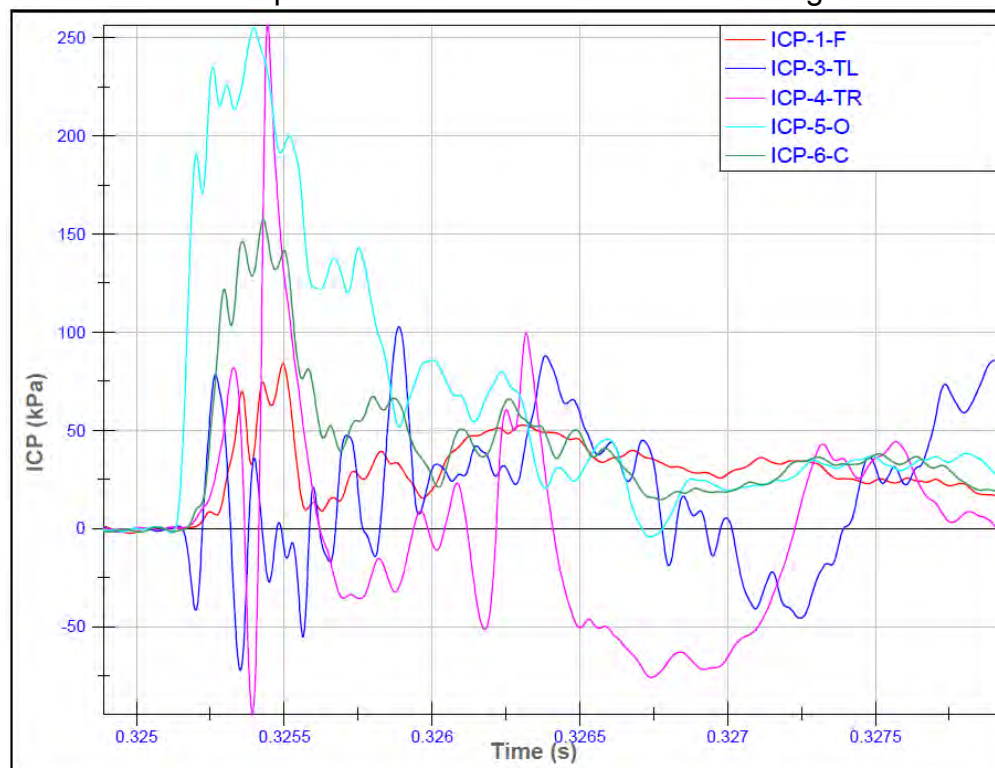

Figure 38. Intracranial pressures at various locations for a low level rear blast
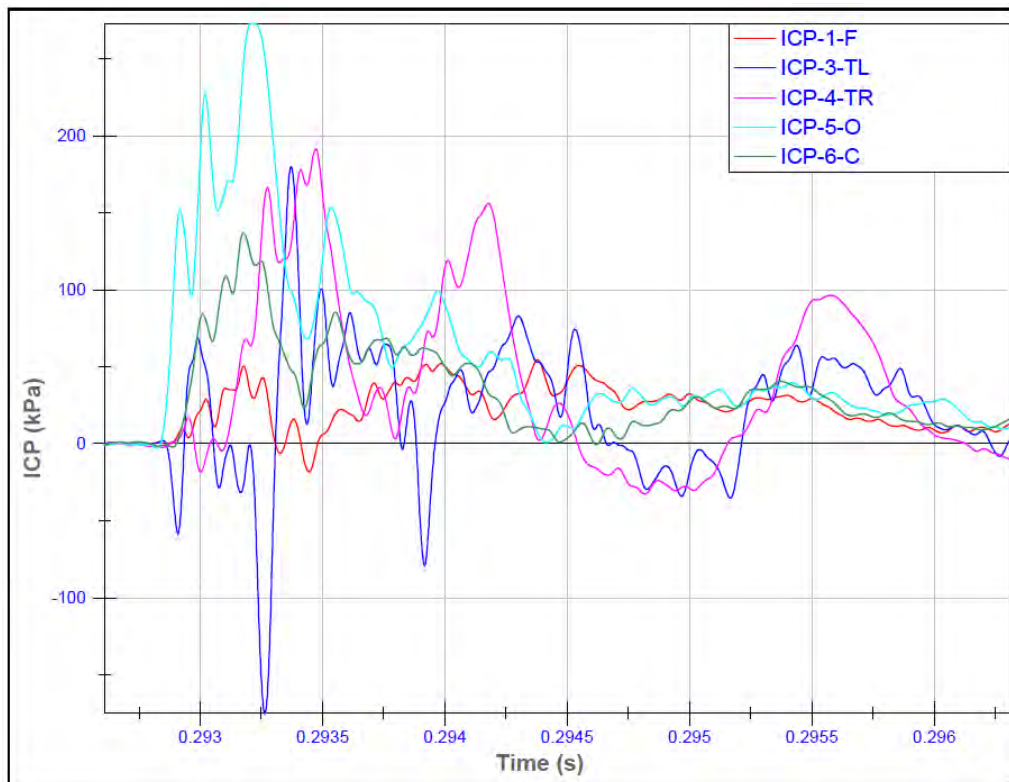
44

Figure 39. Intracranial pressures at various locations for a medium level rear blast

The measured ICP's were generally lower than the IOP but higher than the measurement from cadaver test 1, due possibly to the perfusion performed for this cadaver. There is evidence of a contrecoup (negative) pressure in frontal and side blast tests.

Summary of data from the first two cadaver tests are shown in Table 8.

Table 8. ICP data for two cadaver tests

		Frontal		Parietal		L Temporal		R Temporal		Occipital		Center	
		Test1	Test2	Test1	Test2	Test1	Test2	Test1	Test2	Test1	Test2	Test1	Test2
	Low	90.3	53.8	35.5	n/a	28.1	81.4	18.8	69.7	-35.1	-64.6	27.6	73.7
Frontal	Med	170.4	80.6	103.1	n/a	43.7	59.2	26.9	107.5	-50.6	-83.4	63.3	51.5
	High	354.6	112.3	146.7	119.2	69.3	88.9	27.3	225.3	-84.6	-87.5	n/a	89.8
	Low	44.5	82.5	47.8	n/a	-40.4	136.1	48.3	89.6	63.2	130.3	9.9	53.5
Side	Med	164.4	168.1	105.4	n/a	-57.2	223.9	91.4	119.2	95.5	310.7	32.4	135
	High	235.1	233.7	99.3	n/a	-93.8	431.5	n/a	289.3	157.2	542.8	82.8	224.5
	Low	-220.6	83.5	387.4	n/a	225.1	256.5	n/a	78.6	392	255.3	n/a	157.4
Rear	Med	-75.2	50.8	536.4	n/a	53.5	191.1	n/a	178.9	166.3	272.9	56.9	137.1
	High	-50.1	n/a	213	n/a	50.3	n/a	n/a	n/a	83.3	n/a	-53.6	n/a

No conclusions can be reached with data from these two specimens. We need to continue to analyze the data and collect more test data before we can arrive at some conclusions.

TASK III REPORT

Task III - Develop and validate a computer model of the pig brain simulating the effects of a blast over-pressure

In this reporting period, we worked on three aspects of pig head modeling:

1.   Simulations of the pig head response under blast loading.
2.   Parametric analysis to identify the effect of key parameters on ICP response
3.   Validation of the swine brain model

1.   Simulations of the Pig Head Response under Blast Loading

In this reporting period, a computational parametric study was conducted to evaluate the effect of impulse of incident blast wave on the strain and ICP response in the brain. To reduce computational time, a simplified two-material skull-brain FE model was used instead of a complicated pig head model. The model used was spherical in shape. The outer layer was a polyethylene shell and it was filled with a silicone gel. Such a configuration can be used to mimic a simplified head with skull and brain tissue. The radius of the brain was 60 mm and shell thickness was 16 mm. A similar head surrogate has been used to study the ICP response under blast loading (Zhu et al. 2012). A bilinear elasto-plastic constitutive law, incorporating isotropic and kinematic hardening, was used to represent the mechanical behavior of the polyethylene shell. The material properties are as follows: the mass density (ρ) was 900 kg/m^3, Young's modulus (E) was 0.8 GPa, Poisson's ratio (υ) was 0.4, and yield stress (σ_Y) was 80 MPa. A linear viscoelastic law was adopted to represent the behavior of silicone gel. Its material constants are listed in Table 9 (Zhu et al. 2012).

Table 9. Material properties of the silicone gel

Parameter	Value
Density (ρ)	950 kg/m^3
Bulk modulus (K)	1.0 GPa
Short-term shear modulus (G_0)	3,600 Pa
Long-term shear modulus (G_∞)	586 Pa
Decay constant (β)	0.05 ms^{-1}

CONWEP function was used to model the blast loading, where the pulse shape can be adjusted by changing the mass of charge and stand-off distance. In the current study, fives pulses were generated. The peak pressure magnitude was kept constant (120 kPa) while the duration varied from 1 ms to 8 ms to study the effect of pulse shape on

the biomechanical responses in the brain. The incident pressure – time histories and impulses are shown in Figure 40a and b, respectively.

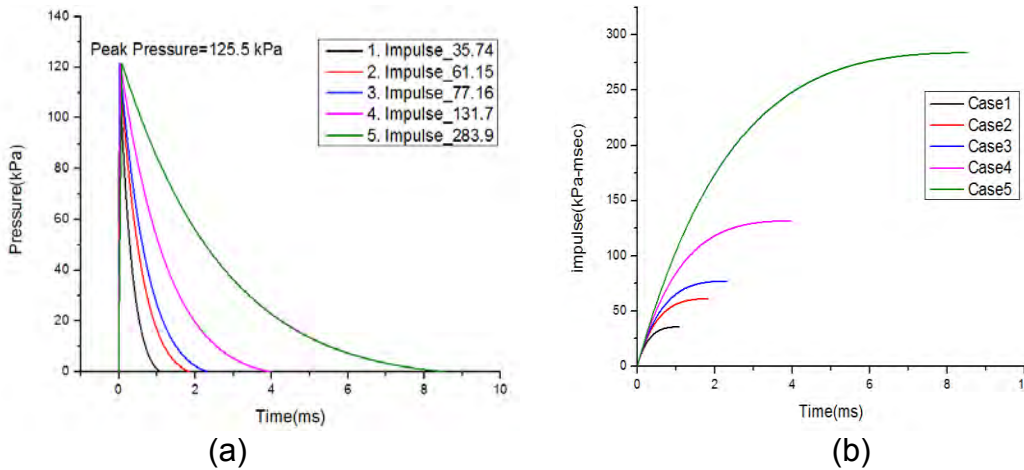
(a)   (b)

Figure 40. The incident pressure – time histories and impulses generated using CONWEP

The conditions of the five simulations and results are given in Table 10. The ICP and strain responses were monitored at the center of brain. Simulation data indicate that in the current scenario, the ICP values increased with the incident impulse. However, increasing the impulse per unit area 8 times from 35.7 Pa•s to 283.9 Pa•s only resulted in a 28% increase in ICP and no change in strain. We surmise from this result that brain response due to blast loading is not sensitive to impulse, but is sensitive to peak pressure. This finding is consistent with the results of our earlier shock tube study on rat brain response (Zhu et al. 2010).

Table 10. Simulated ICP and strain at different impulse levels

Simulation No.	Mass (kg)	Distance (m)	Peak incident pressure (kPa)	Duration (ms)	Impulse (Pa·s)	ICP (kPa)	Strain (%)
1	0.1	1.135	125.3	8.513	283.9	222	0.07
2	0.5	1.94	125.4	3.954	131.7	250	0.07
3	1.0	2.44	125.9	2.308	77.16	260	0.07
4	5.0	4.18	125.4	1.835	65.15	273	0.07
5	50	9.00	125.5	1.073	35,74	285	0.07

2.   Parametric Analysis to Identify the Effect of Key Parameters on ICP
      Response

In this section, a data driven parametric analysis was conducted to identify the effect of
key parameters on ICP response and their interrelationship. These relationships are
very complicated and are usually implicit and "hidden" in a large amount of
simulation/test data. In this section, a data mining method is proposed to explore such
underlying information from the numerical simulation results. A highly simplified model
was built to approximate the real head to save computational time. The model had two
parts, i.e. a spherical brain covered by a skull with an irregular shape as shown in
Figure 41a. The skull was extruded to form a tapered end which mimics the snout of
animals such as rats or pigs. As sketched in Figure 41a, the model consisted of three
geometric parameters, i.e. the radius of brain r, skull thickness t and snout length l.
These three variables can basically describe the dimensions and shape of a head, as
illustrated in Figure 41b.

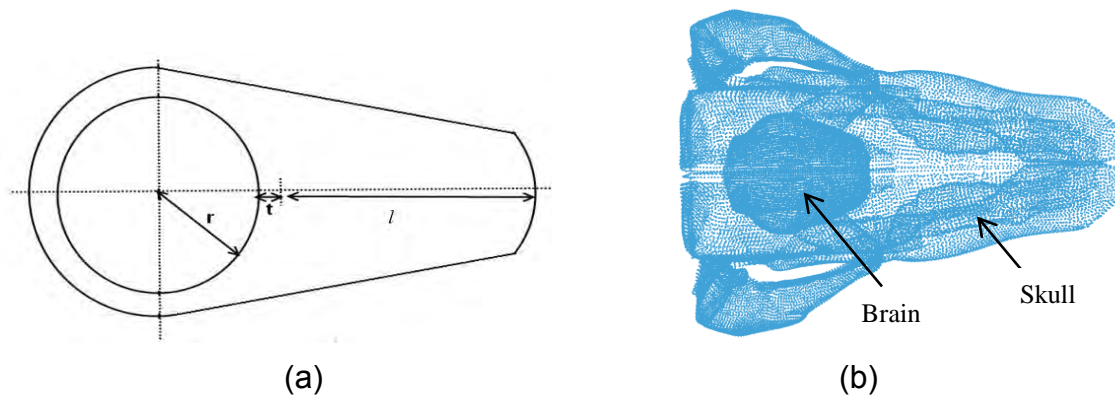(a)   (b)

Figure 41. (a) Sketch of a simplified head model; (b) A FE pig head model (top view)

Since different geometric parameters may have a distinct influence on the response at
the different pressure levels, incident pressure p_{in} was considered as the fourth
parameter. The range of each parameter is given in Table 11. For the intervals
selected, these parameters result in a total of 6900 combinations - the design space for
the current problem.

Table 11. The range of geometric variables in the design space

Variable	Range	Interval	Total no. of values
p_{in}	50-500 kPa	20	23
r	20-200 mm	20	10
t/r	0.1-0.5	0.1	5
l	2r-7r (r<80mm)	1	6
	0.0r-0.5r (r>80mm)	0.1	6

48

Since the design space for simulations is too large, a Latin Hypercube sampling method was used to reduce the number of designs or simulations to 200 with the software modeFrontier (http://www.esteco.com/modefrontier). A uniform Latin Hypercube method is useful when a random sampling space is needed and it guarantees a relatively uniform distribution over each dimension. The sampling of designs is shown in Figure 42 with 3 variables, i.e. pressure, radius and thickness. The data points formed a design space with 200 Design of Computer Experiments (DOCEs) for further analysis.
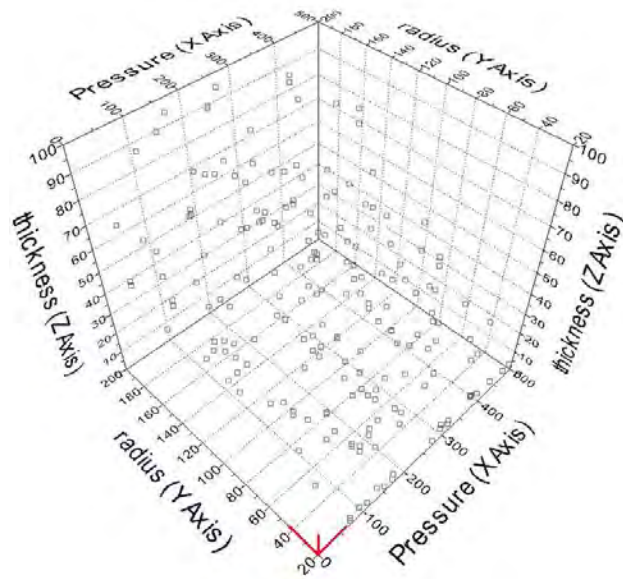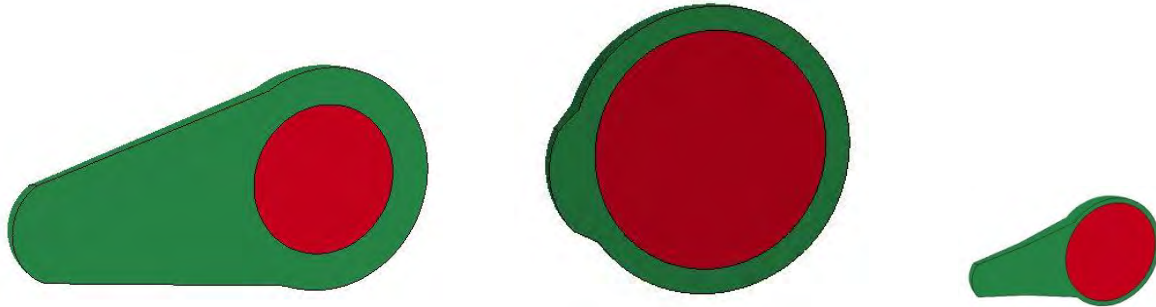

Figure 42. DOCE selection based on Latin Hypercube method

FE models were constructed corresponding to the DOCEs created in this section. Three typical FE model cases, representing a large animal, a human head and a small animal head are shown in Figure 43a, b and c, respectively for illustrative purposes.

r=40 mm; t=20 mm; l=120 mm r=100 mm; t=10 mm; l=20 mm; r=20 mm; t=2 mm; l=40 mm

(a)   (b)   (c)

Figure 43. Three typical FE models to represent: (a) a large animal head; (b) a human head; and (c) a small animal head

The materials for skull and brain in the simplified head surrogate were assumed to be polyethylene plastic and silicone gel, respectively (Zhu et al. 2012). Polyethylene was modeled as a linear elastic solid with a density ρ=900 kg/m^3. The silicone gel was assumed to behave as a visco-elastic material. The material constants are as follows: density ρ=950 kg/m^3; bulk modulus K=1.0 GPa; Short term shear modulus G_0=3,600 Pa, long term shear modulus G_∞=586 Pa; decay constant β=0.05 ms^{-1} (Zhu et al. 2012). Both skull and brain were modeled using brick elements. Mesh sensitivity studies were conducted to guarantee the convergence. The blast loads were created using empirical blast pressure function CONWEP, which can calculate the incident pressure based on two input parameters, that is, the equivalent TNT mass and stand-off distance. In the simulations, these two parameters were adjusted to produce the shock waves with the magnitudes listed in Table 11. The duration of the incident wave pulse was fixed at approximately 1.5 ms since in most cases of nonlethal IED exposures, the blast wave duration is in the range of 1~8 ms. The variation in such a narrow band does not have evident influence on the ICP response (Zhu et al. 2013). A similar model was developed by the authors and validated against shock tube test data (Zhu et al. 2012).

In the present study, the model predicted ICP was for the center of brain. The parameters r, t, l and p_{in} as well as peak ICP response (denoted as P_{ic}) were normalized with Eq.(1) and all of the values are in the range of (0, 1].

$$\bar{x} = \frac{x}{x_{max}} \qquad (x = r, t, l, P_{in}, P_{ic}) \qquad (1)$$

where x_{max} denotes the maximum value of each parameter in the data set.

A typical model predicted $\overline{P_{in}}$ -time trace and $\overline{P_{ic}}$ -time trace with the geometric parameters r=20 mm, t=3 mm and l=3 mm are shown in Figure 44. The two curves

have a similar pattern, which is characterized by a sudden increase in pressure and then an exponential decay. In the current case, the peak ICP is slightly higher than peak incident pressure. The relationship between ICP and incident pressure magnitudes is highly nonlinear and depends on the geometry and dimensions of the head as well as the level of incident pressure.
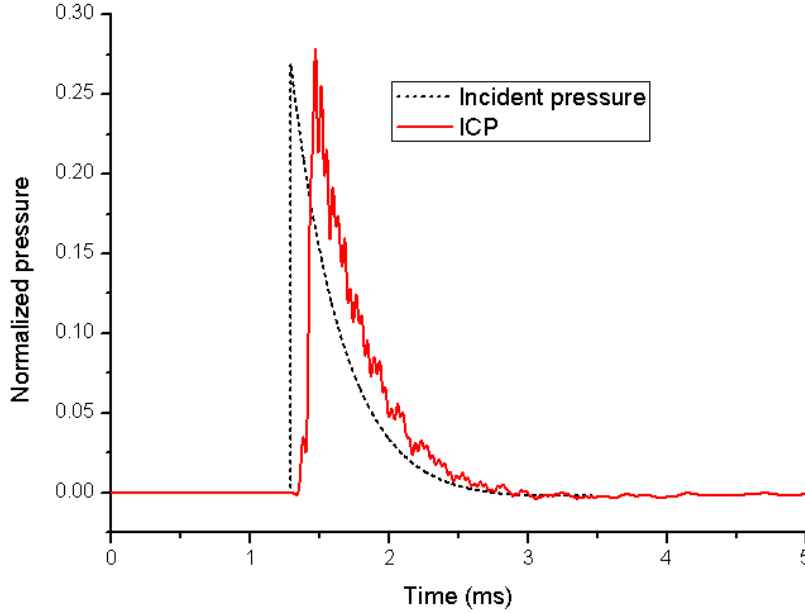

Figure 44. A typical model predicted $\overline{P_{in}}$ -time trace and $\overline{P_{ic}}$ -time trace with the geometric parameters r=20 mm, t=3 mm and l=3 mm

The simulation results, i.e. the model predicted $\overline{P_{ic}}$ and the corresponding input variables $\overline{r}$, $\overline{t}$, $\overline{l}$ and $\overline{P_{in}}$ formed a dataset that was subjected to further data mining and analysis. Data Mining is an analytical process designed to explore data in search of consistent patterns and/or systematic relationships between variables. In the present case, we are going to determine the following relationship from the simulation results through data mining:

$$\overline{P_{ic}} = f(\overline{t},\overline{r},\overline{l},\overline{p_{in}}) \qquad (2)$$

where *f* is an unknown function. Based on the simulation results of the DOCE, a commonly used data mining approach, the Decision Tree method (Han and Kamber 2006; Kantardzic 2003; Witten and Frank 2011), was used to study the interrelationship of the parameters and their influence on ICP response. Decision tree is a decision support tool that uses a tree-like graph to model decisions and their possible consequences. The logic is very similar to a set of "if-then" decision makings in the top-down sequence. This method has been widely employed in dataset classification. To build the decision tree, a number of algorithms are available, including M5P, BFTree, J48, LMT, NBTree, Random Forest, REPTree etc (Han and Kamber 2006; Kantardzic

2003; Witten and Frank 2011). The node on top of the tree is regarded as the root node. Each node represents a test for an attribute (in the present case, the value of parameters $\bar{r}$, $\bar{t}$, $\bar{l}$ and $\overline{P_{in}}$). And each lowest level node is called a leaf, standing for a class or relationship (in the present case, Eq. (2)). The interrelationship/coupling effect of "parents" and "children" nodes is described by the links between them.

The decision tree was developed with software WEKA (http://www.cs.waikato.ac.nz/ml/weka/) based on M5P algorithm, as shown in Figure 45a. In the tree, the top node is the factor which has greatest impact on ICP, which, in the current case, is the peak incident pressure $\overline{P_{in}}$. In each leaf node, a decision rule is obtained by linear regression and it describes the relationship of ICP and key parameters. In the present case, when the normalized peak pressure $\overline{P_{in}}$ is equal to or lower than 0.245, then relationship LM1 is reached. Otherwise, go to the right path and check normalized l. If $\bar{l}$ is smaller or equal to 0.079, the response of the head is governed by LM2. Otherwise, go to LM3. The "if-then" rules and the relationship between ICP and key parameters are shown in Figure 45b. It can be seen that the weight of each parameter varies for different head configurations and loading conditions. For example, the influence of skull thickness $\bar{t}$ in LM2 can be disregarded. In all of the cases, brain radius and snout length have a negative effect on the ICP while incident pressure always influences the ICP positively. Such findings are consistent with our experience.
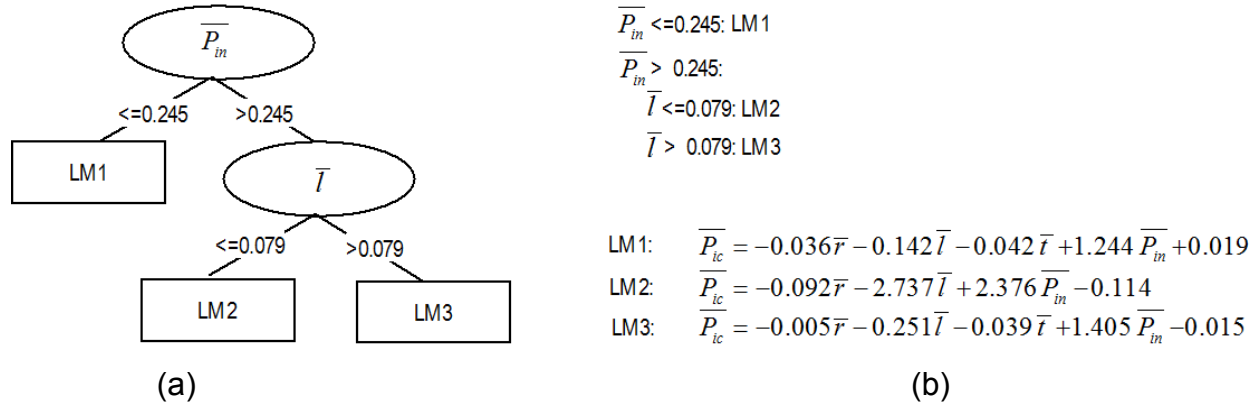
$$\overline{P_{in}} <= 0.245: LM1$$

$$\overline{P_{in}} > 0.245:$$

$$\bar{l} <= 0.079: LM2$$

$$\bar{l} > 0.079: LM3$$

LM1: $\overline{P_{ic}} = -0.036\bar{r} - 0.142\bar{l} - 0.042\bar{t} + 1.244\overline{P_{in}} + 0.019$

LM2: $\overline{P_{ic}} = -0.092\bar{r} - 2.737\bar{l} + 2.376\overline{P_{in}} - 0.114$

LM3: $\overline{P_{ic}} = -0.005\bar{r} - 0.251\bar{l} - 0.039\bar{t} + 1.405\overline{P_{in}} - 0.015$

(a)   (b)

Figure 45. A decision tree built with M5P algorithm in WEKA; (b) "If-then" decision making procedure and the parametric values for LM1, LM2 and LM3

A comparison was made for the results obtained based on the decision tree method and conventional linear regression or linear response surface approach with software SPSS (http://www-01.ibm.com/software/analytics/spss/). The meta model (or response surface) describing the dependence of ICP on the other parameters can be written as

$$\overline{P_{ic}} = -0.004\bar{r} - 0.303\bar{l} - 0.003\bar{t} + 1.574\overline{P_{in}} - 0.1 \quad (3)$$

The model predicted ICP is plotted against simulated results as shown in Figure 46. In the plot, a diagonal line with a slop of 1 indicates a perfect match. It can be seen that the predictions based on the decision tree have a much better agreement with the simulation results than the linear regression method.
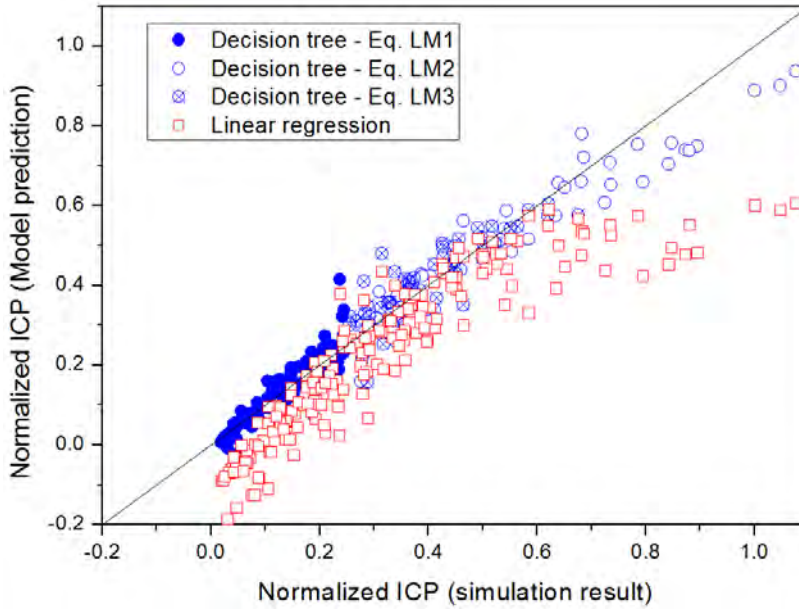

Figure 46. Comparison of the simulated ICP and model predicted ICP by decision tree method and linear regression

A further comparison of statistical significance (indicated by P-value) based on the two models is shown in Table 12. It can be seen that in each of the three sub-design spaces (i.e. the data points governed by LM1, LM2 and LM3, respectively), the parameters have high statistical significance, except $\bar{t}$ in LM2. While in the linear regression model, P-values for $\bar{r}$ and $\bar{l}$ are higher, indicating a lower degree of significance. Therefore one can conclude that a multi-linear model based on the decision tree method has a better performance in terms of correlation of each parameter.

Table 12. Comparison the parametric statistical significance in the decision tree model and conventional linear regression model

Model	P-value			
	$\bar{r}$	$\bar{l}$	$\bar{t}$	$\bar{P}_{in}$
LM1	0	0	0	0
LM2	0	0	1.00	0
LM3	0	0	0	0
Linear regression	0.29	0.01	0.96	0

An additional comparison was made on the performances of the decision tree method and non-linear regression model, which was conducted with SPSS. The non-linear model is given by

$$\bar{P}_{ic} = 0.298\bar{r} + 0.005\bar{l} - 0.052\bar{t} + 1.073\bar{P}_{in} - 0.304\bar{r}^2 + 0.715\bar{l}^2 - 0.215\bar{t}^2 + 1.382\bar{P}_{in}^2$$
$$- 0.539\bar{r} \cdot \bar{l} + 0.218\bar{r} \cdot \bar{t} - 0.118\bar{r} \cdot \bar{P}_{in} - 0.692\bar{l} \cdot \bar{t} - 1.861\bar{l} \cdot \bar{P}_{in} + 0.585\bar{t} \cdot \bar{P}_{in} - 0.045$$

(4)

The model predictions are compared with simulation results in terms of ICP is shown in Figure 47. This comparison demonstrates a similar performance between the decision tree method and non-linear regression. However, the decision tree method allows the revelation of the coupling effect of parameters and yields much simpler equations to estimate ICP. Therefore, it may be concluded that a highly complicated relationship can be split into several sub-models (i.e. LM1, 2 and 3), and each sub-model can be described with a relatively simple linear relationship. In this way, a complex non-linear problem can be simplified and represented by a limited number of linear relationships with high accuracy.
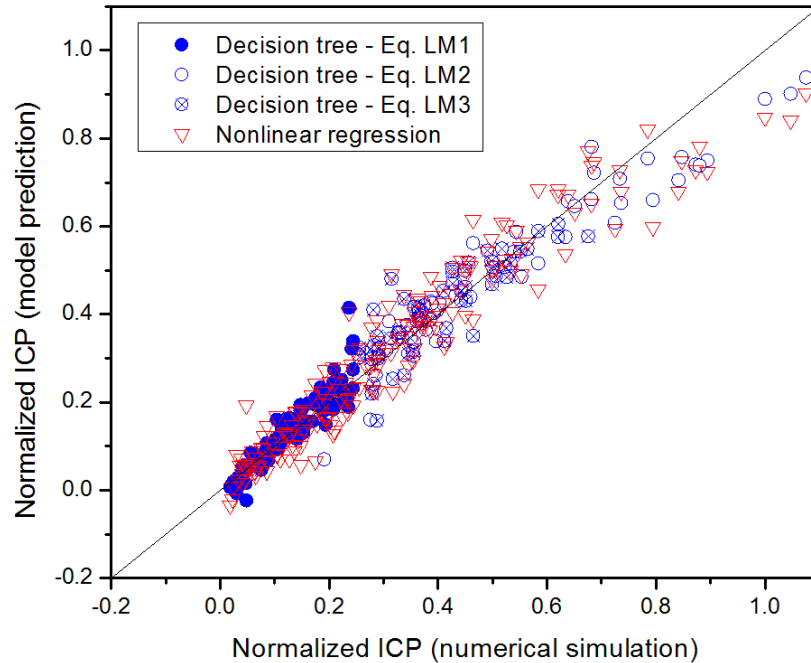
Figure 47. Comparison of the simulated ICP and model predicted ICP by decision tree method and non-linear regression

The results of this study show that the data mining method has a much superior performance over the conventional linear response surface method and it has a similar performance with the non-linear regression method. Considering its capability of exploring implicit information and relatively simple relationships between response and variables, the data mining method can be deemed to be a better tool for a deeper understanding of the mechanisms of bTBI than the use of regression methods. As a general method, this approach can also be applied to other non-linear complex systems.

3,   Validation of the Swine Brain Model

The swine brain model has been partially validated against experimental data. Parametric studies have been conducted to evaluate its performance. The major difficulty we are facing is the mismatch between the model predicted ICP and the measured ICP with the latter being generally lower that the IOP while the model consistently predicts an ICP higher than the IOP. We are examining the boundary conditions of the model, such as small holes in the diploe of the skull, possible presence of air/gas in the brain when the measurements were made or during installation of the pressure sensors and the precise orientation of the head with respect to the incident shock wave.

References

Zhu F, Wagner C, Dal Cengio Leonardi A, Jin X, VandeVord P, Chou C, Yang KH, and King AI. Using a gel/plastic surrogate to study the biomechanical response of the head under air shock loading: A combined experimental and numerical investigation. Biomechancs and Modeling in Mechanobiology, 2012, Vol. 11, pp. 341-353.

Han J and Kamber M. Data Mining: Concepts and Techniques (2nd Edition), 2006, Morgan Kaufmann, San Francisco, CA.

Kantardzic M. Data Mining: Concepts, Models, Methods, and Algorithms, 2003, IEEE Press, Hoboken, NJ.123

Witten IH and Frank E (2011). Data Mining: Practical Machine Learning Tools and Techniques, Third Edition, Morgan Kaufmann, Burlington, MA.

TASK IV REPORT

Task IV - Develop and validate a computer model of the human brain simulating the effects of a blast over-pressure

In this task, we report work on two separate projects:

1. Measurement and Analysis of Incident Overpressure (IOP) in Open Field Blast Test
2. Validation of the Human Brain Model

1. Measurement and Analysis of Incident Overpressure in Open Field Blast Test

As reported previously, the head of the test specimens (swine and cadaver) were positioned 3 ft above the ground in order to avoid the ground reflected wave. It was exposed to the Mach stem which is a single Friedlander blast wave, running along the ground, below the triple point. The blast overpressure was generated by detonating an 8 lb spherically shaped C4 explosive charge which was suspended from a steel chain at 0.66 m (26 inch) above the ground. The nominal blast incident overpressure levels at location of the head of the specimens were 150 (low), 300 (medium) and 400 kPa (high), and achieved by setting the proper standoff distances. The incident overpressure level from each blast test was recorded by PCB pencil probes (Model PCB 137A24, PCB Piezotronics, Inc., Depew, NY) positioned at the same height above the ground and the same standoff distance as the specimen's head. An 8 Channel SIRIUS HS-ACC MODULE (DEWESoft, Slovenia) data acquisition system was used to collect data from pencil probes at a sampling rate of 1 million Hz or samples per second (sps) per channel. The digital data were post processed with a 100 kHz filter.

A total of 50 8-lb C4 explosives were detonated during nine blast testing days performed during the third year. These blast tests were performed on 4 instrumented swine, 6 non-instrumented swine and 1 Post Mortem Human Subject (PMHS). The incident overpressure results were grouped and analyzed for all non-instrumented swine tested so far and including the data collected in 2013, the instrumented swine tested during this reporting period, and the two PMHS blast tests including the data from the first PMHS tested in 2013.

<u>Incident pressure data – Post Mortem Human Subjects</u>

A total of 17 blast tests were performed on a two PMHS specimens, the first of which was tested in 2013 and the second in 2015 (engineering data are described under Task II). The first PMHS received 9 blasts (three directions each at three blast levels while the second PMHS received 8 blasts due to lack of time. The high pressure blast for rear exposure could not be completed before the lab shut down at 5 pm. The testing order started with the frontal blast at low level followed by the medium and high levels. Then the specimen was repositioned to receive blasts from the other two directions, three from the rear at three levels followed by three from the side. For the second PMHS tested in 2015, a total of 8 blasts were performed, short a high level rear blast. Data from the two PMHS tests were combined and analyzed in this report.

Figure 48 shows the average and one standard deviation incident overpressure magnitudes recorded by pencil probes from two the PMHS tests. The measured average incident overpressure of 154.7, 295.2 and 412.8 kPa for low, medium and high blast levels respectively were quite close to each of the target blast levels of 150, 300, and 400 kPa. In particular, the low blast pressure was very consistent (coefficient of variance, cv, = 4%). At the high blast level, the variability of the peak overpressure between tests was high, with a cv of 25%. This variability might be related to short standoff distance where the Friedlander wave was distorted by a ground reflection wave and the specimen was above the triple point. This can be seen in Figures 49a and b. At the low blast level, the incident overpressure time history reassembled a typical Friedlander waveform in a free field. At the high blast level, it appears that there were two peaks distorting the Friedlander waveform. In future tests, the specimen needs to be lowered to stay below the triple point and its exact location will be determined by a calibration test. Figure 50 shows the incident pressure as a function of the standoff distance. The power function fitting the curve is given by:
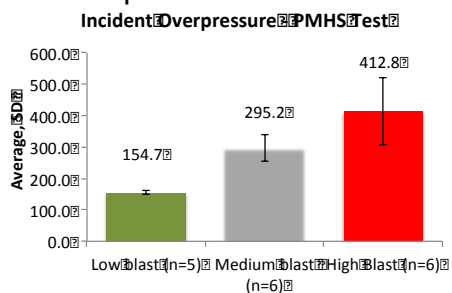Incident pressure = $5709.5x^{-2.338}$ where x is the stand-off distance

Figure 48. Average and standard deviation of the peak incident pressure at the three blast levels in PMHS tests
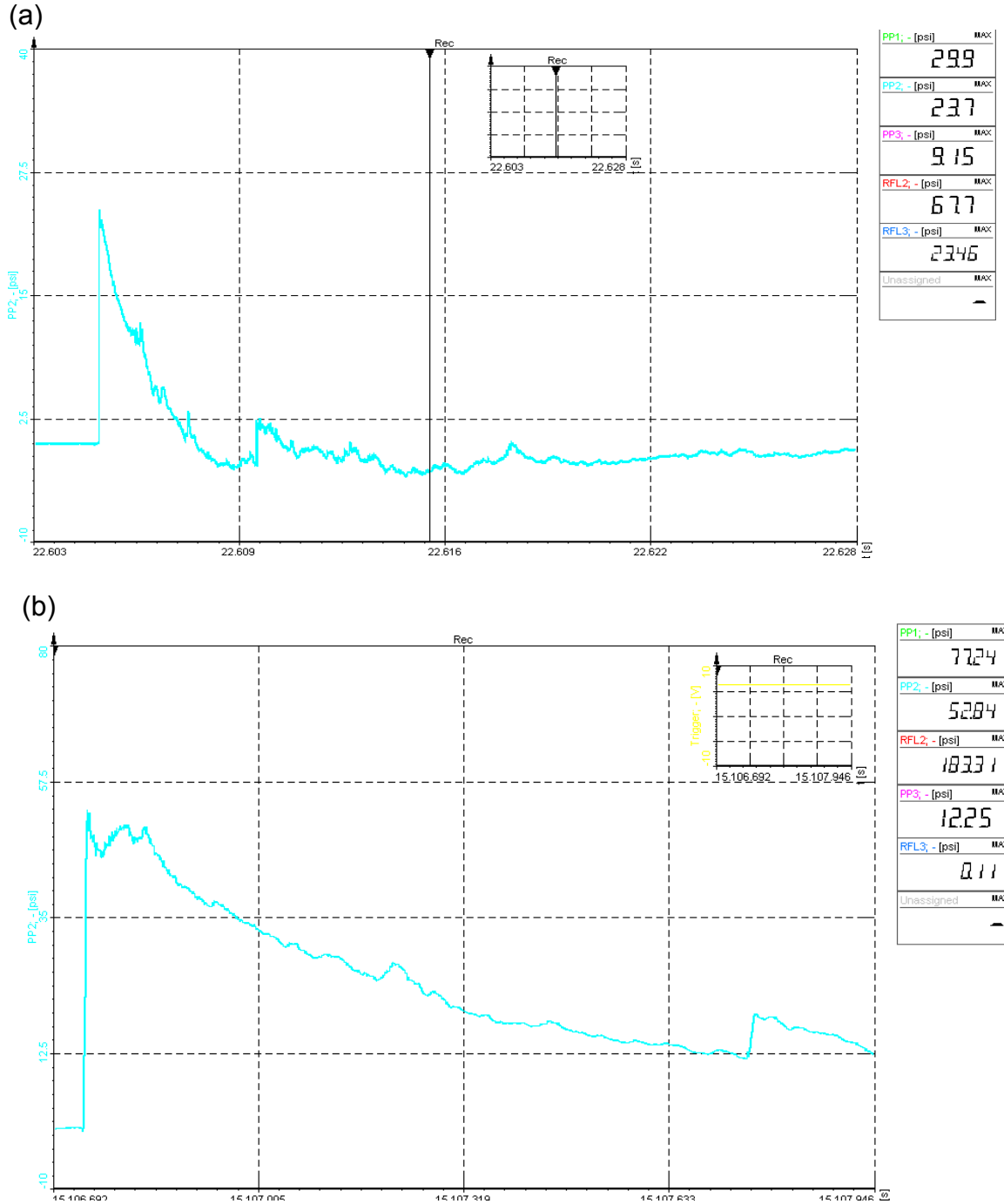
Figure 49: Pressure wave forms measured by pencil probes: a) at the low blast level the waveform reassembled a typical Friedlander wave in a free field; b) at the high blast level the waveform was distorted by ground reflection.
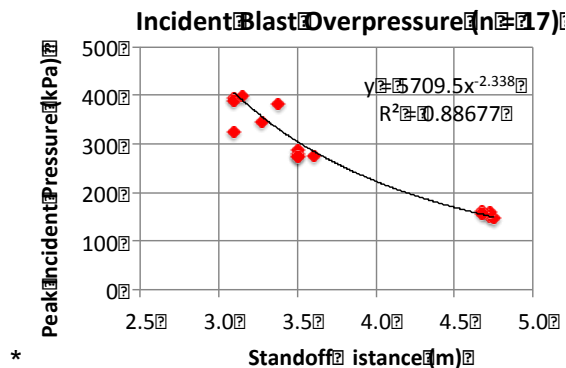
Figure 50: The peak blast pressure vs. standoff distance for PMHS tests

Incident pressure data – non-instrumented swine

A total of 12 non-instrumented swine (Task I for histology data) were exposed to either medium (n=7) or high blast (n=5) blast overpressures in 2013 and 2014. All non-instrumented swine were subjected to frontal blasts. Blast pressure data analyzed and reported here included all 12 non-instrumented swine blast tests that we were scheduled to do.

The average incident pressure was 273 kPa for the medium blast swine group, and 375 kPa for the high blast swine group. Both pressure levels were slightly lower than the targeted nominal pressure levels (Figure 51, Table 13). All non-instrumented pigs were tested in cold weather (around 40 degree) as opposed to 60-80 degree weather for the other blast tests. Whether the temperature difference could affect peak overpressure requires investigation and confirmation.
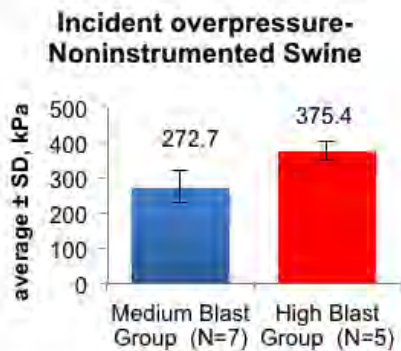

Figure 51. Average incident pressure levels for each non-instrumented swine blast group

Table 13. IOP for non-instrumented swine

Non-Instrumented Pig	Norminal Pressure	Peak Pressure (psi) [filtered]	Peak Pressure (kPa) [filtered]
pig1_non-instrumeted	medium	32.4	223.5
pig2_non-instrumeted	medium	48.2	332.3
pig3_non-instrumeted	medium	44.3	305.4
pig4_non-instrumeted	medium	32.2	222.0
pig5_non-instrumeted	medium	38.1	262.7
pig6_non-instrumeted	medium		
pig7_non-instrumented	high	52.2	359.9
pig8_non-instrumented	high	52.2	359.9
pig9_non-instrumented	high	58.5	403.3
pig10_non-instrumented	high	58.5	403.3
pig11_non-instrumented	medium	42.1	290.3
pig12_non-instrumented	high	50.8	350.3
Medium Blast Group (N=7)		39.6	272.7
High Blast Group (N=5)		54.4	375.4

Blank: data acquisition system was not triggered

Incident pressure data –instrumented swine

A total of 35 8-lb C4 explosives were detonated during 4 testing days performed on 4 instrumented swine during this annual reporting period (June 2014 – June 2015). In two tests, blast pressure data were not recorded due to an issue with the trigger. Figure 52 shows the average and standard deviation of the incident pressures at low, medium and high blast levels. The measured peak overpressure magnitudes were quite close to the target pressure for each blast level (150 kPa, 300 kPa, and 420 kPa). In particular, the low blast pressure was very consistent (cv = 4%). Variability increased as the blast level went up with cv's of 6% and 16% at the medium and high blast levels, respectively.
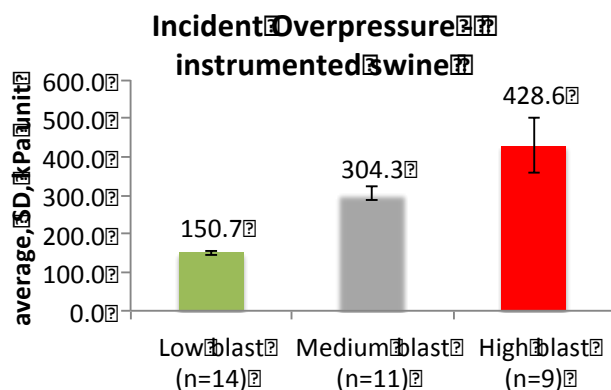

Figure 52. Average incident pressure levels for each non-instrumented swine blast group

Ideally, at a given standoff distance blast pressure generated from a given weight of explosive is constant. During each blast test, the incident pressure at the specimen location for a given blast level was measured by a pencil probe. Two additional pencil probes were also used to monitor the blast overpressures at two other locations during the same event. These measurements help adjust the standoff distance for the next test to match the targeted pressure. Figure 53 shows a total of 100 measurements of the pressure levels and associated standoff distances from a total of 35 blasts during instrumented pig tested conducted during this reporting period. Overall, the peak blast overpressure magnitudes were quite repeatable, particularly at the low and medium blast levels at longer standoff distances.
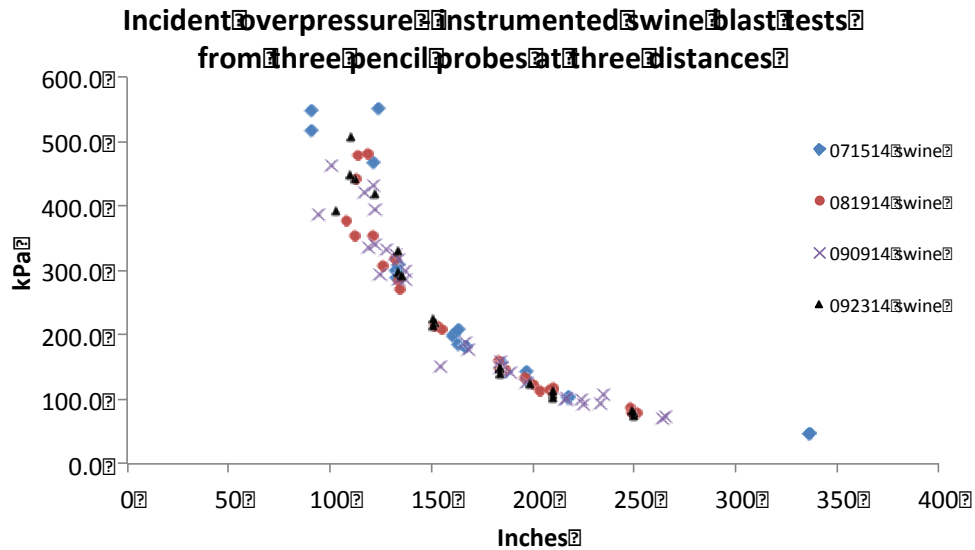
Figure 53: Incident pressure measurements vs distances mesured using three pencil probes for each of the 35 blast tests on instrumented swine.

Conclusions

Incident blast overpressure generated from an 8 lb C4 explosive represents a typical Friedlander waveform in a free field.

The peak blast overpressure magnitudes were repeatable, particularly at the low and medium blast levels.

The peak blast overpressure as a function of standoff distance can be established for the current open field blast test design.

2   Validation of the Human Brain Model

This project was put on hold because of the lack of experimental data needed for validation. It is hoped that the project will be funded beyond its end date so that more cadaver data can be collected and the human brain model project could be completed.

ADDITIONAL STUDIES

Under Task I, we received approval from IACUC of Wayne State University and ACURO of MRMC to add two procedures to our swine testing protocol. One was to monitor the electroencephalographic (EEG) signals from the swine brain pre- and post-blast. The second was to perform MRI scans of the swine brain pre- and post-blast. Both procedures were designed to collect additional information on the effects of primary blast on the brain.

Measurement of Quantitative Electroencephalographic (qEEG) Signals

[The material presented below is a manuscript that was submitted to Brain Injury for review and possible publication]

Blast-related injury is currently a complex problem for the military and civilian populations. A blast event consists of an explosion which produces an associated pressure or primary blast wave that rapidly approaches an individual in its path. It has been reported that Soldiers participating in Operation Iraqi Freedom and Operation Enduring Freedom from October 2001 through January 2005 experienced a greater proportion of head injuries as compared to other previous conflicts. Improvised explosive devices (IEDs) are reported to account for 78% of the injuries, the highest proportion found for any large scale conflict. [1] A survey of over 2500 U.S. Army infantry Soldiers found that they reported loss of consciousness (43.9%), memory problems (24.6%), concentration problems (31.4%), and irritability (56.8%). [2] Blast-exposed Soldiers are categorically different than patients suffering from traditional blunt trauma injuries. [3] A victim exposed to a primary blast wave may appear normal at first but can rapidly demonstrate neurological deficits for a period of time following the blast event indicative of sustained neurological alterations. [4] Early detection of blast -induced brain injury will allow early screening and assessment of brain abnormalities in Soldiers to enable timely therapeutic intervention.

Electroencephalography (EEG) is a commonly used method to study cerebral function. EEG is particularly attractive for field use because the recording device is portable, relatively inexpensive and requires relatively short recording durations. [5] Analysis of EEG data is usually performed qualitatively and routine EEG lacks sufficient sensitivity and specificity for diagnosing mTBI [6-8]. Quantitative analysis of EEG data (qEEG) reduces the amount of data to be recorded and produces results that are readily interpreted.[9] Quantitative EEG (qEEG), together with advanced analysis methods, shows promise for clinical applications and has consistently yielded interesting research results in studies of concussed athletes and mTBI patients [8,10-13], suggesting that qEEG measures can detect brain changes both soon after sustaining mTBI and over a period of time post-injury. Early detection of blast-induced brain injury would allow early assessment of brain abnormality in Soldiers to enable timely therapeutic intervention. However, most qEEG studies have evaluated individuals from civilian settings and individuals who have not been exposed to blast forces. Only a few peer-reviewed

studies have examined EEG-recorded brain activity following blast-related injury among Soldiers, and these did not investigate brain activity in the early post-injury phase.[14-16] A few animal blast studies found waveform amplitude changes using routine EEG without showing diagnostic values. [17,18]   These data are not sufficient to support the widespread clinical use of qEEG to diagnose blast-related mTBI.

The current study reports on the use of qEEG in blast-induced brain injury using a swine model. The purpose was to determine if qEEG can detect brain activity abnormalities early after blast exposure, to develop qEEG data analysis protocols, and to determine the parameters that are of most interest in assessing the neuronal effects of blast exposure.

Methods
Experimental setup
All surgical procedures were approved by the Institutional Animal Care and Use Committee of Wayne State University and the U. S. Army Animal Care and Use Research Office (ACURO). Swine (Yucatan minipigs, 50-kg weight) were used in this initial study. The animals were sedated with ketamine and midazolam, and propofol (0.83-1.66 mg/kg, iv) was given for further anesthesia. They were maintained on propofol (12-20 mg/kg/hr iv) for 2 hours after blast. Ventilatory support via intubation was maintained with an Ambu bag, as needed. Blood pressure, heart rate, and body temperature were monitored over the time. At lower ambient temperatures, supplemental heat (water circulating heating pad, space blanket, Thermacare Heat Wraps) was provided to maintain normal body temperature. The swine was suspended in a sling and restrained for exposure to an open field blast with the chest protected with lead sheet and foam. EEG recording was performed at 15 min before blast, and 15, 30, 120 min, 1, 2, and 3 days post-blast using a Biopac data acquisition system (MP-36, Biopac, Goleta, CA). Non-invasive surface recording electrodes (Model# 502, Biopac, Goleta, CA) were placed on the skin over both the frontal and parietal areas of the skull (Figure 1). Acknowledge software (Version 4.2, Biopac, Goleta, CA) was used for EEG data analysis. Raw EEG data were extracted into different bands including alpha-, beta-, theta-, delta-, gamma-bands. EEG parameters included over all frequency analysis and root mean square (RMS) analysis of alpha band using tools provided by Acknowledge software. Power of analysis (V^2/Hz/Min) of raw data and individual bands were analyzed and compared between pre-blast and post-blast using the power spectral density (PSD) function in the software.

Experimental protocol
Six swine were exposed to blast overpressure with a peak ranging from 420-450 kPa. All tests were performed in an open field test facility owned by ARES Inc. (A manufacturing company engaged in weapon design and testing) located at Lake Erie Business Park in Port Clinton, Ohio. The anesthetized swine was positioned at a appropriate distance from the center of the blast, just outside the "fireball." An 8-lb C4 charge was used to produce the pressure levels of 420-450 kPa at the location of the

head of the swine. The swine wore a protective foam-lined lead vest that protected the torso from physical injury.

Quantitative EEG analysis

A personal computer system was used for the recording of the EEG signals using a Biopac data acquisition system, at 0.53–70 Hz (−3 dB) and a sensitivity of 70 µV/cm. Four pairs of non-invasive surface recording electrodes (model #502 of electrodes, with a diameter of 35 mm) were placed on the skin at the locations corresponding to C3, C4, P3, P4 with a common ground placed at the front of the head (Figure 54)[19]. Offline quantitative EEG analysis was performed using Acknowledge software (Version 4.2, Biopac, Goleta, CA).
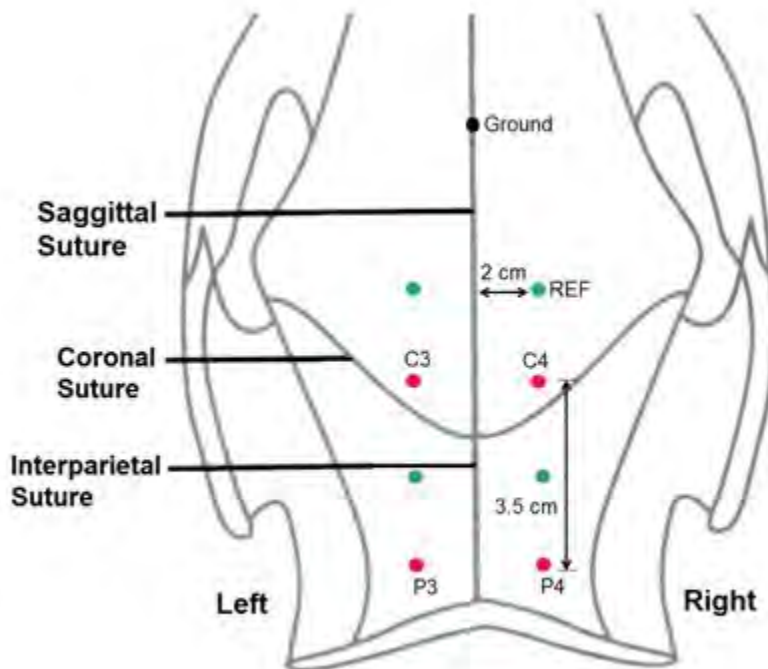

Figure 54. Position of the EEG electrodes is related to the crossing of coronal and sagittal sutures (bregma point). Nomenclature of electrodes (C3, C4, P3, P4) corresponds with the international 10–20 system, distances are adapted to fit the swine skull.

EEG signals were bandpass filtered using a zero-phase 6th order Butterworth filter with cut-off frequencies 0.5 and 30 Hz. A Hamming window was applied before performing a fast Fourier transform of each EEG epoch (2 s of EEG, using Welch's method).[19] EEG parameters including frequency, root mean square (RMS) of the alpha band, and the power (V^2/Hz/Min) of the delta, theta, alpha, and beta bands was analyzed to determine the post-blast changes compared to pre-blast at different recording locations. The qEEG parameters of mean amplitude (MAMP), and spectral edge frequency (SEF90) were also calculated.

MAMP was calculated for each epoch by averaging the mean of the absolute values of the EEG from each channels using a Fast Fourier Transform (FFT) function. The estimate of the power spectral density was calculated using Welch's method with an epoch length of 2 s and 25% overlap resulting in a spectral resolution of 0.5 Hz. SEF_{90} was calculated as the frequency below which 90% of the power between 0.5 and 20 Hz was contained. [20]

<u>Statistical analysis</u>
SPSS 17.0 (SPSS Inc., Chicago, IL) software was used for data analysis. Significance of differences between groups and time points was calculated using One Way ANOVA (PostHoc, LSD) and Repeated Measures of ANOVA (RMANOVA) tests (PostHoc, LSD). *P*<0.05 was considered as a significant difference.

Results

qEEG analysis showed that the power (V^2/Hz) of delta band increased significantly at the 15 minute post-blast time point recorded at left and right parietal locations (P_3 and P_4) (Repeated Measures of ANOVA, PostHoc, p<0.05) (Figure 55) and the delta band power appeared to gradually return to the baseline (the pre-blast level) 30 minutes after blast and later on. Delta band powers recorded at the other post-blast time points were not significantly higher than the pre-blast baseline. Increase of delta power was more predominant in the parietal regions (P3, P4), indicative of the possible neuronal functional inhibition in those regions. The power of other bands including alpha, beta, theta bands only increased slightly after blast without statistical significance (RMANOVA, p>0.05).
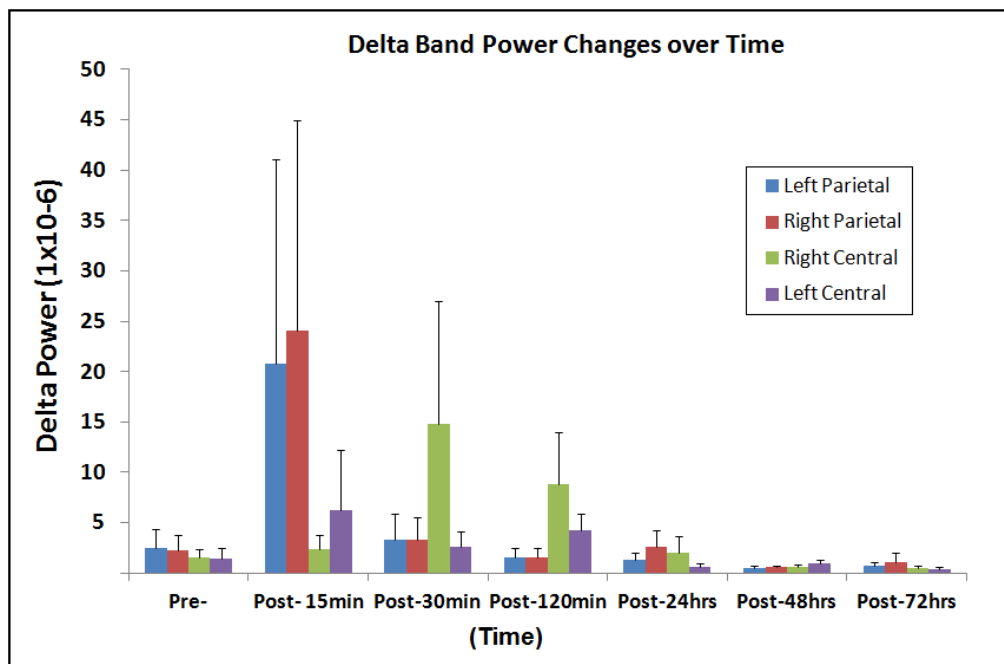
Figure 55 shows the delta band power recorded at different time points and 4 locations on the skull surface. Delta band power (Mean ±SEM) increased significantly 15 minutes after blast, predominantly in the parietal areas.

Alpha band root mean square (RMS) decreased at the 15-minute (RMANOVA, postHoc LSD, $p < 0.05$) and 30-minute ($p < 0.01$) time points after blast and recovered at 120 minutes and later on within 3 days (Figure 56). Decrease of alpha band RMS occurred predominantly in left parietal and left central regions. Alpha band RMSs recorded at the other time points were not statistically different from the pre-blast baseline (RMAVOVA, $p > 0.05$).
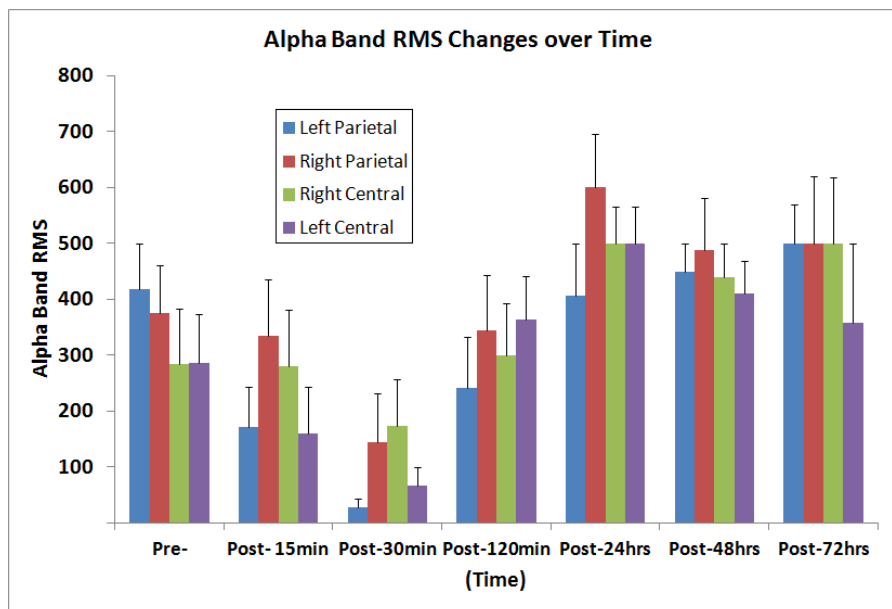
Figure 56 shows the alpha band root mean square (RMS) recorded at different time points. Alpha band RMS (Mean ±SEM) decreased significantly at 15 minutes ($p<0.05$) and 30 minutes ($p<0.01$) after blast.

MAMP appeared to decrease at the time points of 15 minutes (RMANOVA, PostHoc, LSD, $p=0.064$), 1 day ($p=0.082$), 2 days ($p=0.077$) and 3 days ($p=0.134$) post-blast (Figure 57) at all recording locations.
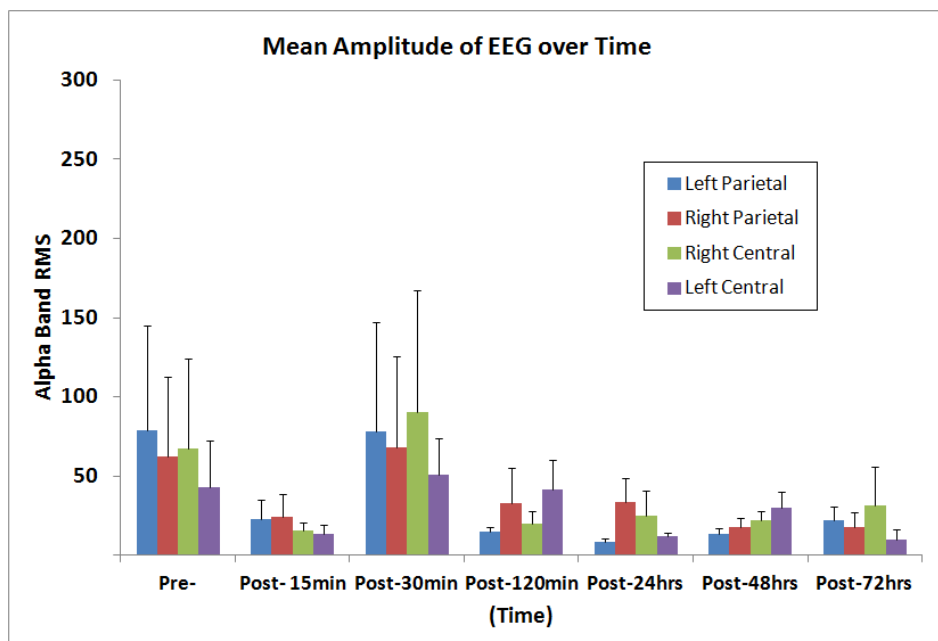

Figure 57 shows the mean amplitude (MAMP) of EEG raw data recorded at different time points. MAMP decreased after blast except for the time point 30 minutes post-blast.

The spectral edge frequency at the 90% margin (SEF_{90}) decreased significantly at 15 minutes (RMANOVA, postHoc LSD, $p=0.027$) and 2 days (RMANAOVA, $p=0.014$) after

blast (Figure 58), indicative of a power spectrum density shift to the left (low frequency domain) and inhibition of neuronal activity.
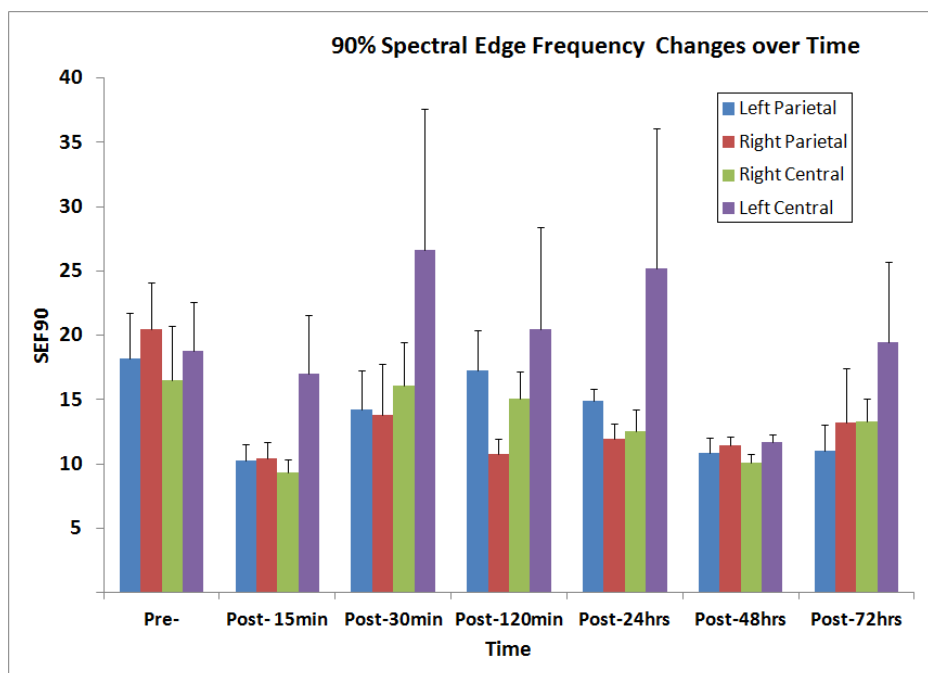

Figure 58 shows the spectral edge frequency at the 90% margin (SEF_{90}) recorded at different time points. SEF_{90} decreased significantly 15 minutes (p=0.027) after blast.

Discussion and Conclusions

Although routine EEG lacks sufficient sensitivity and specificity for diagnosing mTBI, quantitative EEG (qEEG), together with advanced analysis methods, may show promise for clinical applications. It has been reported that qEEG has consistently yielded interesting research results in studies of concussed athletes and mTBI patients.[21] Multiple qEEG parameters appeared to change following mTBI. qEEG abnormalities can appear early after injury. In a subgroup of individuals, qEEG abnormalities can persist over time, reflecting the effects of multiple mTBI exposures and recovery of function. Increase of delta band power was referred to as indicative of subcortical lesions, diffuse lesions, metabolic encephalopathy hydrocephalus and deep midline lesions.[22,23]

Only two peer-reviewed studies have examined EEG-recorded brain activity following blast-related injury, and neither of these investigated brain activity in the early post-injury phase.[14,15] Both studies found EEG abnormalities in individuals who were exposed to blast. In Cernak's study,[14] acute EEG abnormalities were found in 36% of participants with blast injury and 12% of participants without blast injury. The most common observation was hypersynchronous, discontinuous or irregular brain activity with increased theta activity. At 1-year follow-up, persistent alterations were found in 30% of participants with blast injury and 4% of participants without blast injury. These

two studies concluded that conventional EEG data are not sufficient to support the widespread clinical use of qEEG to diagnose blast-related mTBI.[14,15]

We used a swine model of brain injury to determine the value of several qEEG parameters for diagnosis and prognostication in blast-exposed swine. The outcomes demonstrated that 420-450 kPa overpressure led to a large spectrum of brain dysfunction possibly related to brain injury. The parietal region appeared to be vulnerable to dysfunction in this swine blast study because more qEEG parameter including delta band power, alpha RMS, MAPM, and SEF90 were found to have significant changes in parietal regions. Decrease of EEG amplitude was reported in two other blast brain injury research studies using a large animal model.[17,18] This is concordant with our results. The non-invasively obtained qEEG variables MAMP could diagnose and predict severe brain damage in our model and may thus be of clinical value.

Previous studies have found the following qEEG changes in mTBI in civilian settings, including reduction in mean alpha frequency, [24-27] increased theta activity,[28,29] increased theta-alpha ratios (TAR) based on power,[24,30] and decreased alpha delta ratios (ADR).[20,31] In this study, we found that increased delta power 15 minutes after blast was recorded at P_3, P_4 in the parietal region of the swine, decreased alpha RMS in all 4 recording locations 15 minutes ($p<0.05$) and 30 minutes ($p<0.01$) after blast. We also examined other parameters, but did not find statistically significantly changes. This indicates that blast-induced brain dysfunction may be different from mTBI in a civilian setting.

Previous studies have pointed out SEF_{90} as being useful in diagnosing cerebral ischemia [32,33]. General slowing of the EEG, described as a decrease in high frequency (alpha) and an increase in low frequency (delta) activity, results in a decrease in SEF_{90}. In the present study, all these three changes were found in the swine 15 minutes after blast exposure; suggesting a temporary blood circulation disturbance associated with blast exposure at 420-450 kPa and resulting in qEEG abnormalities.

Our experiments were performed under general anesthesia with propofol and ketamine. The former two substances are known to induce dose-dependent changes in EEG pattern, mostly consisting of decrease in high-frequency activity and increase in low-frequency activity.[34] Ketamine can induce an active EEG signal with increase in theta and beta activity.[35] During the perfusion period of propofol, an increase in the power of the alpha band (10% to 40%) and a decrease in the delta band was noticed.[36] Ketamine and propofol are antagonistic to each other in their interaction.[37] In the current study, ketamine was used to induce initial anesthesia, following by intravascular (IV) induction of propofol and IV maintenance of propofol. Hence under the same maintenance dose of anesthesia, parameters of qEEG should remain stable or delta band power should decrease while alpha band RMS should increase. However, after blast exposure, delta power increased with alpha RMS decreased. Hence delta band power decreased and alpha band RMS decreased 15 minutes after blast, suggesting

that these changes resulted from blast exposure rather than from the effects of anesthesia.

This study has some limitations. First, we did not correlate our qEEG findings with clinical outcomes. This is because no acute qEEG blast induced brain injury data have been measured or reported previously in human clinics. Second, a sham group study was not performed. We will perform a sham study in future studies to better understand qEEG measures in anesthetized blasted swine. Associated histological studies need to be performed to validate the qEEG findings. Histological studies of brain tissue are underway in the animals that underwent the qEEG study. Finally, an implantable telemetry technique can be used to measure qEEG in subacute and chronically awake swine models in the future.

References:
1. Owens BD, Kragh JF, Jr., Wenke JC, Macaitis J, Wade CE, Holcomb JB. Combat wounds in operation Iraqi Freedom and operation Enduring Freedom. *The Journal of trauma.* Feb 2008;64(2):295-299.
2. Hoge CW, McGurk D, Thomas JL, Cox AL, Engel CC, Castro CA. Mild traumatic brain injury in U.S. Soldiers returning from Iraq. *The New England journal of medicine.* Jan 31 2008;358(5):453-463.
3. Belanger HG, Kretzmer T, Yoash-Gantz R, Pickett T, Tupler LA. Cognitive sequelae of blast-related versus other mechanisms of brain trauma. *Journal of the International Neuropsychological Society : JINS.* Jan 2009;15(1):1-8.
4. Ciraulo DL, Frykberg ER. The surgeon and acts of civilian terrorism: blast injuries. *Journal of the American College of Surgeons.* Dec 2006;203(6):942-950.
5. Airoldi L, Beghi E, Bogliun G, Crespi V, Frattola L. Rational use of EEG in adults in clinical practice. *Journal of clinical neurophysiology : official publication of the American Electroencephalographic Society.* Sep 1999;16(5):456-461.
6. Gaetz M, Bernstein DM. The current status of electrophysiologic procedures for the assessment of mild traumatic brain injury. *The Journal of head trauma rehabilitation.* Aug 2001;16(4):386-405.
7. Nuwer M. Assessment of digital EEG, quantitative EEG, and EEG brain mapping: report of the American Academy of Neurology and the American Clinical Neurophysiology Society. *Neurology.* Jul 1997;49(1):277-292.
8. Nuwer MR, Hovda DA, Schrader LM, Vespa PM. Routine and quantitative EEG in mild traumatic brain injury. *Clinical neurophysiology : official journal of the International Federation of Clinical Neurophysiology.* Sep 2005;116(9):2001-2025.
9. Jordan KG. Emergency EEG and continuous EEG monitoring in acute ischemic stroke. *Journal of clinical neurophysiology : official publication of the American Electroencephalographic Society.* Sep-Oct 2004;21(5):341-352.
10. Geets W, Louette N. Early EEG in 300 cerebral concussions. *Revue d'electroencephalographie et de neurophysiologie clinique.* Apr 1985;14(4):333-338.

11.   Thatcher RW, Moore N, John ER, Duffy F, Hughes JR, Krieger M. QEEG and traumatic brain injury: rebuttal of the American Academy of Neurology 1997 report by the EEG and Clinical Neuroscience Society. *Clinical EEG.* Jul 1999;30(3):94-98.

12.   Thatcher RW, North DM, Curtin RT, et al. An EEG severity index of traumatic brain injury. *The Journal of neuropsychiatry and clinical neurosciences.* Winter 2001;13(1):77-87.

13.   Thatcher RW, Walker RA, Gerson I, Geisler FH. EEG discriminant analyses of mild head trauma. *Electroencephalography and clinical neurophysiology.* Aug 1989;73(2):94-106.

14.   Cernak I, Savic J, Ignjatovic D, Jevtic M. Blast injury from explosive munitions. *The Journal of trauma.* Jul 1999;47(1):96-103; discussion 103-104.

15.   Trudeau DL, Anderson J, Hansen LM, et al. Findings of mild traumatic brain injury in combat veterans with PTSD and a history of blast concussion. *The Journal of neuropsychiatry and clinical neurosciences.* Summer 1998;10(3):308-313.

16.   Sponheim SR, McGuire KA, Kang SS, et al. Evidence of disrupted functional connectivity in the brain after combat-related blast injury. *NeuroImage.* Jan 2011;54 Suppl 1:S21-29.

17.   Li BC, Li Y, Xu C, et al. Blast-induced traumatic brain injury of goats in confined space. *Neurological research.* Nov 2014;36(11):974-982.

18.   Axelsson H, Hjelmqvist H, Medin A, Persson JK, Suneson A. Physiological changes in pigs exposed to a blast wave from a detonating high-explosive charge. *Military medicine.* Feb 2000;165(2):119-126.

19.   Weenink RP, Vrijdag XC, van Putten MJ, et al. Quantitative electroencephalography in a swine model of cerebral arterial gas embolism. *Clinical neurophysiology : official journal of the International Federation of Clinical Neurophysiology.* Feb 2012;123(2):411-417.

20.   Lee SJ, Hatran DP, Tomimatsu T, Pena JP, McAuley G, Longo LD. Fetal cerebral blood flow, electrocorticographic activity, and oxygenation: responses to acute hypoxia. *The Journal of physiology.* May 1 2009;587(Pt 9):2033-2047.

21.   Slobounov S, Gay M, Johnson B, Zhang K. Concussion in athletics: ongoing clinical and brain imaging research controversies. *Brain imaging and behavior.* Jun 2012;6(2):224-243.

22.   Fraga FJ, Falk TH, Kanda PA, Anghinah R. Characterizing Alzheimer's disease severity via resting-awake EEG amplitude modulation analysis. *PloS one.* 2013;8(8):e72240.

23.   Babiloni C, Frisoni G, Steriade M, et al. Frontal white matter volume and delta EEG sources negatively correlate in awake subjects with mild cognitive impairment and Alzheimer's disease. *Clinical neurophysiology : official journal of the International Federation of Clinical Neurophysiology.* May 2006;117(5):1113-1129.

24. Chen XP, Tao LY, Chen AC. Electroencephalogram and evoked potential parameters examined in Chinese mild head injury patients for forensic medicine. *Neuroscience bulletin.* May 2006;22(3):165-170.

25. Gosselin N, Lassonde M, Petit D, et al. Sleep following sport-related concussions. *Sleep medicine.* Jan 2009;10(1):35-46.

26. Korn A, Golan H, Melamed I, Pascual-Marqui R, Friedman A. Focal cortical dysfunction and blood-brain barrier disruption in patients with Postconcussion syndrome. *Journal of clinical neurophysiology : official publication of the American Electroencephalographic Society.* Jan-Feb 2005;22(1):1-9.

27. Tebano MT, Cameroni M, Gallozzi G, et al. EEG spectral analysis after minor head injury in man. *Electroencephalography and clinical neurophysiology.* Aug 1988;70(2):185-189.

28. Fenton G, McClelland R, Montgomery A, MacFlynn G, Rutherford W. The postconcussional syndrome: social antecedents and psychological sequelae. *The British journal of psychiatry : the journal of mental science.* Apr 1993;162:493-497.

29. McClelland RJ, Fenton GW, Rutherford W. The postconcussional syndrome revisited. *Journal of the Royal Society of Medicine.* Sep 1994;87(9):508-510.

30. Watson MR, Fenton GW, McClelland RJ, Lumsden J, Headley M, Rutherford WH. The post-concussional state: neurophysiological aspects. *The British journal of psychiatry : the journal of mental science.* Oct 1995;167(4):514-521.

31. Claassen J, Hirsch LJ, Kreiter KT, et al. Quantitative continuous EEG for detecting delayed cerebral ischemia in patients with poor-grade subarachnoid hemorrhage. *Clinical neurophysiology : official journal of the International Federation of Clinical Neurophysiology.* Dec 2004;115(12):2699-2710.

32. Finnigan SP, Walsh M, Rose SE, Chalk JB. Quantitative EEG indices of sub-acute ischaemic stroke correlate with clinical outcomes. *Clinical neurophysiology : official journal of the International Federation of Clinical Neurophysiology.* Nov 2007;118(11):2525-2532.

33. Florence G, Guerit JM, Gueguen B. Electroencephalography (EEG) and somatosensory evoked potentials (SEP) to prevent cerebral ischaemia in the operating room. *Neurophysiologie clinique = Clinical neurophysiology.* Feb 2004;34(1):17-32.

34. Brown L, van de Molengraft J, Yazicioglu RF, Torfs T, Penders J, Van Hoof C. A low-power, wireless, 8-channel EEG monitoring headset. *Conference proceedings : ... Annual International Conference of the IEEE Engineering in Medicine and Biology Society. IEEE Engineering in Medicine and Biology Society. Annual Conference.* 2010;2010:4197-4200.

35. Sloan TB. Anesthetic effects on electrophysiologic recordings. *Journal of clinical neurophysiology : official publication of the American Electroencephalographic Society.* May 1998;15(3):217-226.

36. Herregods L, Rolly G, Mortier E, Bogaert M, Mergaert C. EEG and SEMG monitoring during induction and maintenance of anesthesia with propofol. *International journal of clinical monitoring and computing.* Apr 1989;6(2):67-73.

37. Bojak I, Day HC, Liley DT. Ketamine, Propofol, and the EEG: A Neural Field Analysis of HCN1-Mediated Interactions. *Frontiers in computational neuroscience.* 2013;7:22.

Magnetic Resonance Imaging (MRI) of Swine Brain

The second project involved the magnetic resonance imaging (MRI) of swine brain in an attempt to detect MRI changes after sustaining a blast overpressure exposure. Again, these were the noninstrumented animals used for histological studies and were exposed only once to pressures ranging from 420-450 kPa. The pigs were scanned a day or so pre-blast and again on the 3rd day post-blast. Two sham pigs were also scanned, but only once.

We have conducted 12 *in vivo* scans using a 3T MRI scanner. This includes 5 pigs which were scanned pre- and post-blast and 2 sham pigs which were each scanned once. The scanning position was head-first, right- lateral and a 12-channel head coil was used. The pigs were sedated for the duration of the scan.

The *in vivo* study did not show any significant difference between pre- and post-blast MRI. Specifically, we examined the T2-FLAIR images for potential edema and susceptibility weighted imaging (SWI) images for possible bleeds. No abnormalities were identified. Figures 59 and 60 show the T2 FLAIR images for pre and post-blast scan, respectively. Figures 61 and 62 show the SWI images for pre and post-blast scan, respectively.

To further investigate the microstructural white matter injury, which is related to diffuse axonal injury (DAI) or traumatic axonal injury (TAI), high quality (very high-resolution and high signal to noise ratio) diffusion tensor imaging (DTI) needs to be performed. However, due to several factors such as cranial thickness, the large volume of surrounding tissue (skin, fat, and muscles), scan time, and 3T human MRI limitations, we could not collect meaningful DTI images *in vivo* with a decent signal to noise ratio (SNR).

Since the brains were could be scanned ex-vivo after the animal had been sacrificed, it would be possible to verify the *ex vivo* findings with histological images. The *ex vivo* scan protocol requires the specimens to be kept in a material to prevent dehydration. In addition, to achieve the best susceptibility matching, that material must not contain any protons. Fomblin®, or perfluoropolyether (PFPE), has been widely used in the literature as this material. However, to our knowledge, there has been no rigorous study of the possible interactions between PFPE and brain tissue after it was immersed in PFPE. Therefore, there is uncertainty that brain tissue exposed to PFPE would provide suitable samples for complex histological staining. To this end, an additional study is necessary to make this determination.

The last step of our study would be to perform *ex vivo* MRI scans. We anticipate acquiring high quality DTI and SWI data which will allow us to determine the vulnerability of the pig brain to primary blast forces. For reasons given above, the proposed *ex-vivo* study could not be completed under this contract.

Figure 59 T2-FLAIR images of PIG ID# 5027, Pre-blast.

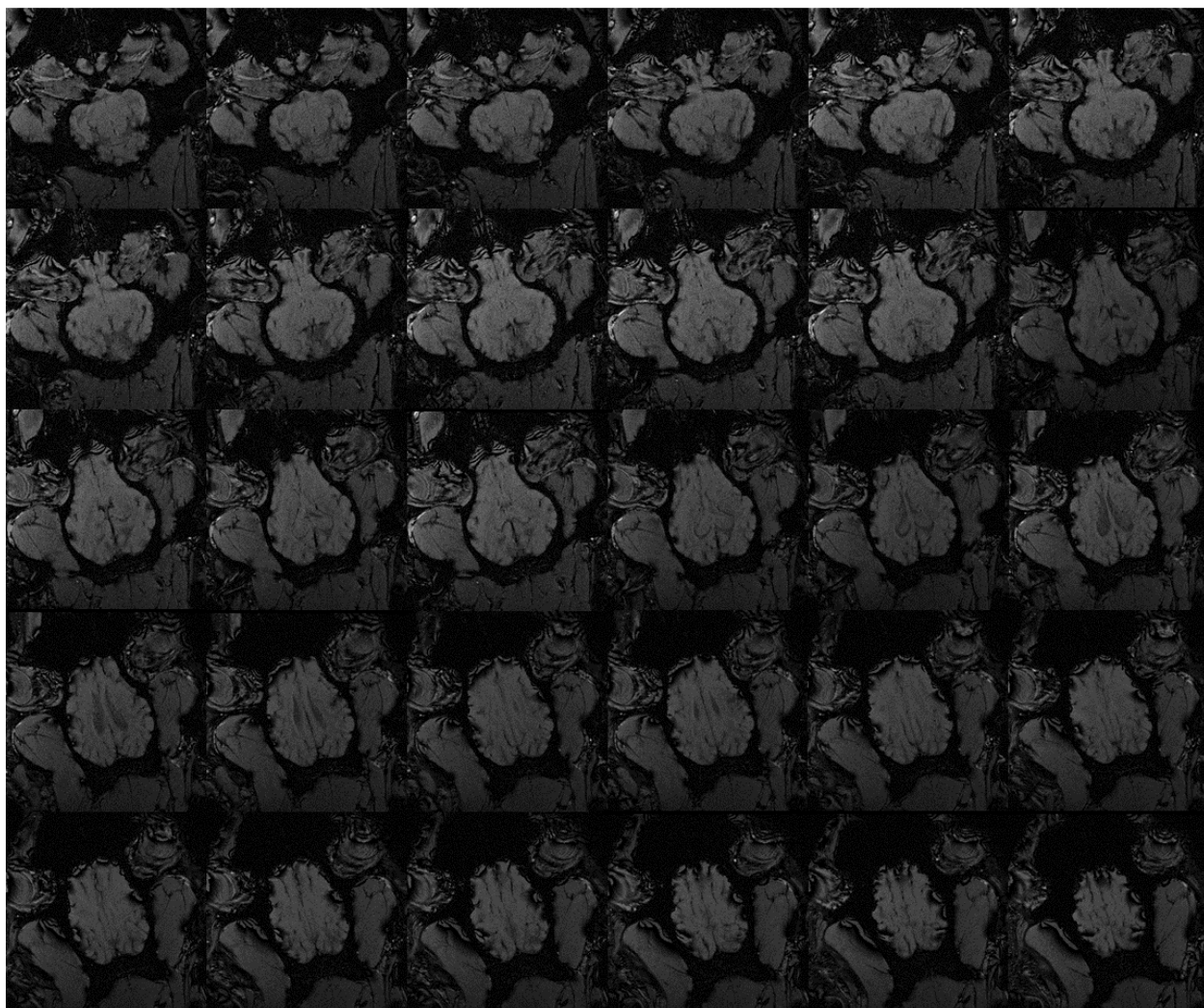Figure 60 T2-FLAIR images of PIG ID# 5027, Post-blast. (420 Kpa)

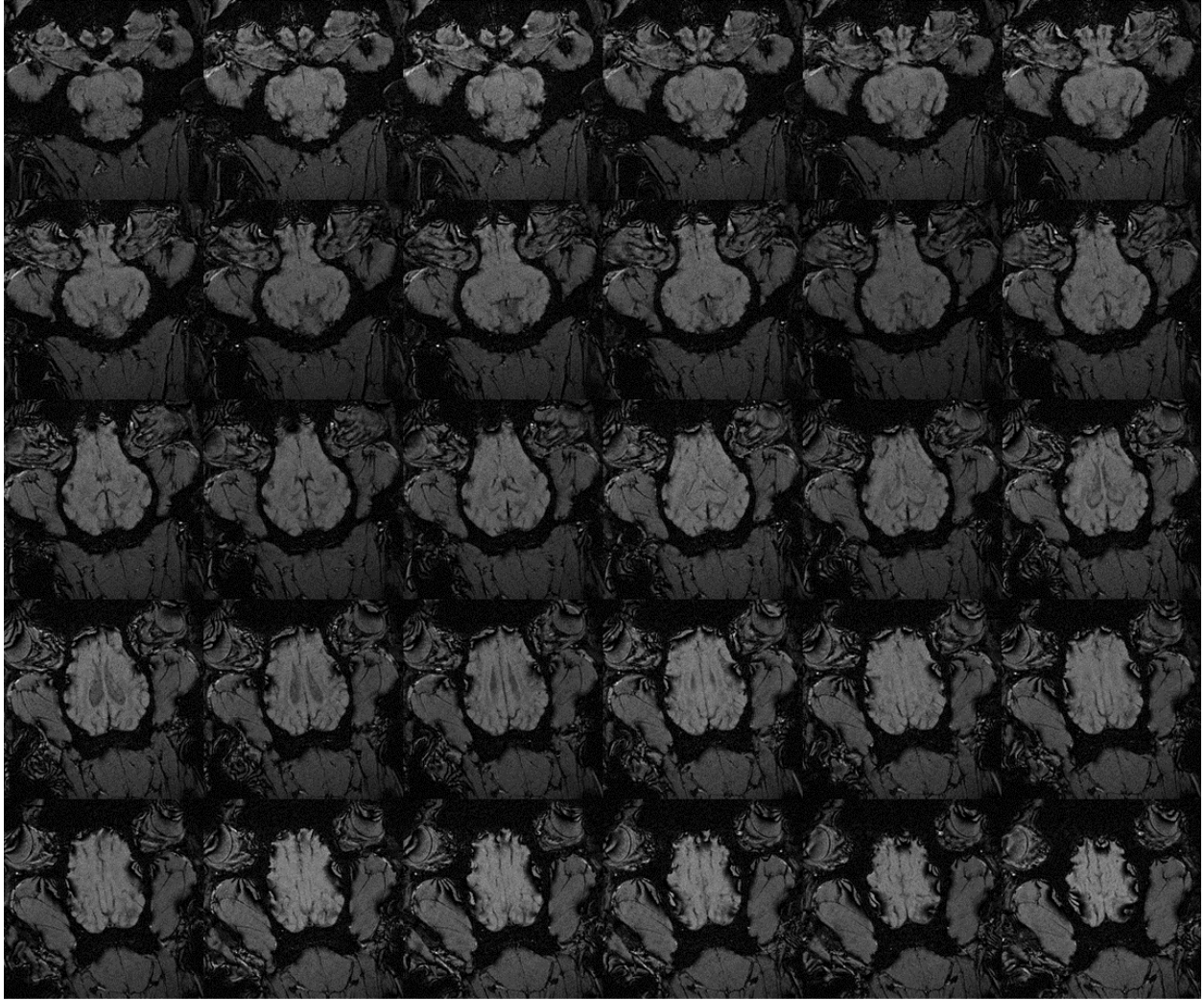Figure 61 SWI images of PIG ID# 5027, Pre-blast.

Figure 62 SWI images of PIG ID #5027, Post-blast (420 kPa)

DISCUSSION

To the extent possible, we have completed all of our blast testing and are making progress on our histological studies of porcine brains. Computer models of the human and swine brain have been completed but validation is held back due to the fact that the predicted ICP is consistently higher than that observed experimentally. Also, we do not have enough cadaver data for validation, having only done 2 of the 6 scheduled cadaver tests.

There is good histological evidence that the porcine brain sustained injury as a result of the primary open field blasts, particularly at high pressures. The various manifestations of axonal and neuronal injuries need to be studied further in order to determine the reasons for the observed changes. Perhaps, direct observation of cellular response to blast needs to be made to ascertain the mechanisms of injury. We have in mind the

construction of a shock tube that can apply a blast wave to a living slice of mouse brain and that will allow observation of the transport of fluorescent molecules across cellular membranes as well as response of subcellular elements to a blast overpressure.

Based on what we know so far, there is injury to the axon as well as to the cell body of the neuron due to blast. The injury mechanism may not be the same as that for blunt impact. That is, in blunt impact, the axons are presumably injured by stretching but since the computed strains in the brain are low due to blast, the observed axonal injury may be due to a dynamic pressure wave. It has long been known that pressure waves can cause concussion but a mechanical explanation of how pressure waves injure brain cells is still unknown. This is another reason for the proposed study to make direct observations of cellular response to a blast wave, as described above.

CONCLUSIONS

1. The porcine brain is susceptible to blast overpressure and sustains both axonal and neuronal cell body injury when the pressure is high enough (above 400 kPa).
2. The measured intracranial pressure (ICP) in the swine brain is generally lower than the incident overpressure (IOP) with the parietal pressures being the highest and almost equal to the IOP.
3. Preliminary data from cadaver testing revealed that the ICP is also lower than the IOP, even with pressurization of the brain with artificial cerebral spinal fluid (CSF).
4. Computer models of the swine and human brain in response to blast have been developed. They predict an ICP larger than the IOP and we are looking for mechanisms that can lower the predicted ICP to match experimental observations.
5. The observed injuries to brain cells require a logical explanation. That is, how does a pressure wave damage cells?
6. Further research involving the observation of cellular response to blast is recommended.

PUBLICATIONS AND PRESENTATIONS

Journal paper

Chen C, Zhou C, Cavanaugh JM, Kallakuri S, Desai A; Zhang L, King AI (2015) Quantitative Electroencephalography in a Swine Model of Blast Induced Brain Injury. Brain Injury. Manuscript under review,

Zhu F, Chou CC, Yang KH and King AI. On the development of a new biomechanical indicator for primary blast-induced brain injury. Chinese Journal of Traumatology (English Edition), 2015, 10.1016/j.cjtee.2014.10.001.

Zhu F, Chou CC, Yang KH and King AI. A theoretical analysis of stress wave propagation in the head under primary blast loading. Proceedings of the Institution of Mechanical Engineers, Part H, Journal of Engineering in Medicine, 2014, Vol. 228(5) 439–445.

Kallakuri S, Desai A, Mathei J, Dawe E, Feng K, Saif T, Jin X, Chen CY, Zhang L, Cavanaugh JM and King AI. Neuronal injury and glial changes are the hallmark of injury changes following open field blast exposure in the brain- an investigation of swine frontal lobe (*Manuscript in Preparation for submission to a major journal)*

Conference papers

Zhu F, Gatti DL and Yang KH. Building a finite element model of axonal microscopic structures. In: Proceedings of WSU 75th Anniversary Symposium Injury Biomechanics, Prevention, Diagnosis & Treatment, August 14-16, 2014, Detroit, MI, USA.

Zhu F, Chou CC, Yang KH and King AI. Analytical modelling of stress wave response in the head under primary blast loading. In: Proceedings of WSU 75th Anniversary Symposium Injury Biomechanics, Prevention, Diagnosis & Treatment, August 14-16, 2014, Detroit, MI, USA.

Kalra A, Zhu F and Yang KH. Key parameters in the blast modeling using 2D to 3D ALE mapping technique. In: Proceedings of 13th International LS-DYNA Users Conference, June 2014, Detroit, MI, USA.

Kalra A, Zhu F, Chen C and Yang KH. A computational modeling of the biomechanical response of pig head under blast loading. In: Proceedings of 17th U.S. National Congress on Theoretical & Applied Mechanics, June, 2014, East Lansing, MI, USA.

Zhang L. Makwana. Biomechanical Responses of Human Head and Headform in Blast Exposure, at the 17th U.S. National Congress on Theoretical and Applied Mechanics, East Lansing, MI, June 16, 2014.

Zhang L, Sharma S, Makwana R, Wang L. Modeling of Brain Responses in Traumatic Blast Exposure. Proceedings of the Wayne State University 75th Anniversary Symposium, August 14th-16th, 2014.

Zhang L, Sharma S. Development and Validation of A Detailed Finite Element Model of Human Eye for Predicting Ocular Trauma. Proceedings of the Wayne State University 75th Anniversary Symposium, August 14th-16th, 2014.

S Kallakuri, A Desai, K Feng CY Chen, T Saif, X Jin, L Zhang, C Zhou, J Mathei, E Dawe, JM Cavanaugh, AI King. Open Field Primary Blast Exposure Induces Changes

in Brain-Preliminary Results from Swine Prefrontal Cortex. Wayne State University Department of Biomedical Engineering 75th Anniversary Symposium, Detroit Marriott, August 14th-16th, 2014.

JM Cavanaugh, K. Feng, L. Zhang, S. Kallakuri, C. Chen, A. I. King. Mechanical Response and Brain Injury in Swine Subjected to Free-Field Blast. World Congress of Biomechanics, Boston, Massachusetts, 2014. Podium.

Kallakuri S, Desai A, Mathei J, Dawe E, Feng K, Chen Cy, Cavanaugh JM, Zhang L, King AI: Open field primary blast exposure induces neuronal and glial alterations in frontal cortex. B3-13; 33rd Annual Symposium of the National Neuortrauma Society, Santa Fe, New Mexico, June 28-July1st , 2015

Poster Presentations

Ke Feng, Liying Zhang, Chaoyang Chen, Srinivasu Kallakuri, John M Cavanaugh, MD, Albert I King, PhD. Biomechanical Response of swine exposed to open-field blasts. The 2015 Military Health System Research Symposium (MHSRS). August 2015.

Srinivasu Kallakuri, Alok Desai, Janine Mathei, Elizabeth Dawe, Ke Feng, Chaoyang Chen, Liying Zhang, John M Cavanaugh, Albert I King, Open field primary blast exposure induces neuronal and glial alterations in the brain - a preliminary investigation of swine frontal cortex. The 2015 Military Health System Research Symposium (MHSRS). August, 2015.

Feng K, Kallakuri S, Zhang LY, Chen CY, Cavanaugh JM, King AI. Mechanical Response and Brain Injury of Swine Subject to Free-Field Blast. Ohio State University, 2014 http://ibrc.osu.edu/symposium/past-symposiums/2014-symposium/2014-posters-manuscripts/